

**LAPPEENRANTA UNIVERSITY OF TECHNOLOGY
DEPARTMENT OF MECHANICAL ENGINEERING**

**MULTIVARIABLE REGRESSION ANALYSIS AND HOT-SPOT STRESS
APPROACH INTO FATIGUE LIFE ESTIMATIONS OF WELDED JOINTS**

Diploma project title has been accepted at the department meeting on 7.12.2005.

Supervisors: Prof. Gary Marquis and Mr. Ilkka Poutiainen (M.Sc.)

Kari J. Salomaa

Signature:

Date:

89 Mill Lane
Sawston, Cambridge
CB2 4HY
United Kingdom
040-044-1562

ABSTRACT

Lappeenranta University of Technology
Department of Mechanical Engineering

Kari J. Salomaa

MULTIVARIABLE REGRESSION ANALYSIS AND HOT-SPOT STRESS APPROACH INTO FATIGUE LIFE ESTIMATIONS OF WELDED JOINTS

Master's Thesis
2006

72 pages, 59 figures, 34 tables, 3 appendices

Examiners: Professor Gary Marquis
Mr. Ilkka Poutiainen

Keywords: multivariable regression, hot-spot stress,
fatigue, welded joints, thin plates

Multivariable regression analysis has been applied to fatigue life prediction of three types of welded joints based on literature search of S-N data. Joint details include butt joints, cruciform joints and longitudinal attachments. Variables considered are stress range, stressed plate thickness and loading mode. Thickness effect regarding stressed plate thickness is re-established for three types of joints in order to check its relevance to fatigue life before moving into multivariable regression. Linear fatigue life estimate equations are derived for all three types of joints considering plate thickness and loading mode. Fatigue life predictions by equations are compared and discussed with chosen test results from literature.

Four case studies are chosen from literature search and different fatigue life prediction methods are used to compute estimated fatigue lives. Results from different methods are compared and discussed with test results. Case studies include 2mm and 6mm thick symmetrical longitudinal attachments, 12.7mm unsymmetrical longitudinal attachment, 38mm symmetric longitudinal attachment under bending and 25mm and 38mm load-carrying cruciform joint under bending. Case studies are modelled as close to test specimens as possible. Fatigue life prediction methods include hot-spot method where structural hot-spot stress is obtained through two linear surface extrapolation methods, quadratic surface extrapolation and through thickness integration at the weld toe. Effective notch method and fracture mechanics methods are applied for cruciform joint.

TIIVISTELMÄ

Lappeenrannan teknillinen yliopisto
Konetekniikan osasto

Kari J. Salomaa

MONIMUUTTUJA REGRESSIO ANALYYSIN JA HOT-SPOT JÄNNITYKSEN SOVELTAMINEN HITSATTUJEN TERÄSRAKENTEIDEN VÄSYMISKESTÄVYYTEEN

Diplomityö
2006

72 sivua, 59 kuvaa, 34 taulukkoa, 3 liitettä

Tarkastajat: Professori Gary Marquis
Diplomi-insinööri Ilkka Poutiainen

Hakusanat: monimuuttuja regressio, hot-spot jännitys,
väsyminen, ohuet levyt

Kolmen eri hitsausliitoksen väsymisikä arvio on analysoitu monimuuttuja regressio analyysin avulla. Regression perustana on laaja S-N tietokanta joka on kerätty kirjallisuudesta. Tarkastellut liitokset ovat tasalevy liitos, krusiformi liitos ja pitkittäisripa levyssä. Muuttujina ovat jännitysvaihtelu, kuormitetun levyn paksuus ja kuormitus tapa. Paksuus efekti on käsitelty uudelleen kaikkia kolmea liitosta ajatellen. Uudelleen käsittelyn avulla on varmistettu paksuus efektin olemassa olo ennen monimuuttuja regressioon siirtymistä. Lineaariset väsymisikä yhtälöt on ajettu kolmelle hitsausliitokselle ottaen huomioon kuormitetun levyn paksuus sekä kuormitus tapa. Väsymisikä yhtälöitä on verrattu ja keskusteltu testi tulosten valossa, jotka on kerätty kirjallisuudesta.

Neljä tutkimusta on tehty kerättyjen väsymistestien joukosta ja erilaisia väsymisikä arvio metodeja on käytetty väsymisiän arviointiin. Tuloksia on tarkasteltu ja niistä keskusteltu oikeiden testien valossa. Tutkimuksissa on katsottu 2mm ja 6mm symmetristä pitkittäisripaa levyssä, 12.7mm epäsymmetristä pitkittäisripaa, 38mm symmetristä pitkittäisripaa vääntökuormituksessa ja 25mm/38mm kuorman kantavaa krusiformi liitosta vääntökuormituksessa. Mallinnus on tehty niin lähelle testi liitosta kuin mahdollista. Väsymisikä arviointi menetit sisältävät hot-spot metodin jossa hot-spot jännitys on laskettu kahta lineaarista ja epälineaarista ekstrapolointia käyttäen sekä paksuuden läpi integrointia käyttäen. Lovijännitys ja murtumismekaniikka metodeja on käytetty krusiformi liitosta laskiessa.

TABLE OF CONTENTS

1	INTRODUCTION.....	1
2	MAIN FACTORS AFFECTING FATIGUE LIFE IN WELDED STRUCTURES.....	2
3	METHODS FOR FATIGUE LIFE PREDICTION IN WELDED STRUCTURES.....	4
3.1	Nominal stress approach.....	4
3.2	Hot-spot stress approach.....	5
3.2.1	Linear surface extrapolation based on thickness - Method 1.....	5
3.2.2	Linear surface extrapolation based on thickness - Method 2.....	5
3.2.3	Quadratic surface extrapolation based on thickness - Method 3.....	5
3.2.4	Through thickness integration at the weld toe – Method 4.....	6
3.3	Effective notch approach.....	7
3.4	Fracture mechanics approach.....	8
4	DATA PROCESSING.....	9
4.1	Least-squares regression.....	10
4.2	Multivariable regression.....	12
5	FINITE ELEMENT ANALYSIS – FOUR CASE STUDIES.....	13
5.1	Finite elements.....	13
5.2	Overview – Four case studies.....	14
6	CASE STUDY I – THIN SYMMETRICAL LONGITUDINAL ATTACHMENT BY GURNEY	14
6.1	Testing procedure.....	15
6.2	Geometry.....	15
6.3	Finite element modeling.....	16
6.4	Boundary conditions and loads.....	17
7	CASE STUDY II – UNSYMMETRICAL LONGITUDINAL ATTACHMENT UNDER TENSILE MODE BY MADDOX.....	19
7.1	Testing procedure.....	19
7.2	Geometry.....	19
7.3	Finite element modeling.....	19
7.4	Boundary conditions and loads.....	20
8	CASE STUDY III – SYMMETRIC LONGITUDINAL ATTACHMENT UNDER BENDING FROM UKOSRP.....	21
8.1	Testing procedure.....	22
8.2	Geometry.....	22
8.3	Finite element modeling – Contact analysis.....	22
8.3.1	Overview – Contact.....	22
8.3.2	Finite element models – Application to welded detail.....	24
8.4	Boundary conditions and loads.....	24

9	CASE STUDY IV – LOAD AND NON-LOAD CARRYING CRUCIFORM JOINTS UNDER FOUR POINT BENDING.....	25
9.1	Testing procedure	25
9.2	Geometry	25
9.3	Finite element modeling	26
9.4	Boundary conditions and loads	30
10	RESULTS.....	30
10.1	Multivariable regression.....	30
10.1.1	Butt joint.....	31
10.1.2	Cruciform joint.....	35
10.1.3	Longitudinal attachment.....	40
10.2	Case study I.....	45
10.3	Case study II	47
10.4	Case study III	48
10.5	Case study IV	48
11	MULTIVARIABLE REGRESSION AGAINST CASE STUDIES.....	50
12	DISCUSSION.....	54
12.1	Multivariable regression.....	54
12.2	Case study I	60
12.3	Case study II	64
12.4	Case study III	68
12.5	Case study IV	68
13	Conclusions.....	70
14	Recommendations.....	72

References
Appendices

Nomenclature

S_{hs}	Estimated structural hot-spot stress
C	Fatigue capacity factor
K_s	Elastic stress concentration factor
FAT	Endurance limit at $2 \cdot 10^6$ cycles
$\frac{da}{dN}$	Fatigue crack growth in mm/cycle
S_{nom}	Nominal stress
ΔK	Stress intensity factor range
M_k	Factor for non-linear portion of total notch stress
$F(a/b)$	Geometric factor – relationship between crack length and thickness
a	Crack length – mm
N	Number of cycles to failure
E	Elastic modulus
ν	Poisson's ratio
CPE8R	8 node plane strain element with reduced integration
CPE8	8 node plane strain element with full integration
CPS8R	8 node plane stress element with reduced integration
CPS8	8 node plane stress element with full integration
CPE4I	4 node incompatible mode element
CPE4	4 node plane strain element with full integration
CPE4R	4 node plane strain element with reduced integration
CPS4	4 node plane stress element with full integration
CPS4R	4 node plane stress element with reduced integration
C_m	Material constant
m	Material constant – slope of S-N curve
ΔS	Stress range - MPa
A_i	Incremental area under dN/da vs. a curve
$\frac{S}{S_{ref}}$	Individual fatigue strength to reference fatigue strength at $2 \cdot 10^6$ cycles
$\frac{t}{t_{ref}}$	Ratio of individual thickness to reference thickness

\mathbf{S}_{notch}	Notch stress based on FAT 225
r^2	Coefficient of determination
r	Loading mode parameter
$R_{b,k}$	Equivalent structural stress parameter
$\mathbf{S}_{k,b}$	Equivalent structural stress due to bending mode
$\mathbf{S}_{k,m}$	Equivalent structural stress due to tensile mode
$[K]$	Stiffness matrix
$\{u\}$	Displacement vector
$\{F\}$	Force vector
C3D8	8 node fully integrated linear hexagonal element
C3D8R	8 node reduced integration linear hexagonal element
C3D8I	8 node incompatible linear hexagonal element
C3D20R	20 node reduced integration quadratic hexagonal element
C3D20	20 node fully integrated quadratic hexagonal element
RSD	Residual standard deviation
UKOSRP	<u>U</u> nited <u>K</u> ingdom <u>O</u> ffshore <u>S</u> teel <u>R</u> esearch <u>P</u> rogram

1 INTRODUCTION

Current fatigue design rules are primarily based on laboratory fatigue testing of various welded details.[21] Based on fatigue tests, welded details are grouped into several classes each having a specific fatigue strength. Results are shown on S-N curve, also known as stress – endurance curve. Generally, the lower bound is chosen for each detail to represent the design curve. However, some peculiarities exist, for example, current fatigue design rules in BS 7608 include so called “thickness effect” beyond 16mm plate thickness. There is a penalty for thicker plate thickness as fatigue strength at least in transverse fillet welded joints is reduced.

Main goal of this project is to investigate the possibility of using multivariable regression in attempt to predict fatigue life of a welded joint. The idea is to derive an equation that would take into account stress range, thickness and loading mode based on collected data for three welded details. As a result, estimated fatigue life could be obtained from single equation given parameters such as stress range, plate thickness and loading mode. Literature search is carried out for butt joints, cruciform joints, and longitudinal attachments.

Relevance of these welded details in practical applications could be as follows. For example, steel sheets in ship structures are butt welded together, reinforcement structure in ship hull is most likely to contain details which follow load or non-load carrying cruciform joint. Longitudinal attachment can be found, for example, in gas tanks as attachment for lifting. Under internal pressure this detail could fit the detail that is investigated in this work, non-load carrying longitudinal attachment.

Finite element analysis has been carried out in the light of four case studies from Gurney, Maddox and UKOSRP, United Kingdom Offshore Steel Research Program. Modeling included thin symmetrical longitudinal attachments tested by Gurney, unsymmetrical longitudinal attachments tested by Maddox and two samples from UKOSRP project, longitudinal attachment and load and non-load carrying cruciform joint. Results from FEA are compared to test results using different fatigue life prediction methods. Methods include linear and quadratic surface extrapolation, through thickness integration, effective notch method and fracture mechanics method. Predicted fatigue lives from multivariable regression equations based on collected data are compared to test results.

However, much more verification, testing and variable consideration is required in order to draw any sound conclusions.

2 MAIN FACTORS AFFECTING FATIGUE LIFE IN WELDED STRUCTURES

Stress range is thought to have the most significance into fatigue life of a welded structure. In a typical fatigue testing set-up slope of the S-N curve is observed to be about three. This means that as stress range is doubled, corresponding fatigue life is reduced by eight times.

$$N = \frac{C}{(\Delta S)^3} \quad (1)$$

Above equation (1) is often used for fatigue life estimation. C is material constant determined by corresponding FAT class of a joint at $2 \cdot 10^6$ cycles. Quite significant and often controversial factor is plate thickness and its significance to fatigue life of a joint. Thickness effect may be explained by three main mechanisms [1] statistical size effect, technological size effect and stress gradient effect. These factors also hold for non-welded materials. *Statistical size effect* refers to the physical dimension of the joint. Probability of finding a defect in a larger joint is greater than in a smaller joint. As a result, it is likely that larger joints would exhibit lower fatigue strength.

Technological size effect refers to difference in manufacturing process. For example, welding residual stresses might be higher in larger and thicker structures.[5]

Stress gradient effect is best illustrated in Figure.1.

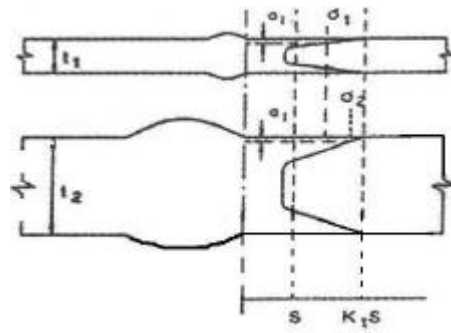


Figure.1. *Stress gradient in a thin plate is shallower than in a thick plate. Fatigue crack grows faster in thick plate as crack propagation reaches deeper.[1]*

Stress gradients are caused by welds and other geometrical discontinuities. Stress gradient in thin plate is shallower than in thick plate.[5] As a result, if same depth crack is present in thin and thick plate, it will grow faster in thick plate because stress gradient reaches deeper. This causes reduction in fatigue strength. Assumption would be that nominal stress is the same in both cases.

Numerous standards describe the thickness effect in welded structures in relation to fatigue strength. In Eurocode 3 the relationship is expressed as follows. [24]

$$\frac{S}{S_{ref}} = \left(\frac{25}{t} \right)^{0.25} \quad (2)$$

where S_{ref} is the fatigue strength for 25mm thickness. Reduction in fatigue strength is taken into account when plate thickness exceeds 25mm. This applies mainly to cases where principal stress acts perpendicular to the weld toe. In BS 7608 thickness effect is expressed as follows.

$$\frac{S}{S_{ref}} = \left(\frac{16}{t} \right)^{0.25} \quad (3)$$

According to British standard reduction in fatigue strength should be considered beyond 16mm. Another standard for steel structures, BSK used in Sweden uses expression as follows.

$$\frac{S}{S_{ref}} = \left(\frac{25}{t} \right)^{0.0763} \quad (4)$$

Here, $S = S_{ref}$ for $t \geq 25mm$. Interestingly, Swedish standard is the only one that takes into account thinness effect.

In the IIW recommendations reduced fatigue strength due to increase in plate thickness is taken into account as follows [22]

$$\frac{S}{S_{ref}} = \left(\frac{25}{t} \right)^n \quad (5)$$

where exponent n takes on different values between 0.1 to 0.3. However, exponent is related to weld profile, weld type and loading mode.

It should be noted that thickness effect based on current standards holds true for fillet welds which are loaded in transverse direction. Gurney [6] found quite different results for complicated longitudinal attachment. Quite well established parameter is loading mode.

In general, bending mode is not as severe as tensile mode as far as fatigue strength of the component is concerned. This is due to linear distribution of bending stress across the thickness being maximum at the surface. Hence, fatigue crack grows toward the region of

lower stress and as a result higher fatigue strength would be expected under bending mode.

Significant parameter for fatigue life is the presence of residual stresses in a welded joint. Welds in real structures are often assumed to exhibit tensile residual stresses up to yield strength. As a result, fatigue life is thought to be independent of the mean stress and depend only on applied stress range.[22] All major fatigue design standards accept this principle. In general, higher residual stress leads to decrease to fatigue life. This brings about a problem of laboratory tested small scale specimens which exhibit lower residual stresses. Currently, no agreed correction factor exists which would bridge the gap between laboratory specimen and real structures which can be ten times as large. Certainly, factors such as environment, loading frequency, welding process, joint specific local and global geometry, amount of weld penetration and material type have effect on fatigue life. However, certain type of joint can be more sensitive to one parameter than other joint or even exhibit opposite behaviour as Gurney [6] found in testing longitudinal attachments under tensile mode. Fatigue strength may not decrease with increasing stressed plate thickness.

3 METHODS FOR FATIGUE LIFE PREDICTION IN WELDED STRUCTURES

3.1 *NOMINAL STRESS APPROACH*

Generally common method for fatigue life assessment is nominal stress method, which is based on the average stress over the section of interest. Most fatigue design curves are based on nominal stress. Definition of nominal stress in real structural details may not be so simple. Due to stress raising details along with complex loading conditions in real structures, definition of nominal stress may be difficult if not impossible to define.[25] In the light of fatigue life assessment for simple geometry, nominal stress method can give useful information. As for more complicated geometry and increased accuracy, more advanced methods have to be considered. Nominal stress method do not take into account stress raising effects due to welded attachments and other structural discontinuities. Hobbacher [24] defines nominal stress as an average stress in area under consideration, calculated by simple and agreed formula, considering global notch effects in the vicinity of the welded joint, but excluding the notch effects of the welded joint geometry itself. Commonly, nominal stress is calculated by basic equations

$$s_{mem} = \frac{F}{A} \quad \text{and} \quad s_{ben} = \frac{Mc}{I} \quad (6)$$

membrane and linearly distributed bending stress, respectively.

3.2 HOT-SPOT STRESS APPROACH

Structural hot-spot stress method estimates stress raising effects in the structure. Structural hot-spot stress consists of membrane stress and shell bending stress caused by the detail, but excludes the non-linear stress peak caused by the local notch at the weld toe. Non-linear portion of the stress is included in the hot-spot S-N curve.[5][25] If nominal S-N curve is used, nominal stress has to multiplied by a relevant stress concentration factor which is calculated from the ratio of hot-spot stress to nominal stress. Figure.2 shows separated stress components.

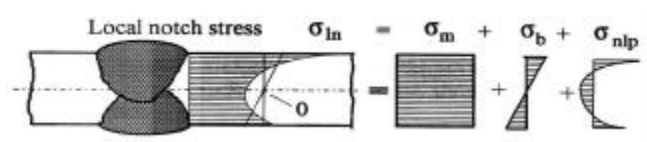


Figure.2. Total stress at the notch consists of membrane stress, bending stress and non-linear stress peak in the vicinity of the notch. Structural stress excludes non-linear portion of the stress.

Hot-spot stress is only applicable to weld toe failure where fatigue cracking might be expected. Weld root failures cannot be assessed with hot-spot method [27]. This rises from the following. Membrane and bending stress after the weld toe collapses in magnitude, due to stiffening in the weld and attachment region. As a result, stress will be lower due to linear elastic material. See Figure.3 for surface extrapolation method and reason for hot-spot failure from weld root.

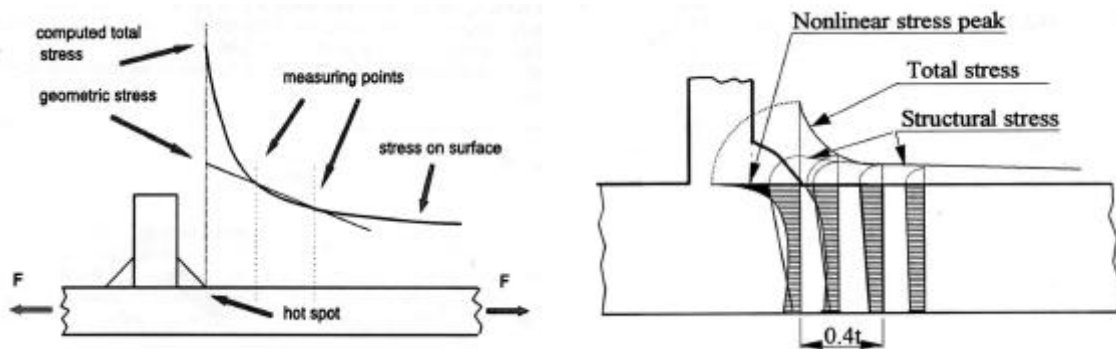


Figure.3. Hot-spot stress is estimated from extrapolation points on surface in front of the weld toe.

3.2.1 Linear extrapolation based on thickness – Method 1

Linear extrapolation method is based on principal stresses from two nodes on the surface at $0.4t$ and t from weld toe, where t is the thickness of stressed plate [4]. Estimated structural hot-spot stress based on linear extrapolation is calculated according to equation

$$\mathbf{s}_{hs} = 1.67\mathbf{s}(0.4t) - 0.67\mathbf{s}(t) \quad (7)$$

Method does not take into account global geometry of the joint. It does take into account for the thickness of the plate.

3.2.2 Linear extrapolation based on thickness – Method 2

Two extrapolation points at distances $0.5t$ and $1.5t$ in front of the weld toe are considered in this method based on thickness [8]. Thickness effect is counted in this method as well. Estimated structural hot-spot stress is calculated according to equation

$$\mathbf{s}_{hs} = 1.5\mathbf{s}(0.5t) - 0.5\mathbf{s}(1.5t) \quad (8)$$

Method is generally recommended in coarser meshes where element length at the weld toe region is equal to the plate thickness. Generally, this method is used in ship building industry.

3.2.3 Quadratic extrapolation based on thickness – Method 3

Three extrapolation points based on stressed plate thickness at $0.4t$, $0.9t$ and $1.4t$ are considered in estimation of structural hot-spot stress at the weld toe [4]. Hot-spot stress is computed according to relationship

$$\mathbf{s}_{hs} = 2.52\mathbf{s}(0.4t) - 2.24\mathbf{s}(0.9t) + 0.72\mathbf{s}(1.4t) \quad (9)$$

Quadratic extrapolation is preferred over linear extrapolation in cases where principal stress increases non-linearly in front of the weld toe. It is assumed that non-linear portion of the stress disappears $0.4t$ from the weld toe. In case of thicker plates non-linear portion of the stress may extend further than $0.4t$ from the weld toe. In such cases, linear extrapolation might underestimate actual hot-spot stress, thus quadratic extrapolation could be used [5]. Other global geometry can also influence the extent of non-linear portion of the stress at the vicinity of the weld toe. Cover plates on beams is one example, where quadratic extrapolation is found to yield better fatigue life estimates over linear extrapolation.

3.2.4 Through thickness integration at the weld toe – Method 4

Through thickness integration at the weld toe takes better into account global and local geometry of the joint. Estimated hot-spot stress is composed of membrane and bending stress.

$$\mathbf{s}_{hs} = \mathbf{s}_{mem} + \mathbf{s}_{ben} \quad (10)$$

$$\mathbf{s}_{mem} = \frac{1}{t} \cdot \int_{x=0}^{x=t} \mathbf{s}(x) \cdot dx \quad (11)$$

$$\mathbf{s}_{ben} = \frac{6}{t^2} \cdot \int_{x=0}^{x=t} \mathbf{s}(x) \cdot \left(\frac{t}{2} - x\right) \cdot dx \quad (12)$$

Structural stress is calculated using (10) that consist of membrane and bending stress, (11) and (12), respectively. [4, 11] Structural stress is obtained through thickness at the weld toe. For finite element applications, results must be processed carefully. Weld toe elements as well as elements directly under the weld toe are deselected in the post-processing phase in order to avoid averaging error due to surrounding elements. Structural stress is obtained through stress linearization in the post-processing phase that separates membrane and bending portions of the total stress which includes the non-linear portion.

3.3 EFFECTIVE NOTCH APPROACH

One of the current procedures for predicting fatigue life of a welded joint is effective notch approach. [24] Considering scatter in actual weld shape and potential non-linear material behavior at the notch, real weld toe is replaced by effective notch. This method is suitable for weld toe and weld root failure investigation where fatigue crack initiation is expected. Method takes better into account the local weld toe geometry. Method is not suitable where significant stress components act parallel to the weld. In these cases nominal stress method would work. This applies to weld toe and weld root side.

Currently, method is restricted to wall thickness greater than 5mm.[24]

In general, fatigue strength tends to increase as weld toe radius is increased as shown in Figure.4. This is due to less severe stress concentration at the notch. Other geometry as well as loading mode has to be considered.

Applying effective notch method reduction in fatigue strength due to plate thickness over 25mm is not taken into account as recommended in Eurocode 3. Generally, maximum

principal stress at the weld toe region transverse to the weld is chosen for fatigue life assessment. Stress concentration factor is computed from maximum principal stress at the notch and nominal stress. Fatigue life estimate is obtained from

$$N = \frac{C}{\mathbf{s}_{notch}^m} \quad (13)$$

where C and m are material constants and \mathbf{s}_{notch} is notch stress, maximum principal stress occurring at the notch. Material constant C is calculated based on FAT 225. [17]

This method has been applied to one of the case studies. Cruciform joint under four point bending from UKOSRP project was studied by using this method. Plate thickness was 38mm with same attachment thickness. Effective notch was modelled with 1mm radius at the weld toe. Effective notch at the weld toe was modelled by smooth transition.

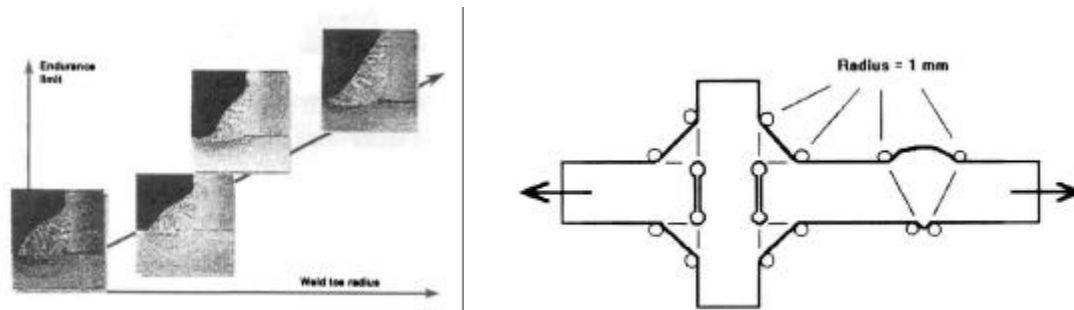


Figure.4. *General effect of weld toe radius to fatigue life and general modeling procedure.*

3.4 FRACTURE MECHANICS APPROACH

Stress intensity factor describes the severity of the crack that depends on applied stress, geometry, and crack length. ABAQUS calculates stress intensity factors based on contour integral method, J-integral. Relationship between Mode I stress intensity factor and J is given as follows [3][13],

$$K_I = \sqrt{\frac{JE}{(1-\mathbf{u}^2)}} \quad (14)$$

Stress analysis is used to determine stress intensity factor range as crack propagates through the plate thickness. This method has been applied to one of the case studies. First, simple plate with edge crack with analytical stress intensity factor solution available was analyzed using ABAQUS before moving into modeling one of the case studies. Plate was 40mm wide and 70mm long with 4mm edge crack in the center. Crack tip in the plate under pure tensile loading was modeled using two different approaches. First, 8-node

plane strain elements were used. Crack tip was located at the corner of the elements.[7]
Refer to Figure.5 for two proposed modeling techniques. [13]

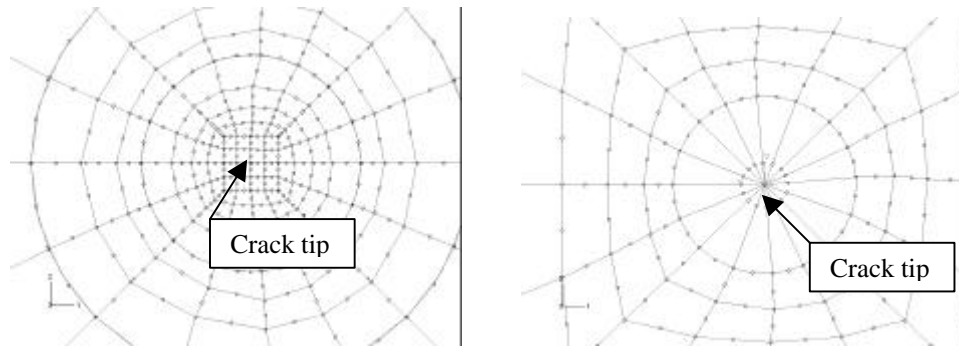


Figure.5. Crack tip modeled using 8-node plane strain quadratic elements, tip located at corner point of elements. Nodes surrounding crack tip are at mid-points and quarter points. Tip element size is 0.01mm in both techniques.

Second, 8-node plane strain collapsed quadratic elements were used with quarter point nodes to introduce $1/\sqrt{r}$ singularity as proposed for linear elastic analysis.[3] Elements were created by modifying input file such that nodes on one side of circumferential elements were assigned crack tip coordinates. Inner nodes were moved to quarter points by assigning cylindrical coordinate system at the crack tip and modifying radial coordinate. Crack tip nodes were constrained together using TIE - command. Stress intensity factor results based on these two modeling techniques are compared with analytical solution.

4 DATA PROCESSING

Literature search was made for three types of welded details under tensile and bending mode. Collected data was S-N data. In all cases, nominal stress versus life was recorded in the database. Measured hot-spot stresses were recorded in cases where they were reported. Welded details included butt joints, cruciform joints and longitudinal attachments. Collected joint types included various global and local geometry. Collected data was broken down in terms of stressed plate thickness and loading mode. Least-squares regression was performed for all joint details based on stressed plate thickness. Various curve fitting techniques were performed to establish relationship between fatigue strength and main plate thickness under tensile and bending mode. Established relationships regarding thickness and fatigue strength based on collected data are compared and discussed with current standards. Multivariable regression was

performed for the three joint types considering stress range, plate thickness and loading mode. Multivariable regression results for fatigue life prediction are compared and discussed with samples from tests and with four finite element case studies.

Goal of first part of the work was to establish relationship between fatigue strength and plate thickness as well as loading mode. General observations from literature search were, fatigue strength under tensile mode was lower than under bending mode. Fatigue test results for bending mode are more limited than for tensile mode. One logical reason might be that based on tensile test results it was concluded that same component under bending mode will be safe. Most data was collected for butt joints. Data set consists of 1556 test results from 50 references. Cruciform joints contain 1189 test results from 29 references. Least amount of data was collected for longitudinal attachment. Data set consists of 456 test results from 11 references.

4.1 Least-squares regression

All fatigue data was analyzed using least-squares regression. Each joint type was treated separately. Each joint type was divided into groups based on stressed plate thickness and loading mode. Coefficients of linear equation were computed as follows. [10]

$$m = \frac{n \sum \log \Delta \mathbf{s}_i \log N_i - \sum \log \Delta \mathbf{s}_i \sum \log N_i}{n \sum \log \Delta \mathbf{s}^2 - (\sum \log \Delta \mathbf{s}_i)^2} \quad (15)$$

$$\log C = \frac{\sum \log N_i}{n} - m \frac{\sum \log \Delta \mathbf{s}_i}{n} \quad (16)$$

where n is the number of data points, $\log \Delta \mathbf{s}_i$ is the stress range and $\log N_i$ is number cycles to failure. Linear equation from S-N curve can be expressed as follows

$$C = N \Delta \mathbf{s}^m \quad (17)$$

S-N relationship (17) was linearized by taking logarithm from both sides which leads to

$$\log C = \log N + m \log \Delta \mathbf{s} \quad (18)$$

and by rearranging

$$\log N = m \log \Delta \mathbf{s} - \log C \quad (19)$$

Stress range and number of cycles to failure were modified by taking logarithm of the variables. Standard deviation based on individual observations was computed as follows

$$S_t = \sum (\log N_i - \log N_{avg.})^2 \quad (20)$$

and standard deviation based on coefficients was expressed by

$$S_r = \sum (\log N_i - \log C - m \log \Delta \mathbf{s}_i)^2 \quad (21)$$

Coefficient of determination or percent fit was computed based on standard deviation of the individual observations and standard deviation based on mean regression line representing data point as

$$PercentFit = \frac{S_t - S_r}{S_t} \quad (22)$$

Based on each regression line fatigue strength at $2 \cdot 10^6$ cycles was computed for each thickness and loading mode. As a result, a series of curves were obtained representing thickness effect as well as loading effect. Relevant plate thickness and loading curves for each joint type were graphed on $\log \Delta \mathbf{s}$ versus $\log N$ curve.

Based on regression lines, reasonable reference thickness was chosen from available plate thicknesses. Based on reference thickness, ratio of actual plate thickness to reference thickness was calculated. Fatigue strength at $2 \cdot 10^6$ cycles was compared with reference fatigue strength that corresponded reference thickness.

Fatigue strength ratio versus thickness ratio were graphed in attempt to establish relationship between fatigue strength and thickness under tensile and bending modes as follows.

$$y(\mathbf{s}) = \frac{\mathbf{s}}{\mathbf{s}_{ref}} \quad x(t) = \frac{t}{t_{ref}} \quad (23)$$

Based on observations, linear and non-linear curve fitting techniques were applied in attempt to derive a function that describes relationship between thickness and fatigue strength under tensile and bending mode for all three joint types. Based on limited amount of available data for bending, relationship was not clear in all cases.

Based on fatigue data collection in this study, several curve fits were examined to see which one best represents the data. Power law fit can be represented as follows

$$\mathbf{s}(t) = a_1 \cdot f(t)^{a_2} \quad (24)$$

After linearization coefficients become easy to solve as follows

$$\log \mathbf{s}(t) = \log a_1 + a_2 \log f(t) \quad (25)$$

Other non-linear curve fitting techniques included exponential fit, saturation fit, and natural logarithm fit.

$$\mathbf{s}(t) = a_1 \cdot e^{a_2 f(t)} \quad (26)$$

which after linearization leads to, however, $\ln e$ becomes 1 that simplifies expression.

$$\ln \mathbf{s}(t) = \ln a_1 + a_2 f(t) \ln e \quad (27)$$

Other model is saturation fit as follows

$$\mathbf{s}(t) = a_1 \cdot \frac{f(t)}{a_2 + f(t)} \quad (28)$$

Linearization is applied as follows

$$\frac{1}{\mathbf{s}(t)} = \frac{a_2}{a_1} \frac{1}{f(t)} + \frac{1}{a_1} \quad (29)$$

Natural logarithm fit is already in correct form for linear regression as

$$\mathbf{s}(t) = a_1 \ln(f(t)) + a_2 \quad (30)$$

As various fits, that in general represented the data, were graphed corresponding coefficient of determination or percent fit was computed. Coefficient of determination (r^2) of 1 represents perfect fit. Coefficient of determination (r^2) represents how many percent of the original scatter has been explained by the curve.

4.2 Multivariable regression

Multivariable regression was considered for all three joints. First, two variables were considered, stress range and plate thickness. It was assumed that power relationship exists between these variables according to general expression. This was done partly because standards suggest power model in thickness and also results from thickness relationship to fatigue strength based on data collection are the same.

As a result, thickness variation in relation to fatigue life in all joints followed closest to power or exponential curves, however, power relationship was assumed in all cases.

$$N = f(\Delta \mathbf{s})^{m_1} f(t)^{m_2} c \quad (31)$$

By taking logarithm of both sides of the equation leads to linear relationship

$$\log N = m_1 \log f(\Delta \mathbf{s}) + m_2 \log f(t) + \log c \quad (32)$$

where $f(\Delta \mathbf{s})$ corresponds to stress range, $f(t)$ to thickness of the main plate and c is the constant. By taking partial derivatives with respect to each one of the variables and rearranging equations into matrix form, coefficients can be solved. This leads to solving 3x 3 matrix with 3 unknown coefficients as follows. [28]

$$\begin{bmatrix} n & \sum \log \Delta \mathbf{s}_i & \sum \log t_i & \Lambda \\ \sum \log \Delta \mathbf{s}_i & \sum \log \Delta \mathbf{s}_i^2 & \sum \log \Delta \mathbf{s}_i \log t_i & \Lambda \\ \sum \log t_i & \sum \log \Delta \mathbf{s}_i \log t_i & \sum \log t_i^2 & \Lambda \\ M & M & M & O \end{bmatrix} \cdot \begin{bmatrix} \log c \\ m_1 \\ m_2 \\ M \end{bmatrix} = \begin{bmatrix} \sum \log N_i \\ \sum \log N_i \cdot \Delta \mathbf{s}_i \\ \sum \log N_i \cdot t_i \\ M \end{bmatrix}$$

This can be extended to n variables and solving n+1 x n+1 matrix, where n is the number of variables. Number of solved coefficients is therefore n+1.[29]

Loading mode parameter in this work is defined as [31]

$$r = \frac{\mathbf{s}_{ben}}{\mathbf{s}_{ben} + \mathbf{s}_{tens}} \quad (33)$$

As a result, for pure bending r is one. For pure tension r is then zero.

Dong [30] has used same parameter in the context for calculating equivalent structural stress for fatigue life estimation. Dong's parameter was defined as follows

$$R_{b,k} = \frac{\mathbf{s}_{k,b}}{\mathbf{s}_{k,m} + \mathbf{s}_{k,b}} \quad (34)$$

However, loading mode parameter used in multivariable regression analysis is in different context than in Dong's work.

5 FINITE ELEMENT ANALYSIS – FOUR CASE STUDIES

5.1 Finite elements

In the context of welded joint modeling element types explored were reduced and fully integrated elements. The term “full / reduced integration” refers to the number of Gauss points required to integrate the element stiffness matrix.

Legitimate question is when to use full integration and reduced integration element. As bending mode is simulated in quite a few cases, reduced versus full integration element plays an important part.

Linear fully integrated elements under predict displacements under bending mode, they tend to be too stiff. As a result, due to linear elastic material, stress will be reduced by same amount as displacement. This can give non-conservative results for fatigue life estimation.

Two dimensional modeling in cruciform joint was done with various plane stress and plane strain elements. Of course, none of the results from FEA cannot be compared to any true value. On the basis of element behavior from FEA theory choice was made which element results were used in fatigue life calculations. Linear fully integrated elements tend to be too stiff under bending because edges are unable to curve and as a result strain energy flows into axial shear deformation versus intended bending. This is referred to as shear locking in FEA terminology. In contrast, linear reduced integration elements tend to be too flexible in bending. Element is unable resist bending deformation due to a single Gauss point in the center of the element. In FEA terms this is called as hour glassing.

Longitudinal attachment was modeled with 3 types of shell elements. Modeling was also done in 3D due to double stress gradient that is present in the longitudinal attachment, through thickness and transverse to the loading direction. Two dimensional model does not accurately represent double stress gradient. Solid modeling was investigated with 5 different elements, linear and quadratic.

5.2 Overview – Four case studies

Four case studies were carried out for symmetrical and unsymmetrical longitudinal attachment and load- and non-load carrying cruciform joint primarily under bending mode. Hot-spot stress method was applied in longitudinal attachments. Hot-spot stress was obtained through linear surface extrapolation and through thickness integration at the weld toe. In addition, effective notch method and fracture mechanics method were applied to cruciform joint. Steel is assumed in all case studies. Material property is linear elastic. See Table.1 for material properties.

Table.1. *Material property used in FE - modeling.*

MATERIAL	E (MPa)	ν
STEEL	210 000	0.30

6 CASE STUDY I – THIN LONGITUDINAL ATTACHMENT BY GURNEY

Gurney [14] carried out experiments for symmetrical longitudinal attachments in thin steel plates. These experiments investigated fatigue strength of joint detail as thickness of main plate decreased to and below 6mm. Results were similar to those found by earlier investigators Castiglioni & Bremen and Castiglioni & Gianola [15] and [16], respectively. Major findings were as follows 1) fatigue strength in longitudinal attachments tends to decrease as plate thickness decreases given other geometry stays constant 2) as main plate width decreases fatigue strength increases but becomes small as width is less than 130mm 3) fatigue strength

increases with decreasing attachment length. Based on Gurney's experiments FAT 67 was established for 6mm plates and FAT 75 for 2mm plates. These were the fatigue strengths of the joints at $2 \cdot 10^6$ cycles.

One of the reasons for the experimental work was to establish fatigue strength for this joint type as thickness of stressed plate falls below cut-off thickness ranging from 16mm to 25mm depending on standard. Part of the project was to investigate whether fatigue strength increases as plate thickness decreases in longitudinal attachment. This is important because, for example, automotive industry has to rely on fatigue tests based on 16mm to 25mm thickness range for the lack of better data even though plate thickness used could be five to six times as thin[14]. As more fatigue data for thin plates become available this trend is due to change.

In the light of structural hot-spot stress approach a finite element study was carried out in longitudinal attachments having thin stressed plate thickness. Gurney experiments were used to validate finite element results. All specimens were tested under tensile mode. All failures in the test program occurred at the weld toe, so structural hot-spot stress should be feasible.

Geometry was taken from [14]. Reference contained specimen geometry along with actual fatigue lives. Finite element study was done to investigate applicability of hot-spot stress approach to predict fatigue life in thin longitudinal attachments.

6.1 TESTING PROCEDURE

Specimen were subjected to tensile load under constant amplitude conditions. Stress ratio, R was zero. Testing frequency range was from 5 to 10 Hz. Only as welded specimens are considered to limit the influence of additional variables such as, post weld treatment procedures. Specimen were tested in air conditions.

6.2 GEOMETRY

Geometry is from Gurney's experiments. Thin longitudinal attachment is just one of the geometry used. Tested specimen consisted of 2mm and 6mm thick plates. Attachment thickness in all cases was same as main plate thickness. Weld profile in 6mm plate was as follows. On average, weld leg length along main plate was 8mm and along attachment 6mm. In 2mm plate weld leg lengths were as follows. Leg length along main plate was 6mm and along the attachment 4mm. These were reported by Gurney. See the Figure.6. for geometry.

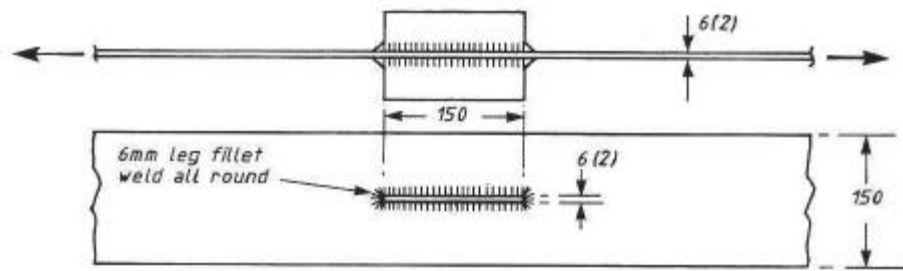


Figure.6. *Geometry for Gurney's tested specimens. Dimensions given as mm. [14]*

6.3 FINITE ELEMENT MODELING

Modeling was made with 4 and 8-node shell elements, also 8 and 20-node solid elements. Shell modeling was made in two ways. Fricke [8] suggests using shell elements without weld modeling with inclined shell elements. Another, approach included weld modeling by using inclined shell elements. Attachment tip was modeled by sweeping shell elements 180°. Obviously, weld toe modeling with shell elements is an approximation as to how represent the stiffness caused by welds as close to real as possible. General guidelines from Fricke [8] were followed.

Shell elements were created in the mid-planes of loaded plate and attachment. This is not a true representation of the joint as shell property definitions overlap in main-plate and attachment intersection. More approximation is created by adding inclined shell elements to represent the welds. Shell element properties overlap even more. Another issue is how to represent weld stiffness using shell elements. For all practical purposes, shell property for welds was defined as weld throat thickness. Welds represented by inclined shell elements in shell model were modeled at 45°.

In addition, same specimens 6mm and 2mm were subjected to four point bending. No test data was available to validate these results, however, results were used and compared to multivariable regression analysis made for longitudinal attachments. Principal stress distributions approaching the weld toe were compared to specimens loaded in tension. This was done for two reasons: 1) to see the effect of element choice and 2) to see how principal stress distribution changes in the vicinity of the weld toe. Are there any correlation between multivariable results and actual test results?

Failure criteria under tensile tests was taken when specimen broke into two pieces. Under bending mode failure criteria was defined as loss of load carrying capacity, it is reported by Gurney that this was about half of the width of the specimen. Clearly, definition of failure criteria adds approximation into the analysis.

6.4 BOUNDARY CONDITIONS AND LOADS

One quarter of the model was built with shell elements. Symmetry boundary conditions were applied to two symmetry planes. One translational and two rotational degrees of freedom were constrained in each symmetry plane. In addition, transverse rigid body motion was constrained in one corner of the joint. Joint detail was given a shell edge load such that nominal stress away from the weld toe was 10 MPa. In 6mm plate this shell edge load was 30 N/mm, this corresponds 10 MPa nominal stress away from the attachment. Load was computed as follows.

$$s = \frac{F}{A} \rightarrow F = s \cdot A = 10MPa \cdot (150mm)(3mm) = 4500N$$

so load per unit length for 6mm thickness becomes

$$F\left(\frac{N}{mm}\right) = \frac{4500N}{150mm} = 30\frac{N}{mm}$$

In 2 mm plate thickness equivalent shell edge load was calculated as $10 \frac{N}{mm}$. Shell model without welds was partitioned at $0.4t$ and t in front of attachment and main plate intersection to enable linear surface extrapolation. Same partitioning was made to shell model with welds. Extrapolation points $0.4t$ and t were chosen from intersection of main plate and inclined shell element. Refer to Figures.7 and 8.

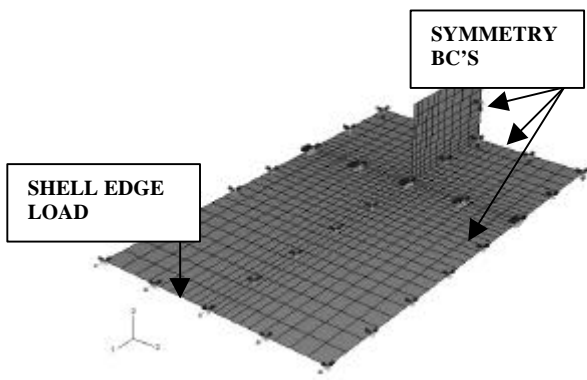


Figure.7. Shell modeling without weld representation.

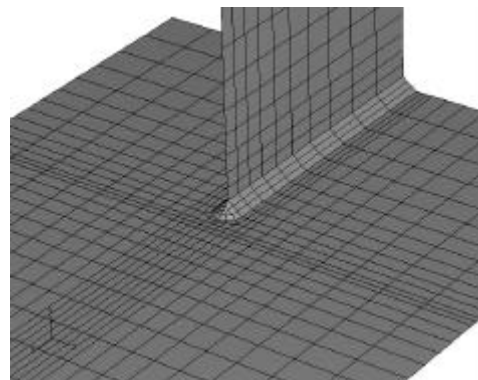


Figure.8. Shell model with inclined shell elements.

Solid modeling of the same detail was made with welds represented. Solid model was subjected to same tensile loading. Evenly distributed pressure load of 10 MPa was applied to

the edge of the attachment. Boundary conditions are same as in shell model with exception of rotational degrees of freedom which do not exist in solid elements. Refer to Figures.9 and 10.

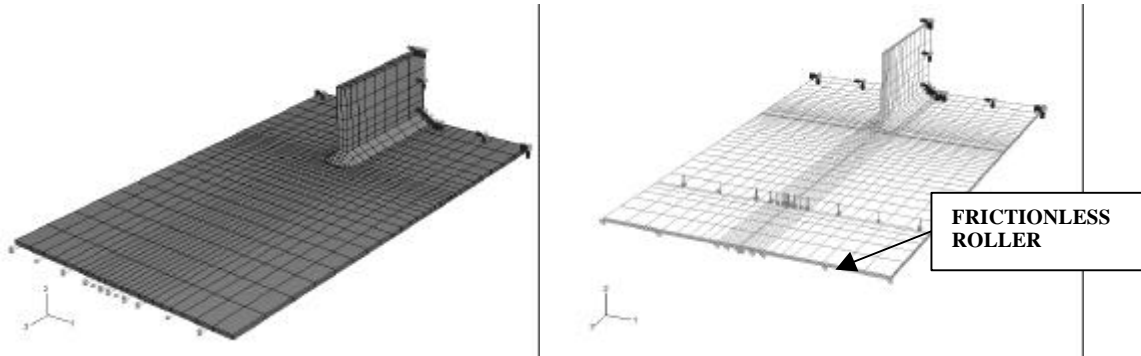


Figure.9. Solid model under tensile mode.

Figure.10. Solid model under bending mode.

Both, 6mm and 2mm joints in solid modeling were also subjected to four point bending. One half of the joint was modeled with solid elements. Symmetry boundary condition was applied to the middle of the joint. One translational degree of freedom was constrained in the symmetry plane. Rigid body motion in transverse direction was constrained in one corner of the symmetry plane. Due to the nature of four point bending test the other end of the joint detail was idealized as resting on frictionless roller. Two translational degrees of freedom were constrained at this location. Obviously, this is a contact problem with friction for elastic support and loading point. This was one of the assumptions.

Pressure load was applied along the width of the plate for 2mm area strip. Loading center lied 50mm from the end of the detail. Pressure was adjusted such as to cause extreme fiber stress caused by bending to be 10 MPa. Applied loading was far enough from the attachment end to cause evenly distributed fiber stress as approaching the weld toe. No membrane stress was developed due to axial translation being free. Transverse pressure for 6mm thick plate was calculated as follows

$$s_{ben} = \frac{6FL}{bh^2} = \frac{6F(50mm)}{(150mm)(6mm)^2}$$

where $s_{ben} = 10MPa$ and F becomes 180 N. Force is distributed over 2mm strip of area and therefore

$$s_{trans} = \frac{F}{A} = \frac{180N}{(2mm)(150mm)} = 0.6MPa$$

For 2mm thick plate transverse pressure load was computed as 0.0666 MPa.

7 CASE STUDY II: UNSYMMETRICAL LONGITUDINAL ATTACHMENT UNDER TENSILE MODE BY MADDOX

Maddox tested unsymmetrical longitudinal stiffeners under tensile mode. Analysis has been carried out to predict fatigue lives of corresponding geometry using linear surface extrapolation and through thickness integration at the weld toe. Fatigue life prediction methods are compared to test results by Maddox. Results from multivariable regression are compared and discussed with test results.

7.1 TESTING PROCEDURE

Fatigue testing were carried under different stress ratios and various type of stress-relief methods. Tested specimens were subjected to tensile loading. However, comparison from FEA results have been made to tested specimens with $R = 0$ and “as-welded” condition. Maddox reported cycles to through plate cracking and cycles to failure. Failure criteria here is chosen as complete failure of the specimen.

7.2 GEOMETRY

Unsymmetrical longitudinal attachment used in fatigue testing is shown in Figure.11.[18]

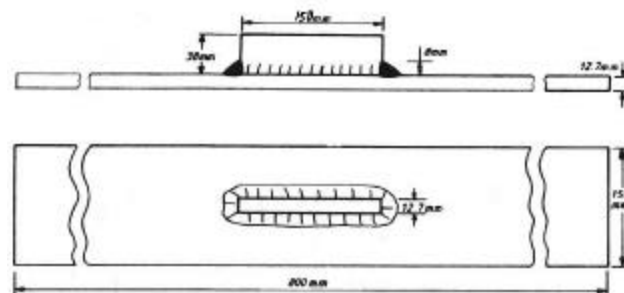


Figure.11. *Geometry for Maddox's experiments.*

7.3 FINITE ELEMENT MODELING

Longitudinal stiffener was investigated with finite elements using shell and solid modeling techniques. One half of the shell model was built in similar fashion as in case study I. Stressed plate shell property was given as full thickness of the main plate. Attachment property was given as full plate thickness. Element type was varied in shell and solid model. Results were obtained with coarse and fine mesh. Element size in coarse shell mesh was ~5mm and in fine mesh ~2.5mm, in the solid model ~2.5mm and ~1.5mm, respectively. Solid modeling enabled additional through thickness integration at the weld toe to estimate structural hot-spot stress.

7.4 BOUNDARY CONDITIONS AND LOADS

Care is needed to apply boundary conditions correctly in the case of unsymmetrical longitudinal attachment. Boundary conditions were set up as in testing conditions. Due to one sided attachment, a secondary bending stress is introduced in the attachment region because attachment side is stiffer. This causes welded detail to curve in the attachment region such that attachment side forms into concave shape. Relevant boundary conditions are shown in Figures. 12 and 13.

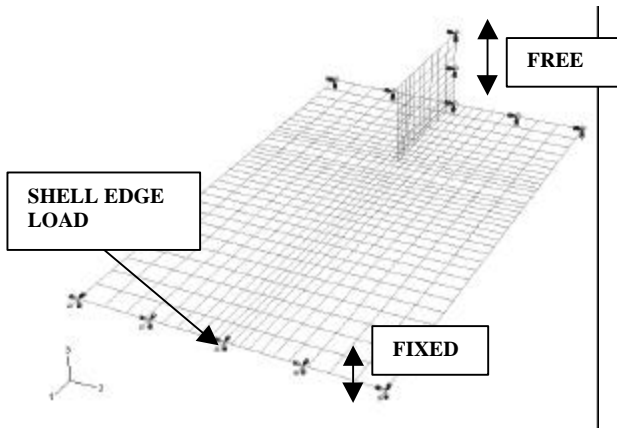


Figure.12. *Shell model of unsymmetrical longitudinal attachment.*

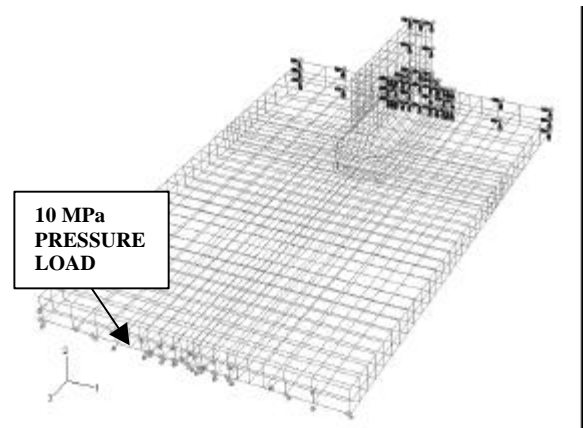


Figure.13. *Solid model of unsymmetrical longitudinal attachment.*

Evenly distributed shell edge load was applied to the end to cause nominal stress of 10 MPa. Equivalent shell edge load was calculated as $127 \frac{N}{mm}$. In the case of solid model, 10 MPa pressure load was applied to the end surface. Resulting deformation plots are shown in Figure.14.

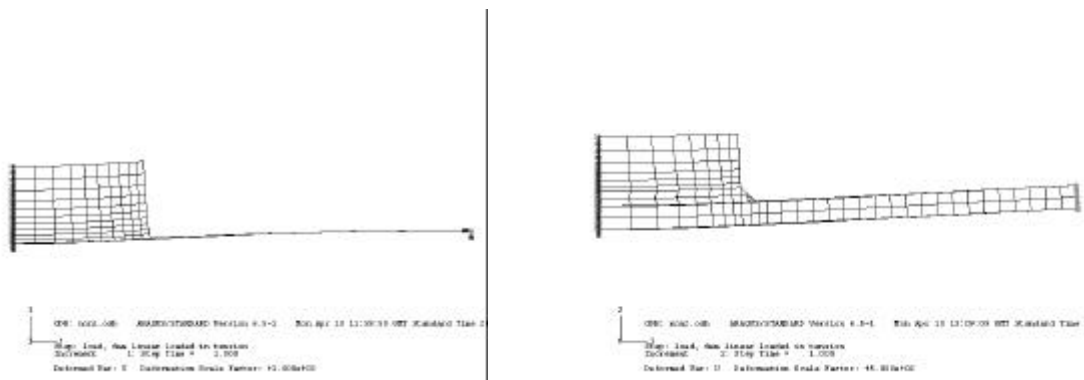


Figure.14. *Deformation plots for shell and solid model in the case of unsymmetrical longitudinal attachment.*

Fatigue strength for the detail was chosen as FAT 90 based on UKOSRP project where symmetrical 25mm thick longitudinal attachments were tested under tensile mode. Material constant C was calculated based on FAT 90 at $2 \cdot 10^6$ cycles and $m = 3$.

$$C = 1.458 \cdot 10^{12} \text{ cycles} \cdot (\text{MPa})^m \quad m = 3$$

Fatigue strength of unsymmetrical detail might be higher due to secondary bending stress in the toe region. However, as reported by Gurney, fatigue strength tends to decrease with decreasing plate thickness in longitudinal attachment. As a result, secondary bending stress may have increasing effect in fatigue strength and tendency of fatigue strength to decrease with decreasing plate thickness might counteract each other, so no adjustment for fatigue class was made in this case study.

Tested shell elements included S8R, so called thick shell element. This is 8-node shell element with reduced integration. It has six degrees of freedom per node. These elements allow transverse shear deformation. Two other types of shell elements included S4R and S4, linear reduced and full integration shell elements.

Elastic stress concentration factor was computed from finite element models as follows.

$$K_s = \frac{\mathbf{s}_{hs}}{\mathbf{s}_{nom}} \quad (35)$$

Hot-spot stress at the weld toe was obtained through linear surface extrapolation in shell models and through thickness integration at the weld toe in solid models as well as linear surface extrapolation.

Clearly, value of stress concentration factor depends on element type used as well as method. Element type chosen in shell model was 8-node shell element with reduced integration. It should work well under tensile load. Element type in solid model was 20-node brick element with reduced integration. Stress concentration factors were calculated based on these elements.

8 CASE STUDY III – UKOSRP 38mm SYMMETRIC LONGITUDINAL ATTACHMENT UNDER FOUR POINT BENDING

Thick 38mm plate from UKOSRP project was studied under four point bending. Fatigue life prediction methods are linear and quadratic extrapolation and through thickness integration at the weld toe. Modeling was carried out in two different ways, idealized and 3D contact.

Contact modeling was made due to true nature of the actual test.

8.1 TESTING PROCEDURE

Only “as-welded” specimens tested in air are considered in this case study. Testing was carried out with frequency of about 3 Hz. Stress ratio was zero. In practice, test was carried out with slight positive stress ratio to prevent movement of the joint in between the support points.

8.2 GEOMETRY

Attachment thickness was 13mm and weld leg length 10mm with full penetration. Width of the stressed plate is 125mm. Test specimen is shown in Figure.15.

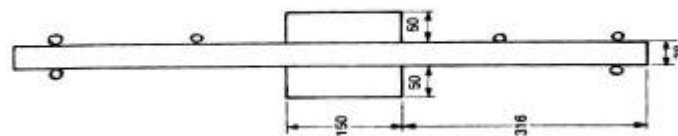


Fig.15. Longitudinal attachment from UKOSRP project loaded in four point bending. Dimensions given in (mm).

8.3 FINITE ELEMENT MODELING – CONTACT ANALYSIS

In the modeling procedure a series of assumptions are often made. Often, these assumptions are reasonable as far as structural integrity of the component is concerned. In the light of assumptions, more rigorous approach was taken to analyze longitudinal attachment under four point bending. Joint was modelled with 3D contact and more idealized evenly distributed pressure load over an area. Aim of the contact modeling was to simulate the relative motion between the loading point and joint detail. In the real world, four point fatigue bending test is a contact problem with friction. Bending test was simulated with frictionless contact. FEA stress results were used to calculate estimated fatigue life and are compared to test results along with preliminary multivariable regression results.

8.3.1 OVERVIEW - CONTACT

A contact problem is a non-linear problem even if linear elastic material behavior is assumed. Search algorithm must be present as contact is the driving force for deformation.[19] As in numerous engineering problems, linear approximation cannot be used in contact problem.

$$[K]\{u\} = \{F\} \quad (36)$$

where

$[K]$ is the stiffness matrix, $\{u\}$ is the displacement vector and $\{F\}$ is the force vector. In linear problems, as shown in (12), displacements are directly proportional to the load. If load doubles so does displacement. Also, stiffness of the structure is independent of the load in linear problem. However, in contact problem stiffness of the structure is dependent of the load. Non-linear problem uses incremental and iterative solution procedure. Main points are as follows. Refer to Fig.16 for outline of the procedure and main points that follow.

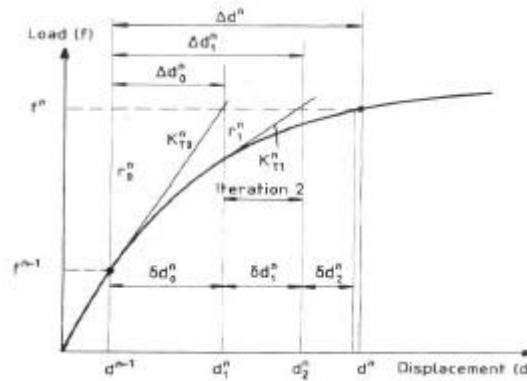


Fig.16. *Standard Newton's method for solving a non-linear problem.*

First, direct sparse solver, in ABAQUS direct linear equation solver is used which uses Gauss elimination procedure. A set of linear equations is solved at each iteration.

ABAQUS uses Newton's method for solving non-linear problems. Total load, F , is divided into load increments, F_n . ABAQUS uses structure's tangential stiffness matrix which is based on displacement where non-linearity starts and load increment to calculate displacement correction for the structure. Using displacement correction, structure's internal forces are calculated. Same process is repeated, for new tangential stiffness matrix is calculated from remaining load in the increment. Iterations within time increment are repeated until tolerance value is reached. This was 0.5%. ABAQUS also checks displacement correction from previous iteration. This tolerance was 1%. These were default values. Automatic incrementation control was used.

Stiffness of the assembly is dependent of the contact state, that is, how much bodies are touching each other. In addition, on contact surface friction will be present which is dependent on the normal force across the interface. Material and geometric non-linearity will add complexity into the analysis.

Structural stress obtained through contact analysis and more simplified analysis are compared.

8.3.2 FINITE ELEMENT MODELS - APPLICATION TO WELDED DETAIL

One quarter of the joint detail was modeled in both cases. Four point bending was simulated through two rigid cylindrical surfaces and uniform pressure load over an area. Refer to Figure.17 for two FE - modeling techniques.

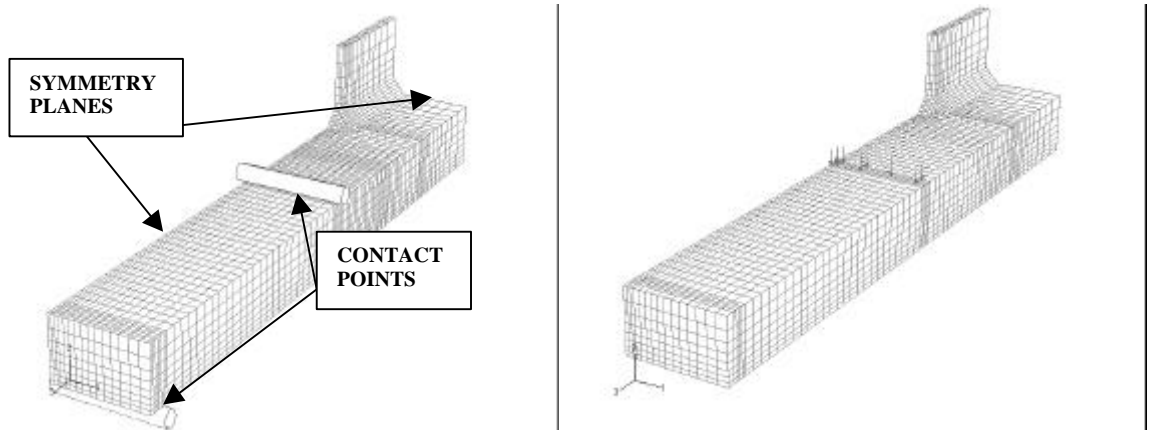


Fig.17. Four point bending modeled with contact and uniform pressure over an area.

First, contact was modeled as a surface based contact between a rigid and deformable body. A contact pair was defined between a rigid surface and surface of the deformable body. Rigid surface was defined as a master surface and deformable body surface was the slave surface. Normal behavior at the contact surface was defined as hard contact. This means that rigid surface does not penetrate slave surface as the load is applied. Tangential behavior was defined as frictionless. This means that no shear stresses develop between the rigid surface and deformable body as load is applied. ABAQUS has two options for sliding formulation - *finite sliding* and *small sliding*. As a rule of thumb, if the relative motion in between surfaces is less than an element length at the contact point then small sliding is valid. However, relative motion between contact points in actual test can be significant depending on stress range. As a result, finite sliding was applied.[20]

Second, uniformly distributed pressure load was applied over the strip of area to simulate four point bending. This is clearly an approximation.

8.4 BOUNDARY CONDITIONS AND LOADS

In contact problem, two rigid surfaces were defined a reference point at the center of the cylinder. Boundary conditions and load were applied to this reference point. All surfaces were initially in contact. All translational and rotational degrees of freedom were initially constrained for the support and loading point. Symmetry boundary conditions were applied on

two planes in the model. In addition, vertical rigid body mode of the joint was constrained initially from one corner. At the second time step, initial displacement of 0.5mm was given to the loading point to establish contact. Only vertical translation was free. Vertical boundary condition for the joint was held at this time step. Now, joint detail has deformed and contact has been established. During third time step vertical translation was made inactive and vertical boundary condition for the joint was free. Load was determined such that extreme fiber stress at the surface away from the weld toe due to bending was 10 MPa. No membrane stress was developed because frictionless surfaces had been defined. Load was determined as follows.

$s_{ben} = \frac{6M}{bh^2}$ where $M = FL$ and L is the distance between support and loading point. Due to symmetry load was divided by two. As a result required concentrated force for the cylinder was equal to $F = 791.6N$.

Same symmetry boundary conditions were given for the simplified joint. Support was modeled by constraining transverse and vertical translational degrees of freedom at the same location as in contact model. Pressure load was determined such as to cause extreme fiber stress to be equal to 10 MPa away from the weld toe. No membrane stress was developed because axial translation was free. Pressure load to cause 10 MPa bending stress was determined as follows. Same load was distributed over a strip of area of 10mm wide. As a result, applied transverse pressure load was 1.26 MPa.

9 CASE STUDY IV: LOAD- AND NON-LOAD CARRYING CRUCIFORM JOINTS UNDER FOUR POINT BENDING

9.1 TESTING PROCEDURE

Analyzed joints were tested in four point bending. This caused constant bending moment in the attachment region. Testing frequency was approximately 3 Hz. In all cases failure criteria was defined when fatigue crack had propagated half way through the thickness of stressed plate. All specimen were subjected to constant amplitude loading. In practice, zero stress ratios were slightly on the positive side to prevent movement of the joint.[1]

9.2 GEOMETRY

Four point bending specimens tested in UKOSRP project are shown in Figure.18 along with relevant dimensions. Only as-welded specimens tested in air are considered in this study to limit the influence of other variables. Ends of the beam were tightened enough to

prevent backlash in the case where $R = -1$, but slack enough to maintain simply supported beam situation.[1]

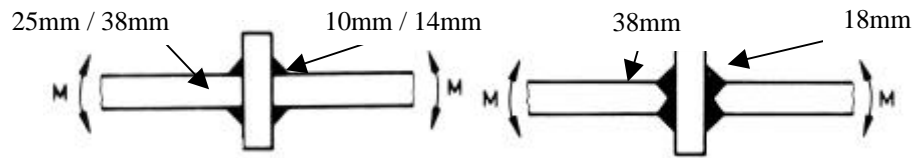


Fig.18. Tested specimens [1]

Stressed plates were 25mm and 38mm thick. Weld leg lengths were 10mm and 14mm in 25mm thick plates. Weld leg length was 18mm in 38mm specimen.

9.3 FINITE ELEMENT MODELING

FEA was carried out with ABAQUS v.6.5 as linear elastic analysis. Models were built using ABAQUS CAE. Joint detail in all cases was modeled in 2D. First part of the study included exploratory work using various 2D-element types under plane strain and plane stress conditions. Elements were specified unit thickness property. Effort was made to see how much does element selection and mesh size affect the results. Fillet welded and full penetration cruciform joints were analyzed using several different 2D-element types. Typical global view of symmetrical cruciform joint is shown in Figure.19. Element size in the weld region varied from 5mm in the coarse mesh model to 2mm in the fine mesh model.

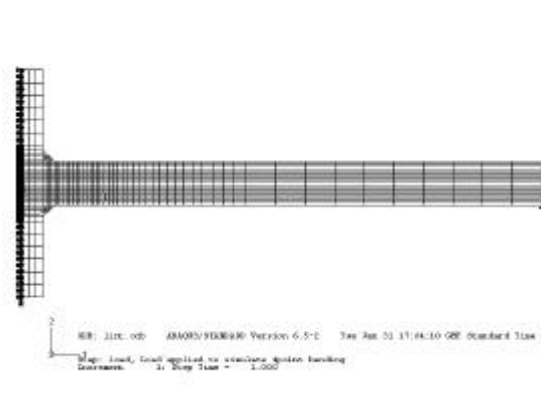


Figure.19. Global FE – model of the cruciform joint used in surface extrapolation methods and through thickness integration.

In addition, effective notch method was used in estimation of fatigue life. 38mm plate was modeled with coarse and fine mesh in the vicinity of the weld toe. Local geometry at the weld toe is shown in Figure.20. [23] Element size at the notch in the coarse model was about 0.4mm and in the fine mesh model about 0.13mm.

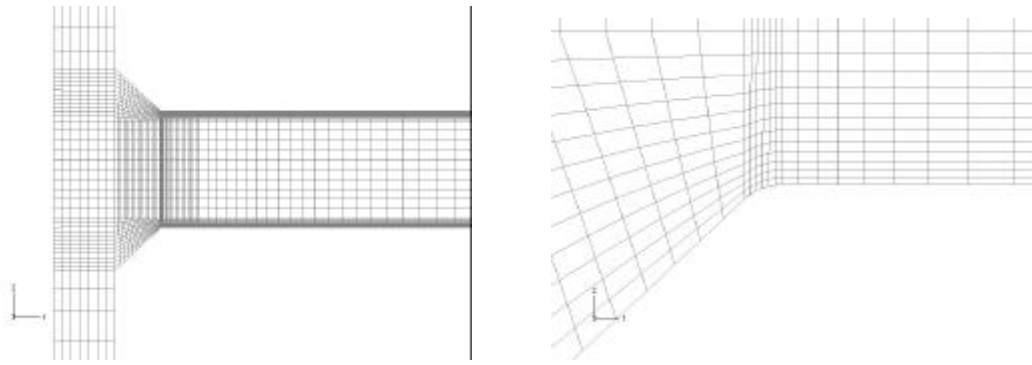


Figure.20. *Effective notch modeled with 1mm radius for full penetration cruciform joint. Fine mesh model. Element size at the notch ~0.13mm.*

Lastly, fracture mechanics method has been considered in fatigue life estimation for cruciform joint under four point bending. Overall joint was modeled with 8-node plane strain elements. Crack geometry was created by using partitioning and crack itself was created using SEAM-command in ABAQUS. Command allows nodes that are initially in same geometrical location to move apart as load is applied. Elements used in the crack tip were 8-node, not collapsed plane strain elements.

Detail used in fracture mechanics calculations was 38mm thick main plate with fillet welds having leg length of 14mm. Six different crack lengths were modeled at the weld toe in the tensile side of the joint. Crack lengths were 0.05mm, 0.5mm, 3mm, 7mm, 15mm and 22mm. Mode I stress intensity factors were obtained from ABAQUS and are listed in Table.2.

Table.2. Crack lengths with Mode I stress intensity factors and calculated dN/da.

Crack length (mm)	Mode I SIF $MPa\sqrt{mm}$	dN / da (cycles / mm)
0.05	289.5	224972.2
0.5	461	55714.9
3	684	17057.1
7	930	6786.2
15	1555	1451.7
22	2680	283.5

Element size at the crack tip for the sample mesh shown in Figure.21 is about 0.1mm. Mesh size at the crack tip for all crack lengths ranged from 0.05mm to 0.1mm. Figure.22 shows procedure for determining the estimated fatigue life of a joint by fracture mechanics.

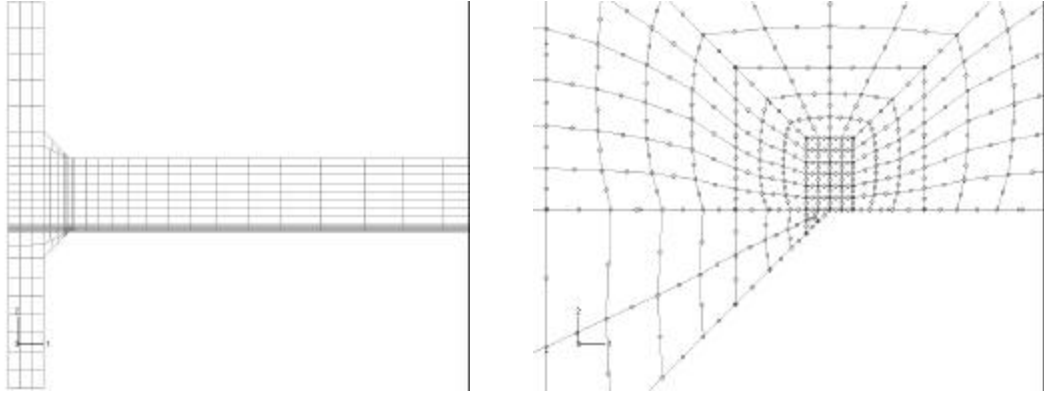


Figure.21. Sample mesh for 0.5mm crack modeled at the weld toe.

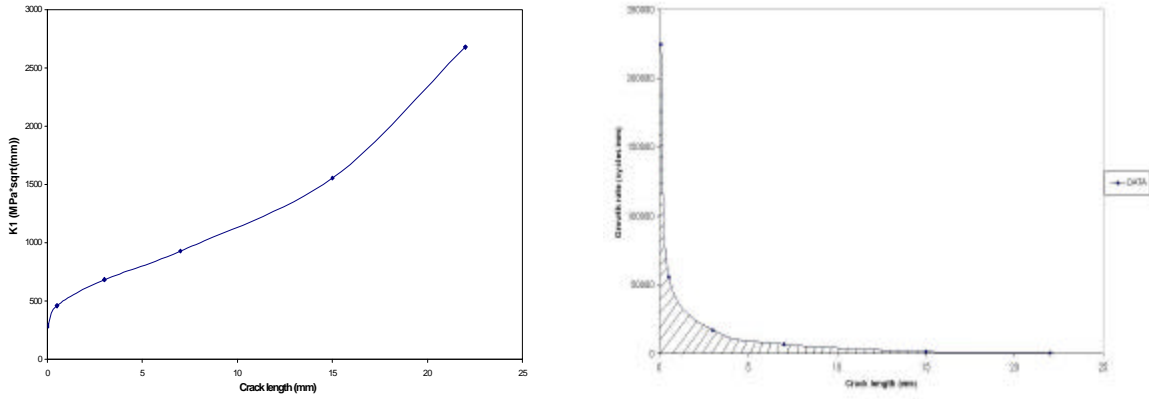


Figure.22. K_1 stress intensity factor history for cruciform under four point bending and inverted Paris law relationship.

Fracture mechanics calculations were based on Paris law that relates fatigue crack growth and stress intensity factor range as follows.

$$\frac{da}{dN} = C(\Delta K)^m \quad (37)$$

where

$$\Delta K = M_k F \Delta S \sqrt{pa} \quad (38)$$

in which M_k is the factor taking into account global geometry, F is factor relating crack depth into thickness of the plate, ΔS is the stress range and a is the crack length.

Three loading cases were considered that corresponded testing conditions. Stress intensity factor solution was obtained from ABAQUS for six different crack lengths. Material constants C and m were taken from experiments by Gurney [7].

$$C = 1.83 \cdot 10^{-13} \frac{mm/cycle}{(MPa\sqrt{mm})^m} \quad \text{and} \quad m = 3$$

As a comparison, fatigue life was estimated having ΔK as constant. Geometry was 38mm thick plate with 14mm leg full penetration welds. Nominal stress was 200 MPa. It was assumed that when crack length was 3mm crack growth was stable, thus Paris law could be applied. This resulted fatigue life of 341 500 cycles as compared to test result of 171 520 cycles.

Of course, this is idealization. In the light of idealization, more rigorous approach was taken and more crack lengths were considered.

If Paris law is reversed, result can be used to generate a graph that represents number of cycles to grow a crack a unit distance.[10] Estimate of fatigue life is found by curve fitting technique and this function is integrated numerically from initial crack size to final crack size. As a result, area under the curve represents the number of cycles to failure according to

$$N_{if} = \int_{a_i}^{a_f} \frac{dN}{da} da \quad (39)$$

Least-squares regression was performed to all three loading cases that produced dN/da (cycles/mm) versus a (mm) graphs. Power fit, exponential fit and natural logarithmic fit were examined and coefficient of determination was calculated to see which curve best represents the data. In all cases exponential fit showed best correlation. Selection of “best fit” to continue with numerical integration was based on coefficient of determination. Numerical integration was performed using trapezoidal rule according to relationship.[11]

$$A_i = (a_{i+1} - a_i) \left(\frac{f(a_i) + f(a_{i+1})}{2} \right) \quad (40)$$

where

$f(a_i)$ is a function value at initial crack size

$f(a_{i+1})$ is a function value at next increment crack size

Increment size was 0.025mm. During integration it was assumed that geometry function $F(a/b)$ and M_k factor caused by global geometry stay constant.

9.4 BOUNDARY CONDITIONS AND LOADS

Half model was built due to symmetry. Four point bending was simulated by applying symmetry boundary conditions to the mid-plane of the joint. Attachment end of the structure was rigidly supported. Rotation and axial translation at the end were free.

Concentrated force, 100 N, was applied in the mid-span of the joint, 250mm from supported end. Any reasonable load will work that causes bending stress that is less than yield strength of typical steel, because stress concentration factors were computed. Nominal stress in the region of the weld was calculated using beam equation.

$$s_{ben} = \frac{6M}{bh^2} \quad (41)$$

s_{ben} or nominal bending stress was equal to 103.88 MPa in the surface of the plate at weld region. Concentrated force was adjusted in 25 mm thick plate to cause same bending stress in the weld region. Membrane stress was not introduced under these conditions, because joint end was supported on rollers thus causing pure bending stress in the weld region. This was assumption in FE - modeling. Real situation is something in between fixed and roller support.

10 RESULTS

Thickness effect was re-established, mainly due to multivariable regression. No assumptions were made regarding thickness effect. Results of multivariable regression considering three joint types and case studies are presented here.

10.1 Multivariable regression

For all three joints under bending mode it was found that correlation coefficients were poor. Therefore, any reasonable curve fitting technique investigated does not adequately represent the data. Due to lack of data in bending mode, especially for longitudinal attachment, it would seem reasonable to treat derived functions as an approximation. It is clear that results act only as a guide to specific kind of fatigue behavior of the joint. This is due to the fact that, for example, looking at thickness effect under tensile and bending mode all different local geometry was included. This included different attachment thickness, attachment length, weld leg length and weld toe angle. Toe angle, however, in most cases was at 45°. In several tests, toe angle was not recorded. Table.3 and table.4 lists correlation coefficients for butt and cruciform joints. Longitudinal attachment was not considered due to limited data.

Table.3. Best fit curve criteria for butt joints.

MODEL	Exponential	Saturation	Power	Logarithmic
r^2 - tensile	0.42	0.13	0.29	0.22
r^2 - bending	0.4	0.01	0.63	Linear 0.47

Table.4. Best fit curve criteria for cruciform joints.

<i>MODEL</i>	<i>Exponential</i>	<i>Saturation</i>	<i>Power</i>	<i>Logarithmic</i>
r^2 - tensile	~0	0.12	0.058	0.103
r^2 - bending	0.51	-	0.82	0.505

10.1.1 Butt joint

All collected butt joint data were graphed on S-N curve. Tensile test results included 1 531 fatigue test results. However, factors such as axial and angular misalignment, weld cap width, welding process, amount of weld penetration and stress ratio are not considered. Certainly, these factors have an effect in fatigue life of a joint, however, as a starting point for multivariable regression only thickness is considered.

Linear regression was performed for tensile and bending mode data. Exponential fit produced highest r^2 , coefficient of determination under tensile mode. Most scatter was observed at thickness ~20mm. As expected, fatigue strength decreased with increasing thickness.

Under bending mode power law fit produced highest r^2 . Same observation was made as with tensile specimens, fatigue strength in general decreases with increasing thickness. For same thickness, fatigue strength under bending was higher than under tensile loading. Corresponding fitted equations are as follows. Under tensile mode reference thickness was chosen as 20mm and reference fatigue strength was calculated as 171.3 MPa. Under bending, 10mm and 162.6 MPa, respectively. For tensile loading

$$\frac{\mathbf{s}}{\mathbf{s}_{ref}} = 0.77e^{-.382 \frac{t}{t_{ref}}} \quad (42)$$

Bending data resulted following power law relationship.

$$\frac{\mathbf{s}}{\mathbf{s}_{ref}} = 0.956 \cdot \left(\frac{t}{t_{ref}} \right)^{-.174} \quad (43)$$

Thirteen different plate thicknesses were recorded ranging from 2mm to 50mm. S-N curves based on data collection that show all butt joint data are shown in Figure.23.

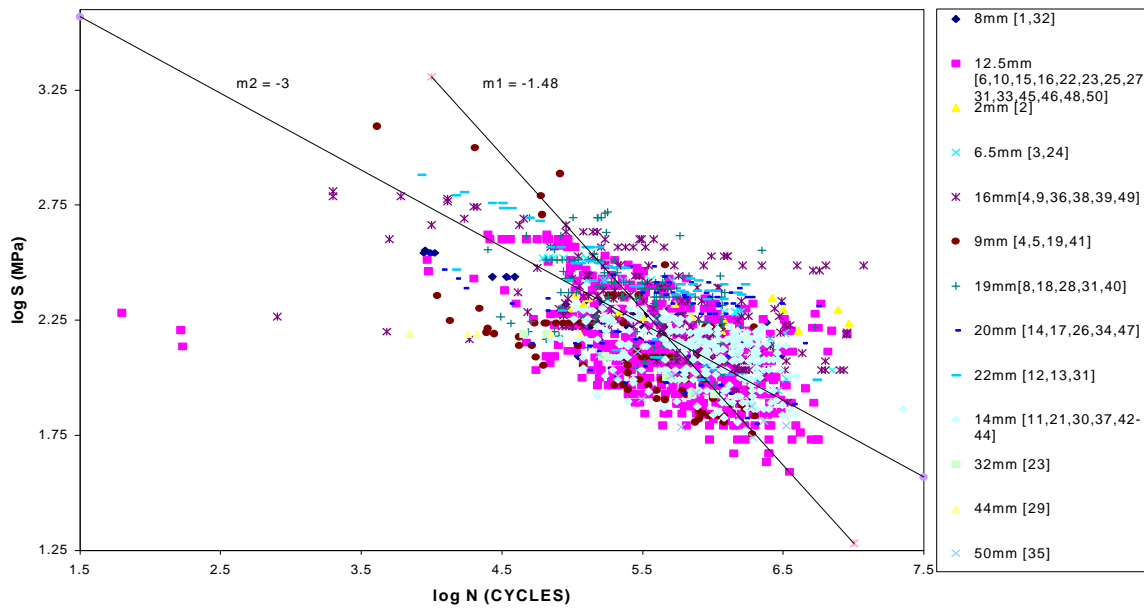


Figure.23. Collected butt joint data under tensile mode.

As a result linear regression was performed to each thickness data set and clear thickness effect was established as shown in Figure.24. Slope was forced to $m = -3$.

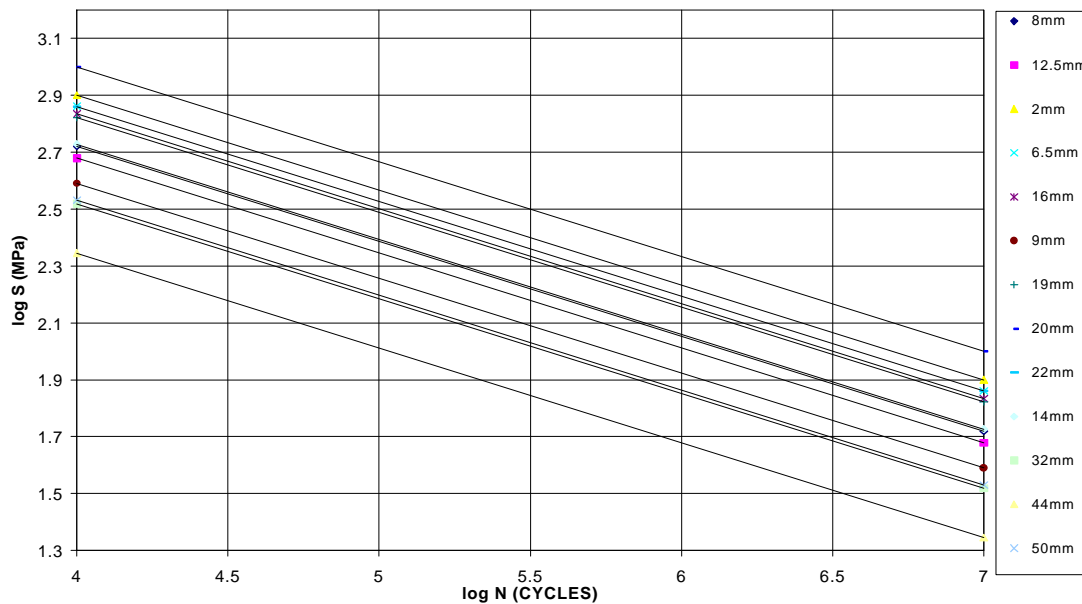


Figure.24. Butt joints under tensile mode by thickness.

Linear regression was performed for tensile results not considering different plate thickness. Line representative of the data was also graphed with forced slope of -3 .

Thickness order starting from the top is as follows along with fatigue strength representing each thickness based on collected data. Fatigue strength at $2 \cdot 10^6$ cycles is calculated based on $m = -3$.

Table.5. Descending order of plate thickness for butt joints under tensile mode.

Thickness from the top	Fatigue strength at $2 \cdot 10^6$ cycles
20 mm	171 MPa
2 mm	136 MPa
22 mm	124 MPa
6.5 mm	124 MPa
16 mm	117 MPa
19 mm	114 MPa
14 mm	91 MPa
8 mm	90 MPa
12.5 mm	82 MPa
9 mm	67 MPa
50 mm	58 MPa
32 mm	57 MPa
44 mm	38 MPa

Having established a thickness effect, it is of interest how does thickness relate to fatigue strength. Following relationships were established. Refer to Figures.25 and 26, tensile and bending modes, respectively.

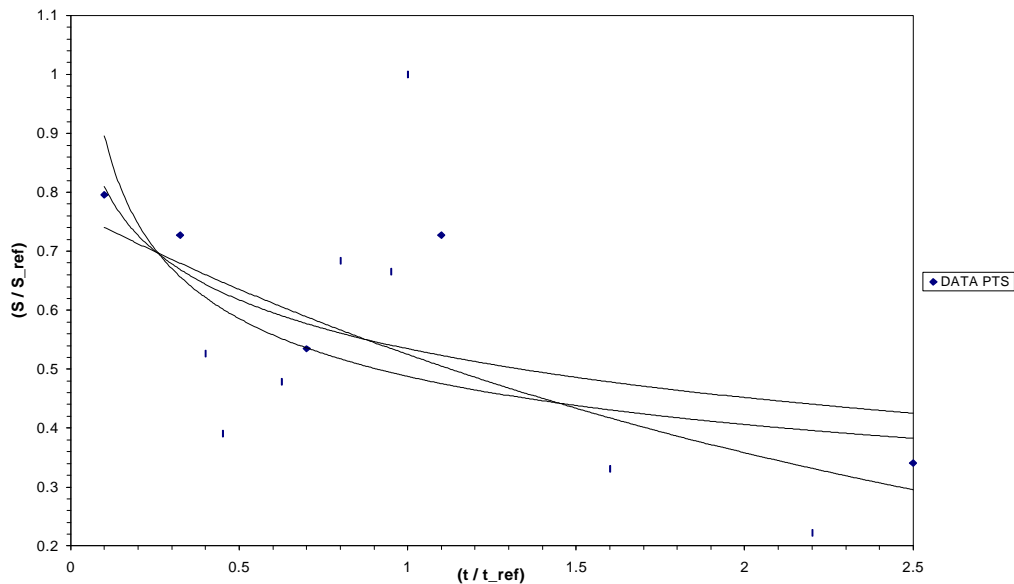


Figure.25. Butt joint data points under tensile mode relating thickness to the fatigue strength at $2 \cdot 10^6$ cycles.

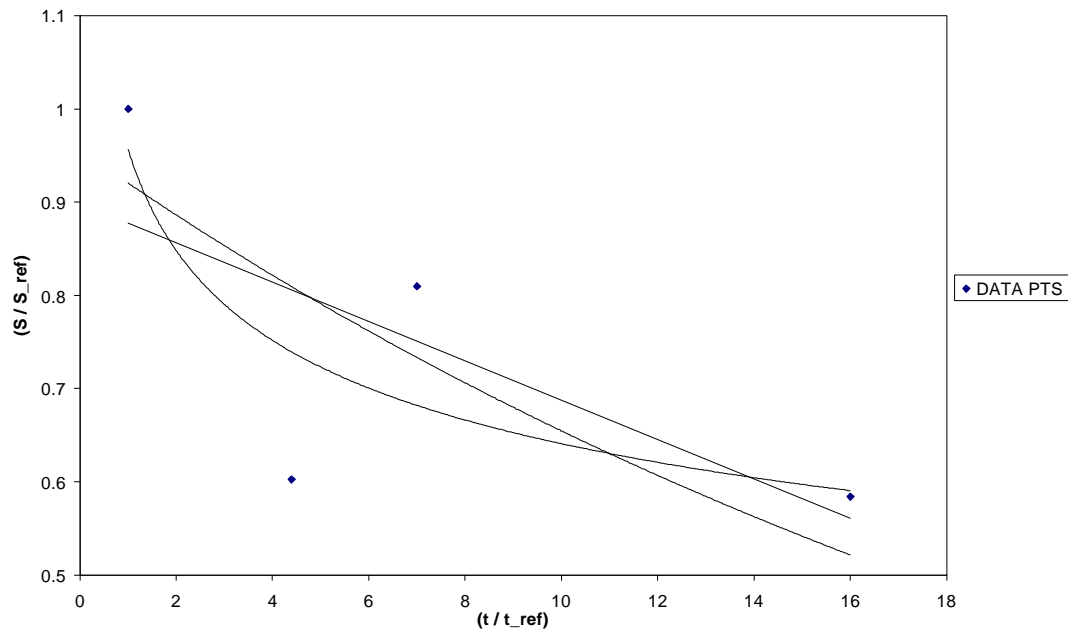


Figure.26. Butt joint data points under bending mode relating thickness to the fatigue strength at $2 \cdot 10^6$ cycles.

Much scatter is observed under tensile and bending mode. Due to lack of data for the bending mode, relationship is hard to define. Based on four test results, fatigue strength might decrease with increasing plate thickness. It appears that same is true for tensile loading. No clear relationship is observed under 20mm, however, sudden drop in fatigue strength is observed beyond 20mm. Applying multivariable regression the results are as follows.

First, two variables were considered that affect fatigue life in butt joints, stress range and plate thickness. As least-squares regression line was calculated solely based on data points results was $m = -1.4807$. Moving into multivariable regression resulted nearly same coefficient for stress range, however, coefficient in thickness was small enough to cause no variation for thickness effect. Estimate of this relationship could be expressed as

$$\log N = -1.478 \cdot \log s - 0.03317 \cdot \log t + 8.929 \quad (44)$$

There is an alarming issue to be noticed here. Coefficient in thickness term is quite small although negative as suggested in earlier results. This suggests that stress range and thickness are not well correlated in butt joints even though both exhibit a clear relationship to fatigue life. At this point it seems meaningless to move on to add additional variables as thickness effect in

butt joints do not work using multivariable regression. Next, additional variable is added, namely bending mode. Solving for coefficients leads to

$$\log N = -1.4809 \cdot \log S - 0.070115 \cdot \log t + 0.3315 \cdot \log r + 8.9763 \quad (45)$$

As a result, a series of curves are obtained that should describe the fatigue strength as a function of stress range, thickness and loading mode. Interestingly, bending mode exhibits higher fatigue strength and decreases as a function of plate thickness. Still, all bending mode data according to (45) with relevant thickness are well above tensile curves. Figure.27 shows multivariable regression results for the butt joint.

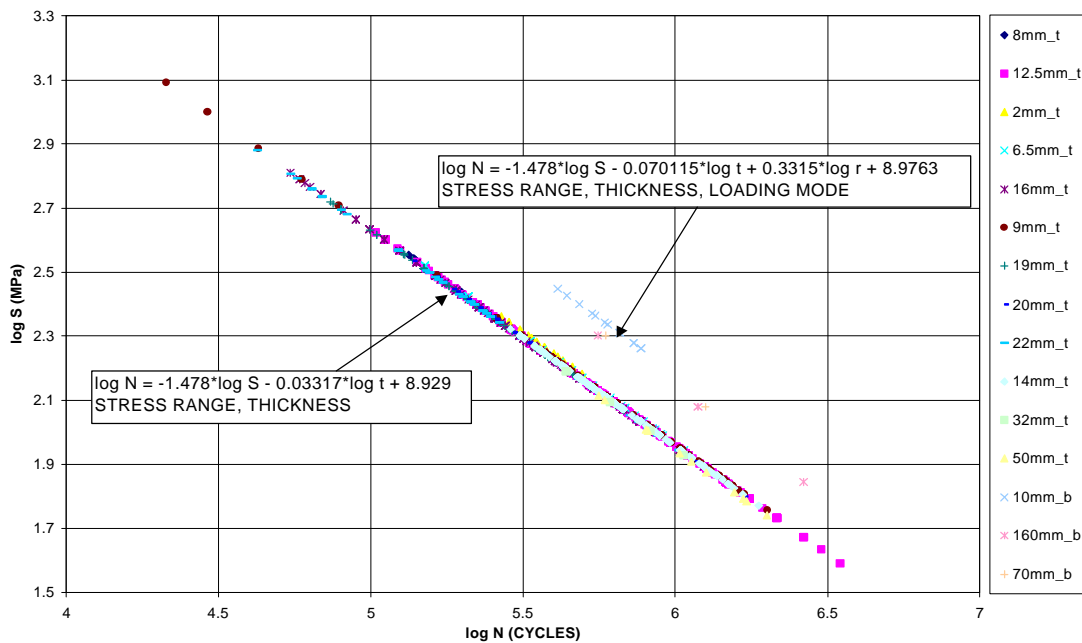


Figure.27. Multivariable regression results taking into account plate thickness and loading mode.

Similar procedure has been carried out for the cruciform joints. Due to more data, tensile and bending mode were separated. First, linear regression was carried out for tensile and bending data sets that were further separated by stressed plate thickness.

10.1.2 Cruciform joint

Scatter in tensile tests was significant. Power fit provided best, yet poor coefficient of determination with r^2 .06. For tensile loading the relationship was established as follows

$$\frac{S}{S_{ref}} = 0.83 \cdot \left(\frac{t}{t_{ref}} \right)^{-0.525} \quad (46)$$

In bending mode relationship most closely obeyed power law as follows with r^2 equal to 0.82.

$$\frac{S}{S_{ref}} = 0.851 \left(\frac{t}{t_{ref}} \right)^{-2.49} \quad (47)$$

More data was available for tensile mode than bending mode. Refer to Figures.28 and 29 for the data.

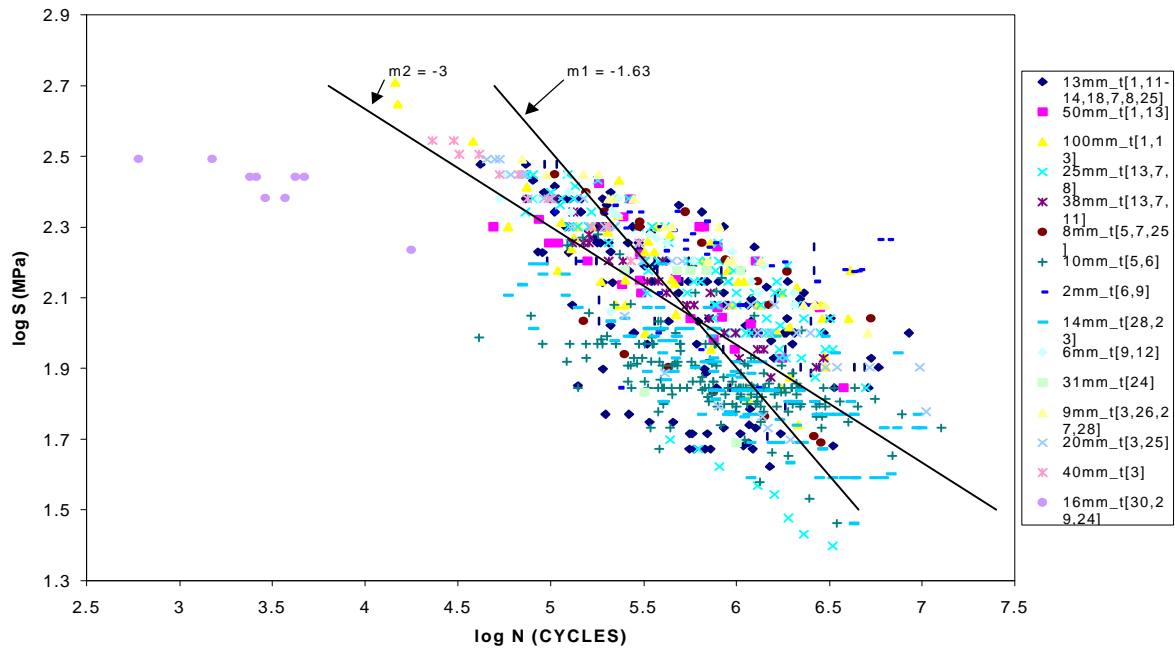


Figure.28. Cruciform joints under tensile mode separated by stressed plate thickness.

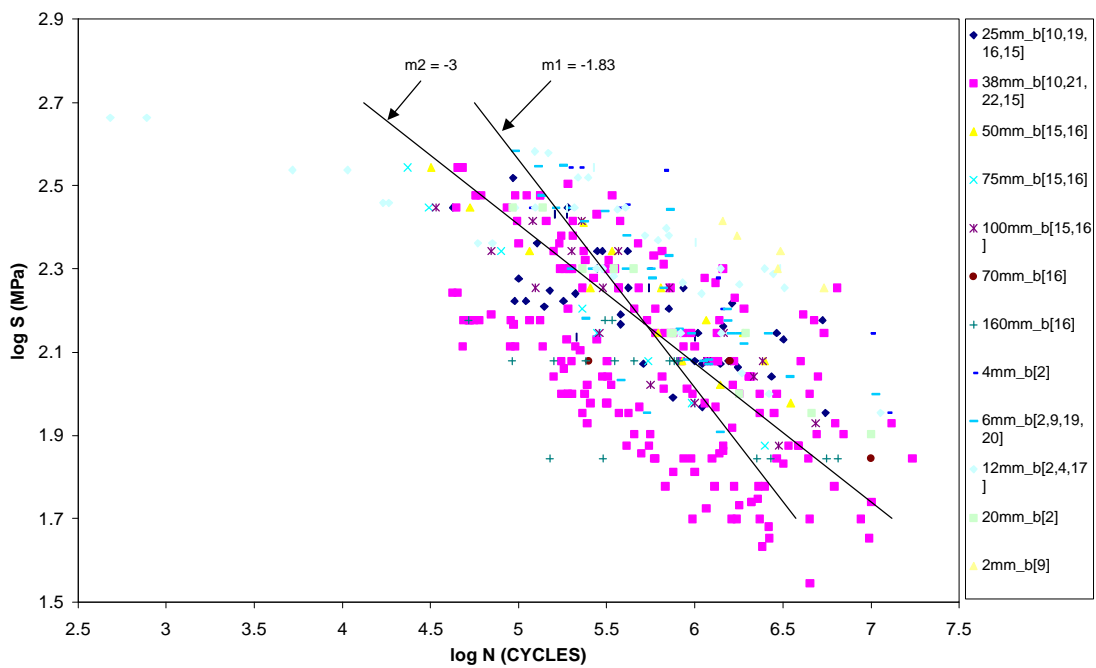


Figure.29. Cruciform joints under bending mode separated by stressed plate thickness.

As linear regression was performed for each data set following curves resulted. Refer to Figures.30 and 31.

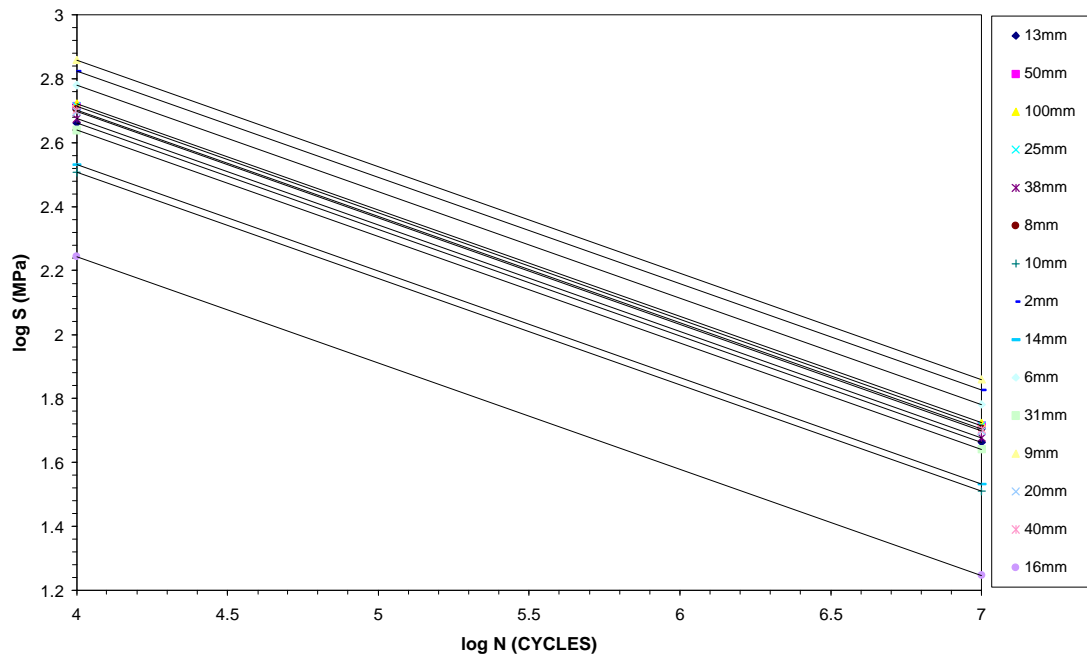


Figure.30. Thickness effect in cruciform joints under tensile mode.

Other global or local geometry is not taken into account. Cruciform joints still, generally, exhibit decrease in fatigue strength as stressed plate thickness increases.

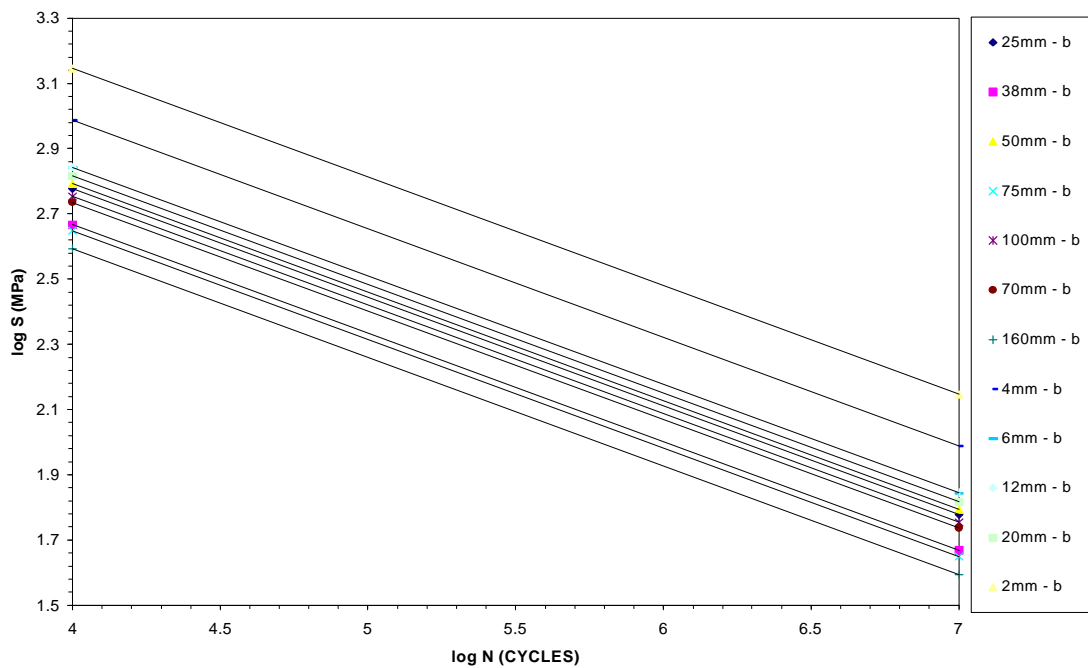


Figure.31. Thickness effect in cruciform joints under bending mode.

Moving into establishing the relationship between thickness of stressed plate and fatigue strength at $2 \cdot 10^6$ cycles. Tensile mode is considered first. Refer to Figure.32.

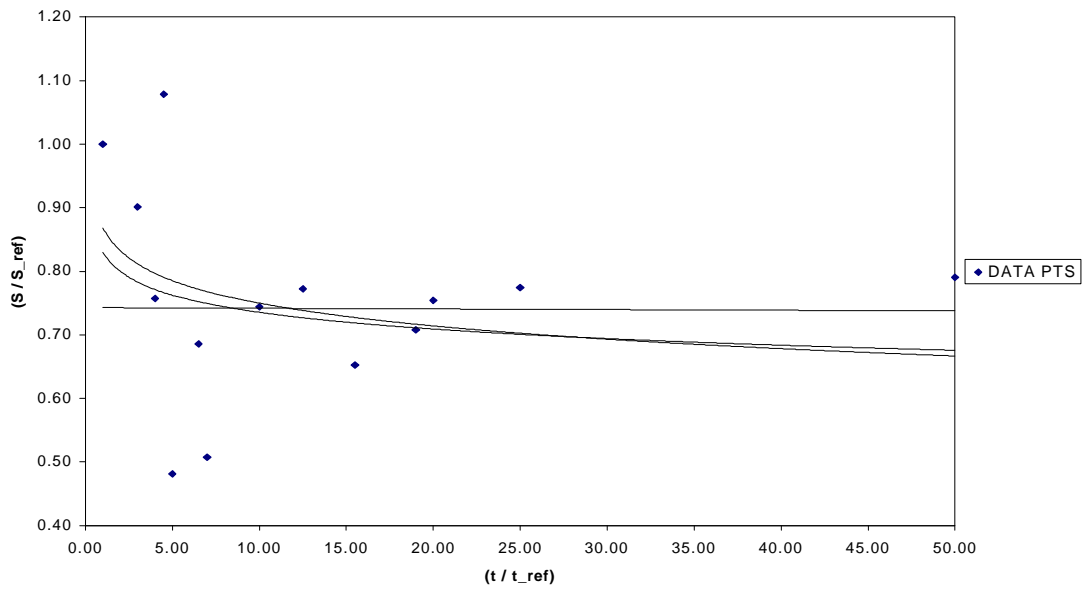


Figure.32. Relationship between thickness and fatigue strength at $2 \cdot 10^6$ cycles for cruciform joint under tensile mode.

More consistent relationship was seen under bending mode. Refer to Figure.33.

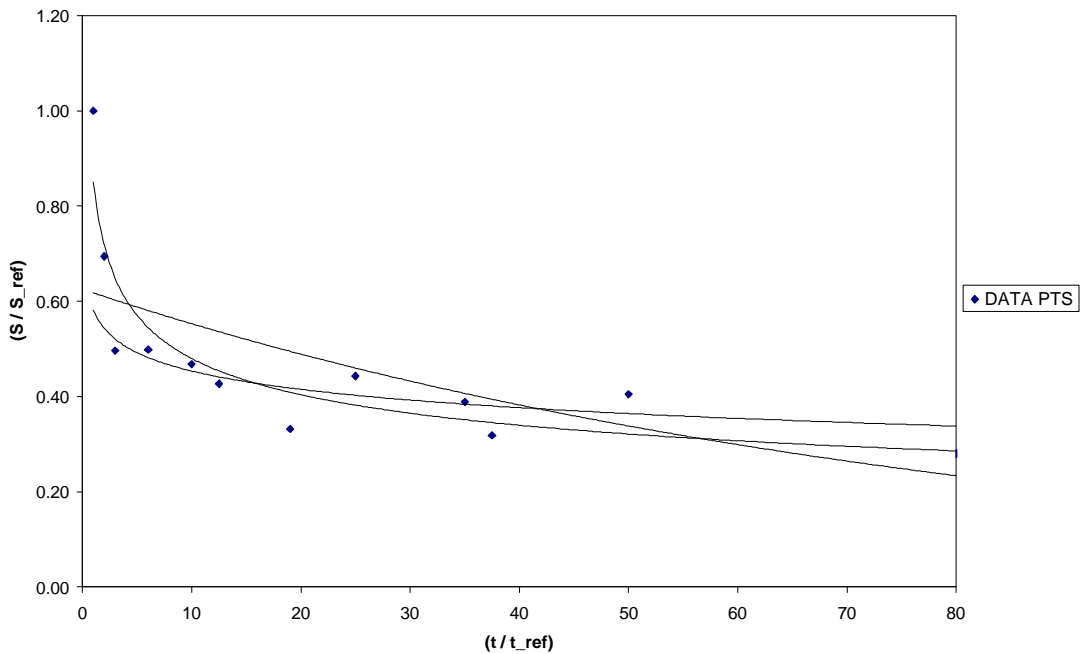


Figure.33. Relationship between thickness and fatigue strength at $2 \cdot 10^6$ cycles for cruciform joint under bending mode.

Tensile mode relationship is quite scattered, however, decreasing relationship is observable under bending mode. Reference thickness under tensile and bending mode was chosen as 2mm. Fatigue strength at $2 \cdot 10^6$ cycles was calculated based on 2mm regression line with $m = -3$.

Based on linear relationship assumption between variables, multivariable regression was applied to the collected data. Following equation considering two variables, stress range and plate thickness, was obtained.

$$\log N = -1.6337 \cdot \log s - 0.049517 \cdot \log t + 9.16535 \quad (48)$$

If bending mode was considered as a third variable result was

$$\log N = -1.41 \cdot \log s - 0.1 \cdot \log t + 0.165 \cdot \log r + 8.765 \quad (49)$$

where $r = \frac{s_{ben}}{s_{structural}} = \frac{s_{ben}}{s_{mem} + s_{ben}}$ thus under pure tension $r = 0$ and pure bending $r = 1$. All

collected data are either under pure tension or pure bending. Figure.34 shows multivariable regression results for all cruciform joint data.

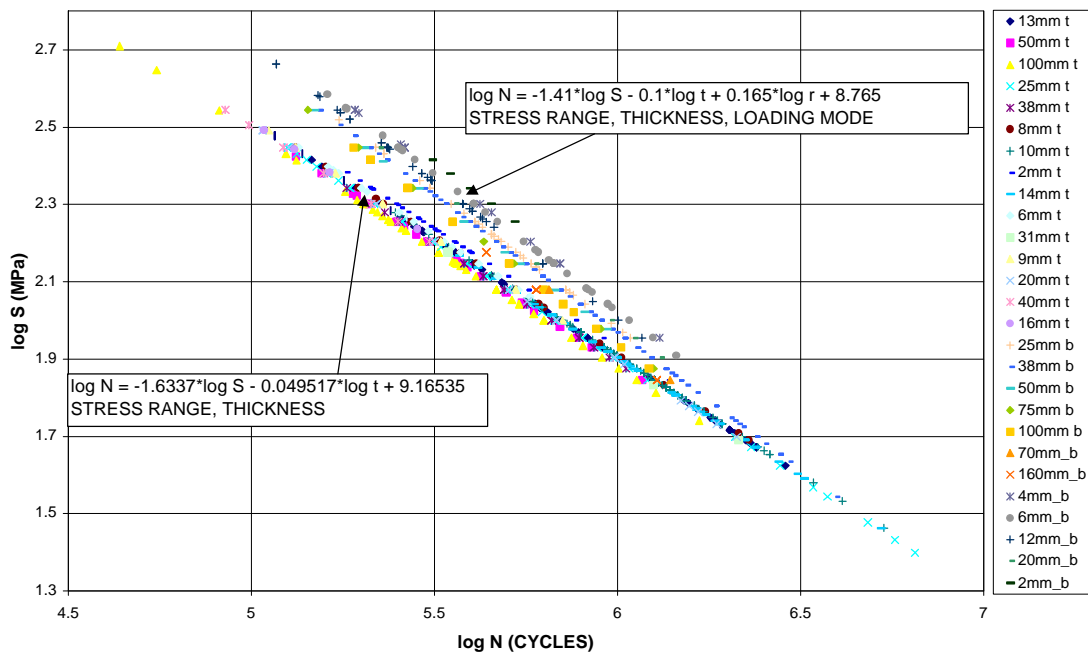


Figure.34. Multivariable regression performed for cruciform joint under tensile and bending mode.

Bending mode results exhibit better fatigue strength than tensile mode as would be expected. In addition, fatigue strength tends to decrease as the thickness increases under bending mode. Under tensile mode, generally, same observation can be made – fatigue

strength decreases as thickness increases. However, effect of thickness under bending mode is more clear than under tensile mode. Also, bending specimens have slightly steeper slope as compared to tensile specimen.

10.1.3 Longitudinal attachment

Longitudinal stiffener on flat plate was studied lastly. Least amount of data was available for this type of joint. Data is broken down in terms of stressed plate thickness and loading mode, tensile mode and bending mode. Regression analysis with resulting slope and forced slope were fitted to the data set. Raw tensile data points and regression lines are shown in Figure.35 and 36, tensile and bending modes, respectively.

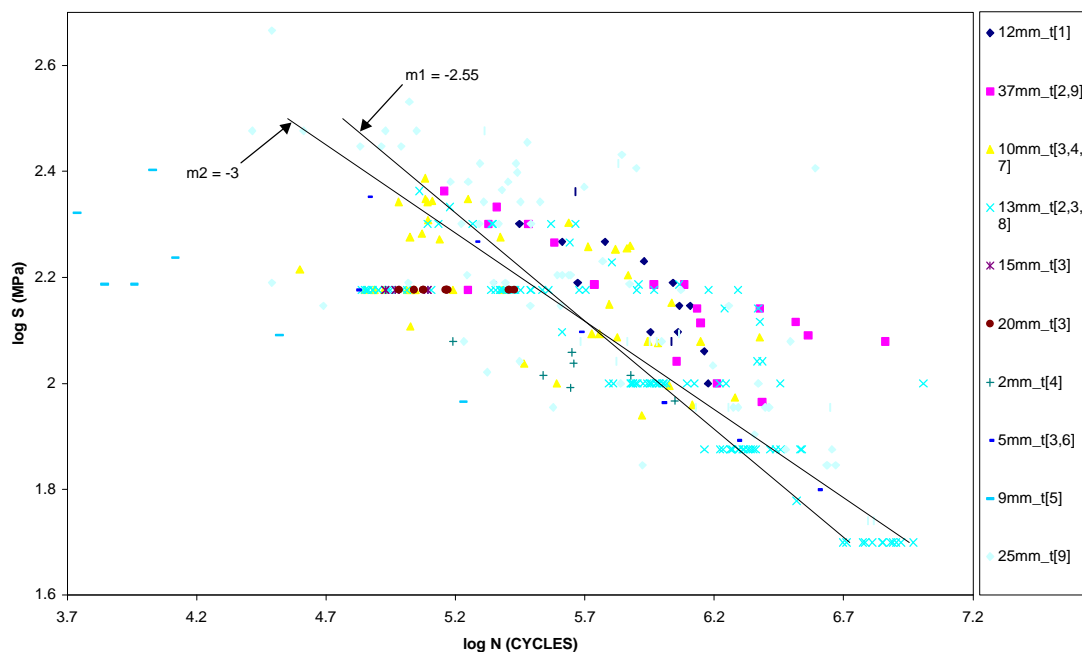


Figure.35. Longitudinal attachment under tensile mode. Data is broken down in terms of stressed plate thickness. Regression based on data and forced slope of $m=-3$.

Regression slope of 2.6 was close to generally accepted slope of $m = 3$. One of factors that contributed to this was a lack of data. As more data is added data point clouds form on S-N curve. Tight cloud in certain region of the curve can alter regression slope significantly as was seen the case of butt joint data.

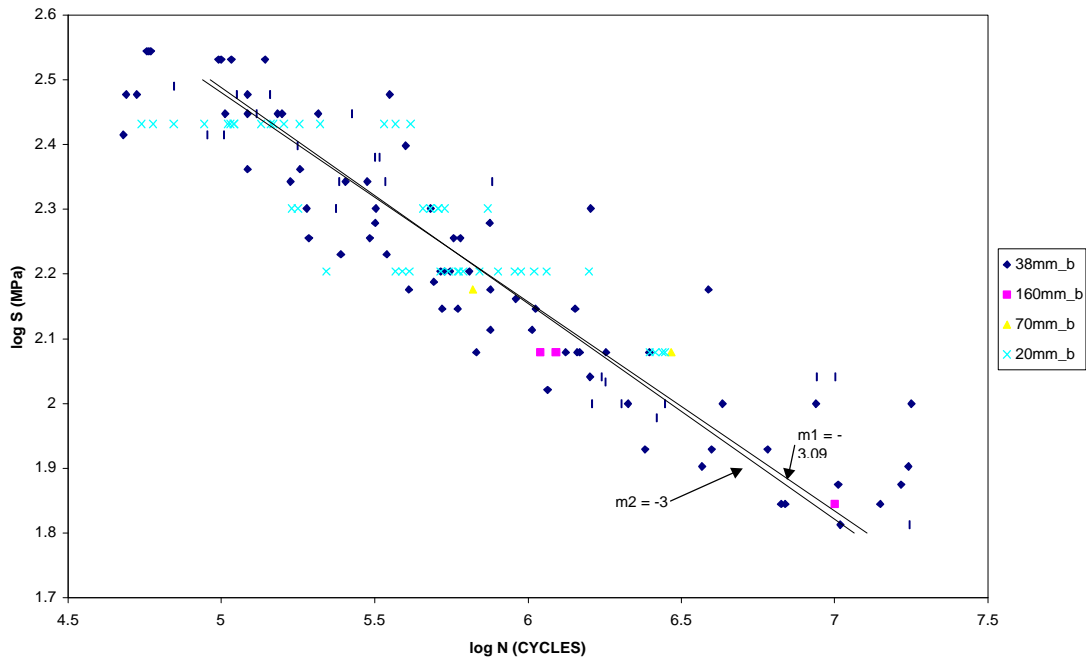


Figure.36. Longitudinal attachment under bending mode and regression and forced based slopes.

Wide scatter was observed in tensile data. Power law fit provided best fit as follows with r^2 equal to 0.13.

$$\frac{\mathbf{S}}{\mathbf{S}_{ref}} = 0.846 \cdot \left(\frac{t}{t_{ref}} \right)^{-1.62} \quad (50)$$

Scatter was quite large under bending mode. General trend based on collected data is not obvious, however, least-squares regression was applied. Best correlation resulted from linear fit. Linear equation was as follows with r^2 equal to 0.41.

$$\frac{\mathbf{S}}{\mathbf{S}_{ref}} = -0.00951 \cdot \left(\frac{t}{t_{ref}} \right) + 1.033 \quad (51)$$

Tensile mode relationship was established as shown in Figure.37.

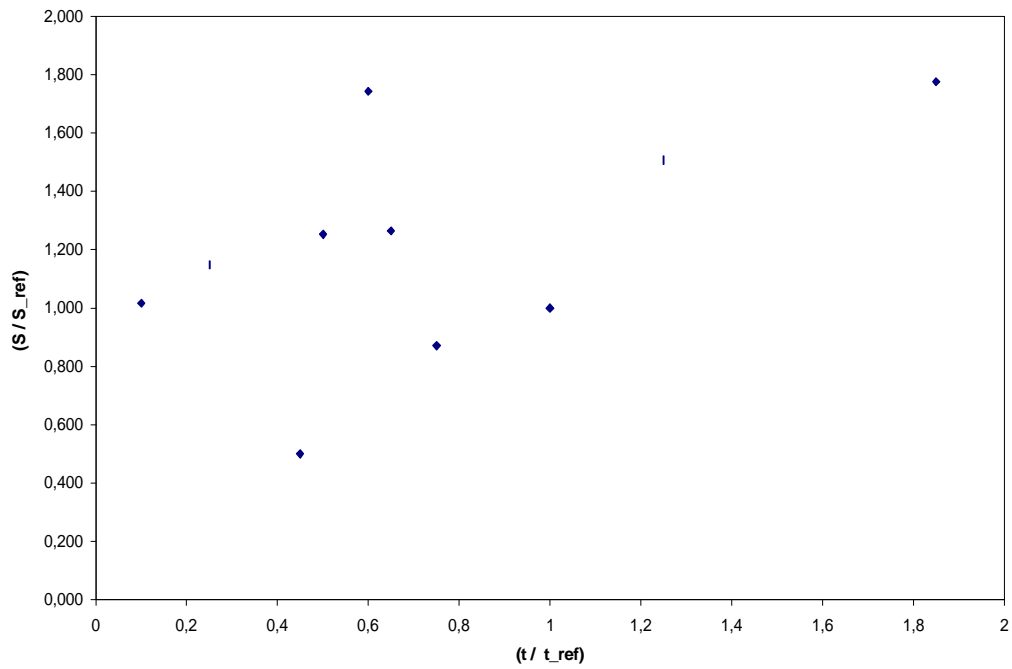


Figure.37. Relationship between plate thickness and fatigue strength at $2 \cdot 10^6$ cycles for longitudinal attachment under tensile mode.

Actually, by visual inspection collected data for longitudinal attachment suggests that fatigue strength would increase with increasing plate thickness. Based on results from this literature search, relationship between thickness and fatigue strength in longitudinal attachment under bending should be treated as a rough estimate. Clearly, more data points are needed to draw further conclusions. Bending mode relationship was established as in Figure.38.

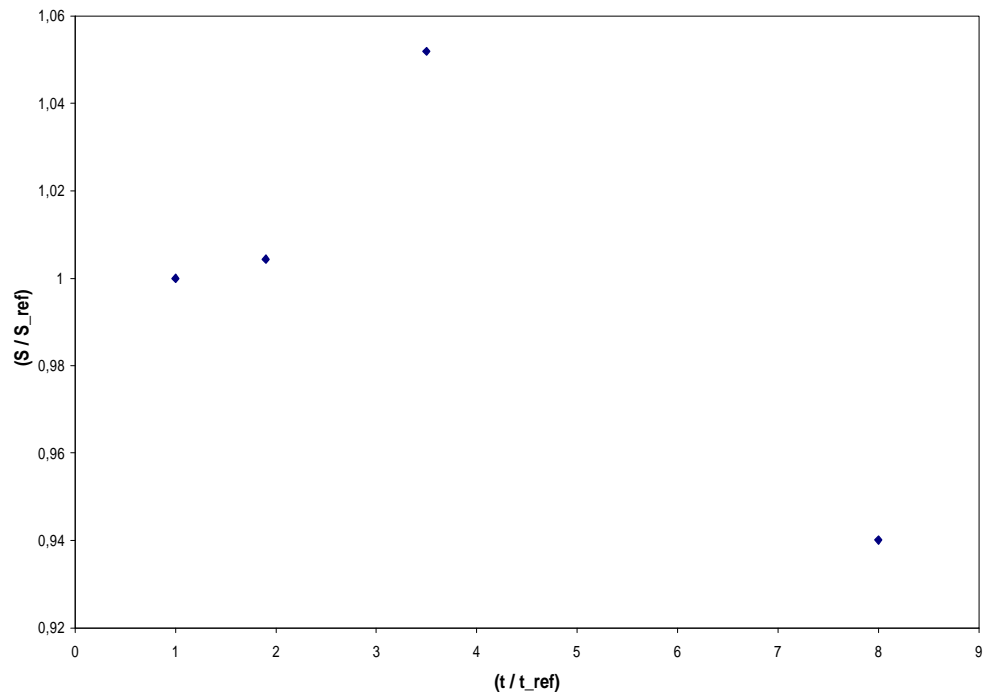


Figure.38. Relationship between plate thickness and fatigue strength at $2 \cdot 10^6$ cycles for longitudinal attachment under bending mode.

Regression analysis for longitudinal attachment taking into account stress range and plate thickness resulted following relationship

$$\log N = -2.564 \log S + 0.577 \log t + 10.452 \quad (52)$$

Limited data was available in bending mode, however, relationship was established as follows

$$\log N = -2.692 \log S + 0.4939 \log t - 0.2073 \log r + 10.821 \quad (53)$$

Scatter, especially in bending mode was large. Based on multivariable regression, fatigue strength decreases as plate thickness decreases. Based on data collection same holds for tensile loading. Thinnest plate showed lowest fatigue strength. It is important to keep in mind that the attachment length, width and height have not been considered among other variables. These geometry changes have effect on fatigue strength.

Another regression analysis has been performed to individual thicknesses represented in Figure.39. Slope was forced to be $m=-3$.

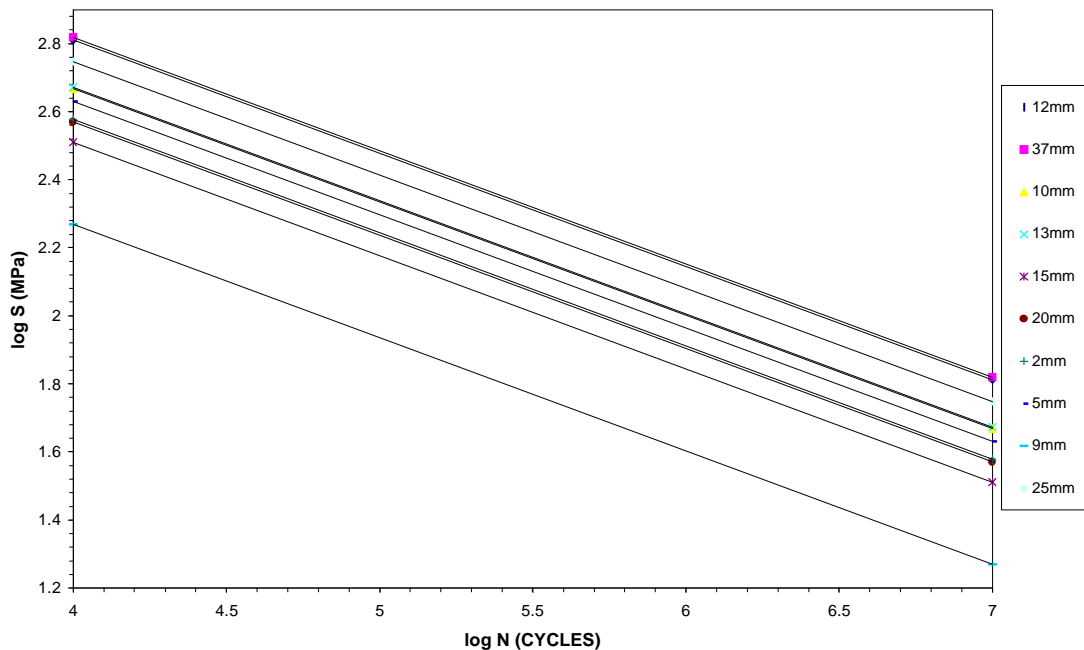


Figure.39. Thickness effect under tensile mode for longitudinal attachment.

In general, fatigue strength tended to decrease as stressed plate thickness decreased based on collected data. Again, only main plate thickness has been considered under tensile mode. Other factors in longitudinal attachment have an effect in fatigue strength. In the light of this, regression was performed on limited data under bending mode. Refer to Figure.40.

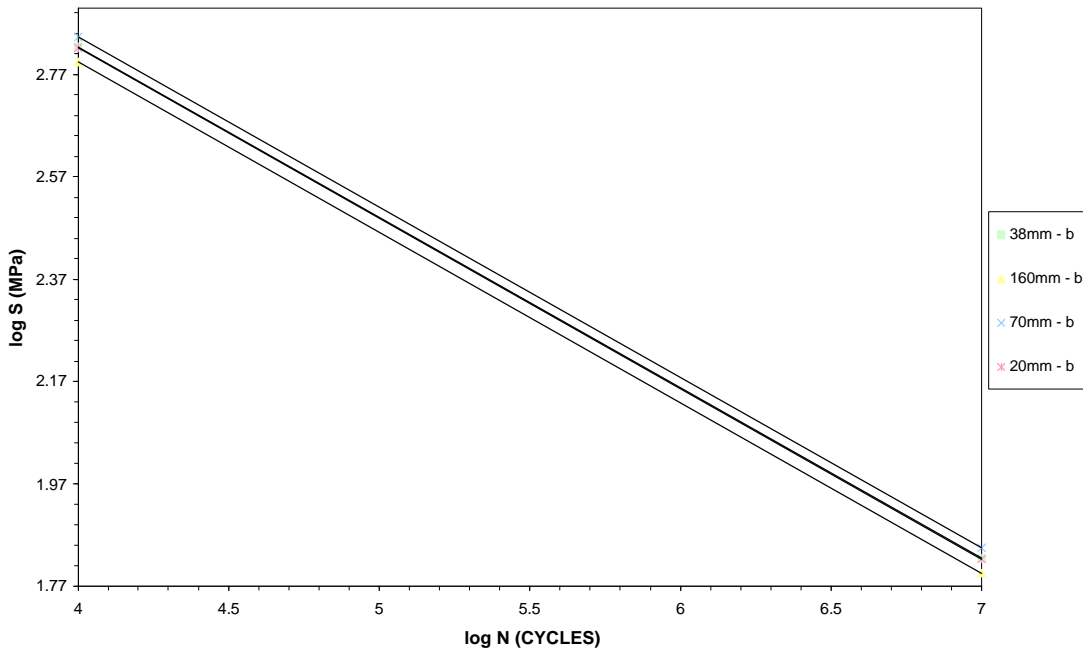


Figure.40. Thickness effect under bending mode for longitudinal attachment with $m = -3$.

It may be that under bending mode fatigue strength in longitudinal attachment would decrease with increasing plate thickness. Clearly, only few test results have been analyzed and local/global geometry is different from tensile results as a result it is questionable whether this might be the case. Fatigue testing would be required.

To the task of interest, multivariable regression was performed considering plate thickness and loading mode. Refer to Figure.41 for tensile mode specimens.

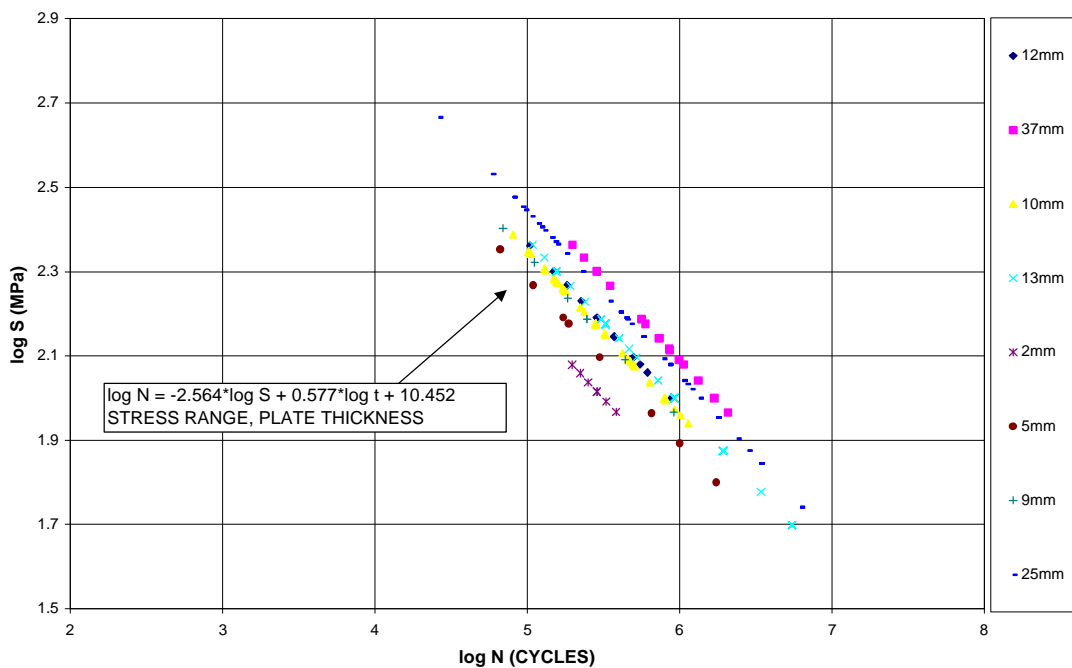


Figure.41. Multivariable regression results considering two variables. Longitudinal attachment under tensile mode.

In general, multivariable regression equation for longitudinal attachment based on collected data predicts that fatigue strength would decrease with decreasing thickness. In the light of earlier relationship between fatigue strength and stressed plate thickness under bending mode, multivariable regression was performed. Refer to Figure.42 for bending mode relationship.

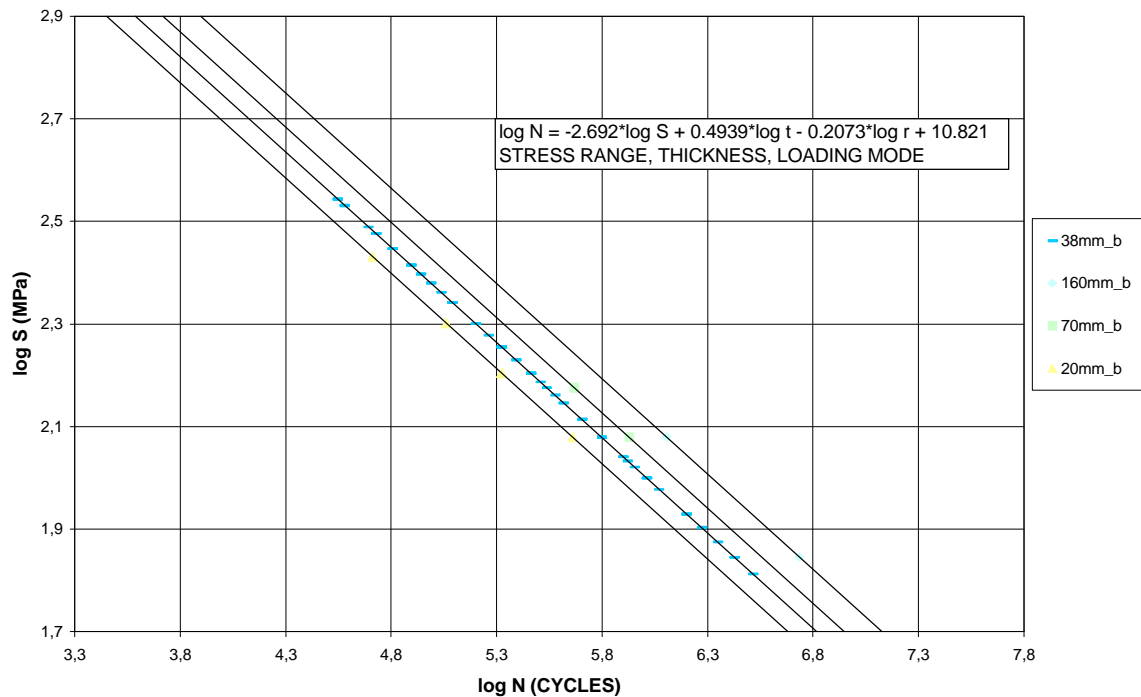


Figure.42. *Multivariable regression performed for longitudinal attachment based on collected data under bending mode.*

Under bending mode fatigue strength tends to decrease as plate thickness decreases. Only four plate thicknesses are considered here due to limited amount of data.

10.2 CASE STUDY I

All shell models were subjected to tensile mode. Nominal stress was 10 MPa given as shell edge load. Hot-spot stress was obtained through linear and quadratic surface extrapolation. In all four shell models stress concentration factors were found to be greater than 2. Material constants C and m were obtained as follows. Linear regression was performed to the actual test data for 6mm and 2mm specimens. Value of m was found by regression analysis and was used in calculation for material constant C . Fatigue strengths at $2 \cdot 10^6$ cycles were established from test program. Table.6 lists material constants and corresponding fatigue strengths.

Table.6. Material constants for 6mm and 2mm loaded plates.

	<i>m</i>	<i>C</i>	FAT @ $2 \cdot 10^6$
<i>6mm</i>	2.98	$5.53e+11$	75
<i>2mm</i>	3.35	$3.82e+12$	67

Stress concentration factors were calculated based on linear and quadratic surface extrapolation. Through thickness integration was applied in solid models. Refer to Tables.7 through 11 for the results.

Table.7. 6mm shell model results without welds

ELEMENT TYPE	0.4t	t	Hot-spot	SCF	
S8R	18.81	14.65	21.6	2.16	
S4R	16.11	14.06	17.48	1.74	
S4	20.16	15.55	23.25	2.32	
	0.4t	0.9t	1.4t	Hot-spot	SCF
S8R	18.85	15.11	13.69	23.51	2.35
S4R	16.17	14.3	13.2	18.22	1.82
S4	20.3	16.02	13.87	25.26	2.52

Table.8. 2mm shell model results without welds

ELEMENT TYPE	0.4t	t	Hot-spot	SCF	
S8R	25.6	19.37	29.77	2.98	
S4R	20.86	17.65	23.01	2.3	
S4	27.04	19.05	32.39	3.24	
	0.4t	0.9t	1.4t	Hot-spot	SCF
S8R	23.74	20.2	17.88	27.45	2.75
S4R	17.65	16.52	15.32	18.5	1.85
S4	23.99	21.27	18.36	26.03	2.6

Table.9. 6mm shell model with inclined welds modeled

ELEMENT TYPE	0.4t	t	Hot-spot	SCF
S8R	20.81	16.97	23.38	2.34
S4R	20	16.43	22.39	2.24
S4	20.87	16.79	23.6	2.36

Table.10. 2mm shell model with inclined welds modeled

ELEMENT TYPE	0.4t	t	Hot-spot	SCF
S8R	26.87	23.89	28.87	2.88
S4R	26.25	22.71	28.62	2.86
S4	26.94	23.33	29.36	2.93

Table.11. Solid modeling results for 6mm and 2mm plates

ELEMENT 6mm	0.4t	t	Hot-spot	THICKNESS
C3D8	15.61	14.32	16.47	18.45
C3D8R	15.25	14.15	15.99	18.12
C3D8I	16.01	14.37	17.11	17.08
C3D20R	15.18	14.19	15.84	21.55
C3D20	14.86	14.1	15.37	21.8
2mm				
C3D8	19.14	17.7	20.1	23.2
C3D8R	18.77	17.65	19.52	22.09
C3D8I	19.38	17.66	20.53	24.7

C3D20R	18.84	17.94	19.44	25.4
C3D20	18.56	17.95	18.97	25.65

Considering tensile mode, result from 8-node reduced integration element, S8R, in shell model was chosen for fatigue life calculation. In solid model 20-node reduced integration element was chosen, because two elements were modeled in thickness direction.

Tables.12 and 13 lists the test results and fatigue life estimates by surface extrapolation.

Table.12. Test results from Gurney for 6mm longitudinal non-load carrying fillet welds under tensile mode for R = 0.

<i>GURNEY</i>		<i>SHELL MODEL – NO WELDS</i>		<i>SOLID MODEL</i>	
<i>MPa</i>	<i>CYCLES</i>	<i>LIN. (CYCLES)</i>	<i>QUAD.(CYCLES)</i>	<i>LIN. (CYCLES)</i>	<i>THICK (CYCLES)</i>
180	131 000	10 600	8 200	29 000	10 300
140	274 000	22 400	17 400	61 400	21 800
110	388 000	46 000	35 700	126 000	44 700
100	494 000	119 000	92 400	325 600	115 600
<i>FOUR POINT BENDING</i>		-	-	<i>LIN. (CYCLES)</i>	<i>THICK (CYCLES)</i>
	180	-	-	8 700	6 700
	140	-	-	18 300	14 100

Table.13. Test results from Gurney for 2mm longitudinal non-load carrying fillet welds under tensile mode for R = 0.

<i>GURNEY</i>		<i>SHELL MODEL – NO WELDS</i>		<i>SOLID MODEL</i>	
<i>MPa</i>	<i>CYCLES</i>	<i>LIN. (CYCLES)</i>	<i>QUAD.(CYCLES)</i>	<i>LIN. (CYCLES)</i>	<i>THICK (CYCLES)</i>
180	102 000	2 700	3 600	12 600	4 500
160	184 000	6 300	8 300	29 300	10 600
140	276 000	19 700	25 700	90 400	32 700
120	352 000	41 500	54 300	191 000	69 100
<i>FOUR POINT BENDING</i>		-	-	<i>LIN. (CYCLES)</i>	<i>THICK (CYCLES)</i>
	180	-	-	1 900	1 600
	140	-	-	4 300	3 800

10.2 CASE STUDY II

In shell model 8-node reduced integration element was used for fatigue life estimation. In the solid model 20-node reduced integration element was used. Material constant C and slope m were taken from UKOSRP as mentioned earlier. Only pure tensile modes were considered, however, some bending was present due to secondary bending caused by the attachment.

Table.14. Unsymmetrical shell model under tensile mode with coarse and fine mesh.

<i>ELEMENT TYPE</i>	<i>0.4t (coarse / fine) MPa</i>	<i>t (coarse / fine) MPa</i>	<i>S_{hs} (fine) MPa</i>
<i>S8R</i>	<i>10.5 / 10.52</i>	<i>10.15 / 10.15</i>	<i>10.77</i>
<i>S4</i>	<i>11.24 / 10.85</i>	<i>10.24 / 10.18</i>	<i>11.3</i>
<i>S4R</i>	<i>10.42 / 10.46</i>	<i>10.14 / 10.13</i>	<i>10.68</i>

Table.15. Unsymmetrical solid model under tensile mode with coarse and fine mesh.

<i>ELEMENT TYPE</i>	<i>0.4t (coarse / fine)</i>	<i>t (coarse / fine)</i>	<i>S_{hs} (fine)</i>	<i>Through thickness</i>
<i>C3D8</i>	<i>12.55 /</i>	<i>11.49 /</i>	<i>13.26</i>	<i>13.37</i>
<i>C3D8R</i>	<i>11.91 /</i>	<i>11.28 /</i>	<i>12.33</i>	<i>12.65</i>
<i>C3D8I</i>	<i>13.18 / 13.24</i>	<i>11.89 / 11.6</i>	<i>14.34</i>	<i>14 / 14.1</i>
<i>C3D20R</i>	<i>12.99 / 13.05</i>	<i>11.58 / 11.63</i>	<i>14</i>	<i>14.28 / same</i>
<i>C3D20</i>	<i>13.23 / 13.21</i>	<i>11.56 / 11.6</i>	<i>14.29</i>	<i>14.35 / same</i>

Nominal stress was 10 MPa in all cases and thus stress concentration factors were computed for selected elements used in fatigue life calculation.

Table.16. Fatigue life comparison.

<i>MADDOX / MPa</i>	<i>MADDOX / CYCLES</i>	<i>SHELL MODEL</i>	<i>SOLID MODEL</i>
<i>150</i>	<i>266 350</i>	<i>350 000</i>	<i>148 000</i>
<i>100</i>	<i>787 880</i>	<i>1 179 000</i>	<i>499 000</i>
<i>50</i>	<i>8 014 700</i>	<i>9 430 000</i>	<i>3 947 000</i>

10.3 CASE STUDY III

No significant difference was observed from two different modeling approaches. Predicted structural hot-spot stress was the same using contact approach versus simplified modeling approach. Elements used were 20-node reduced integration hexagonal elements. Refer to Table.17 for the fatigue life estimates.

Table.17. Contact model from UKOSRP project for longitudinal attachment under bending mode.

UKOSRP	UKOSRP	PREDICTED		
		LINEAR	QUADRATIC	THROUGH THICKNESS
280	207 300	105 600	93 300	60 800
200	482 000	289 700	256 000	167 000
140	1426 400	1 426 000	746 600	486 800

10.5 CASE STUDY IV

Quadratic plane strain elements with reduced integration (CPE8R) were primarily used in all fatigue life prediction methods. All three surface extrapolation methods failed in this study. First extrapolation point was located in the region of lower principal stress, thus causing problem with extrapolation. As a result, hot-spot stress was lower than nominal stress. No fatigue lives were calculated as they would be meaningless. Element size did not have effect for extrapolation methods. Element type had effect on results.

Linear incompatible mode elements (CPE4I) gave comparable results with quadratic elements. As long as element distortion was not present, these linear elements gave good results. Advantage would come more evident in larger models. No difference was noticed in small models. Incompatible mode element has enhanced formulation for deformation gradient. This enhancement to deformation gradient is internal to the element, it is not associated with nodes on element edges.[2] Refer to Tables.18 and 19 for fatigue life estimates based on structural stress through thickness integration at the weld toe.

Appendix 3 contains surface extrapolation results.

Table.18. *Through thickness integration results at weld toe for 38mm plate, 14mm leg*

σ_{nom} (MPa)	σ_{hs} / N(cycles) $m = 3.57$	σ_{hs} / N(cycles) $m = 2.7$	UKOSRP (cycles)
200	203.1 / 159 400	204.1 / 253 700	171 520
120	121.8 / 989 100	122.4 / 1 009 000	833 000
90	91.35 / 2 762 400	91.8 / 2 193 800	2 326 700

Table.19. *Through thickness integration results at weld toe for 25mm plate, 10mm leg*

σ_{nom} (MPa)	σ_{hs} / N (cycles) $m = 3.57$	σ_{hs} / N (cycles) $m = 2.7$	UKOSRP (cycles)
230	233.6 / 96 700	234.55 / 174 300	127 300
160	162.5 / 353 400	163.2 / 464 000	712 400
100	101.6 / 1 889 700	102 / 1 650 500	2 915 400

Full penetration welds were considered as a sensitivity study. In the light of failure, fatigue lives based on nominal stress of 200 MPa were computed for 38mm fillet welded joint as 268 000 cycles. For 25mm fillet welded plate at nominal stress of 230 MPa result was 183 500 cycles. Material constant C and slope were taken from UKOSRP program and are mentioned earlier.

Through thickness integration to obtain structural stress at the weld toe was done to 38mm plate with 14mm leg length and 25mm plate with 10mm leg length. Stress concentration factor and thickness penalty were ignored in this method as these effects are included in the procedure. Load was adjusted such that nominal bending stress corresponded testing conditions. Nominal stresses are from UKOSRP tests.

In fracture mechanics approach simple plate with edge crack was analyzed first.

Analytical solution for stress intensity factor was calculated from the following relationship.[10]

$$K_1 = F_s \sqrt{p \cdot a} = 1.12 \cdot 100 \text{MPa} \sqrt{p \cdot 4 \text{mm}} = 397 \text{MPa} \sqrt{\text{mm}}$$

Both crack tip modeling techniques gave same results, $K_1 = 412.1 \text{MPa} \sqrt{\text{mm}}$. Difference to analytical solution was about 3.5 %.

Next, crack modeling was extended a step further into cruciform joint. Crack tips in cruciform joint were modeled using 8-node quadratic elements without collapsed elements. This was done because solutions from Mode 1 fracture in simple plate were same under both crack tip modeling techniques. Cruciform joint, atleast during initial stages exhibits Mode 1 failure. Fracture mechanics analysis gave comparable results with actual testing data. Refer to Table.20 for method and predicted fatigue life. Appendix 1 and 2 contains simple plate mesh and load/non-load carrying cruciform joint under four point bending.

Table.20. *Fracture mechanics results compared to testing results from UKOSRP.*

EXPERIMENTAL, UKOSRP		LEFM / PREDICTED	
RANGE (MPa)	LIFE (cycles)	RANGE (MPa)	LIFE (cycles)
200	171 520	200	416 500
120	833 000	120	1 117 400
90	2 326 700	90	2 760 000

Effective notch approach was applied to 38mm thick plate with 14mm weld leg length with full penetration welds. Element type was 8-node reduced integration shell element. Principal stress at the notch was 279.8 MPa with 100 MPa nominal stress. In this case nominal stress was equal to bending stress. Mesh was refined at the notch location such that element size was 0.13mm by using same element type. Principal stress was calculated as 276.6 MPa. Elastic stress concentration factor therefore was computed as 2.76 with 1mm radius. Quite severely conservative results with 200 MPa nominal stress predicted fatigue life of 5 100 cycles versus 171 000 cycles.

Element type was modified to plane strain condition. Fully integrated 8-node plane strain element with same mesh predicted 282.7 MPa which will result even more conservative fatigue life estimation.

11 MULTIVARIABLE REGRESSION AGAINST CASE STUDIES

Multivariable regression did not predict thickness effect in butt joints. Coefficient in thickness was small enough not to predict any difference even if thickness of the plate changed from 2mm to 50mm. Multivariable regression equation predicts only 300 000 cycles difference in fatigue life going from 2mm plate to 50mm plate.

Two derived equations based on collected data have been compared to Gurney's experiments on thin longitudinal attachments. Attachments were loaded in tension. Equations derived were

(54) where stress range and stressed plate thickness were considered and (55) where loading mode was added.

$$\log N = -2.564 \cdot \log s + 0.577 \cdot \log t + 10.452 \quad (54)$$

$$\log N = -2.692 \cdot \log s + 0.4939 \cdot \log t - 0.2073 \cdot \log r + 10.821 \quad (55)$$

Equation (55) presents a problem if tensile mode is considered. It was established earlier that r was zero for tensile mode. Observation to (55) reveals that $\log r$ tends to negative infinity for $r = 0$. Therefore, equation (55) would be valid only for bending mode. However, legitimate question might be whether tensile tests are truly tensile loaded. As a sensitivity study r in (55) was made small (0.25/0.025) and estimated fatigue life computed. Results for 6mm and 2mm specimens are shown in Tables.21 through 24.

Table.21. Multivariable prediction for 6mm thickness. Three variable equation under tensile mode. $r = 0.25 / 0.025$

Gurney / MPa	Gurney / Cycles	MVR / log N	MVR / N
180	131 000	5.26 / 5.47	181 500 / 292 500
140	274 000	5.55 / 5.76	357 000 / 575 500
110	388 000	5.83 / 6.04	683 500 / 1 101 500
100	494 000	5.95 / 6.15	883 400 / 1 424 000

Table.22. Multivariable prediction for 6mm thickness. Two variable equation under tensile mode.

Gurney / MPa	Gurney / Cycles	MVR / log N	MVR / N
180	131 000	5.12	131 400
140	274 000	5.40	250 200
110	388 000	5.67	464 400
100	494 000	5.77	593 000

Table.23. Multivariable regression prediction for 2mm thickness. Three variable equation under tensile mode. $r = 0.25 / 0.025$

Gurney / MPa	Gurney / Cycles	MVR / log N	MVR / N
180	102 000	5.02 / 5.23	105 500 / 170 000
140	184 000	5.32 / 5.52	207 500 / 334 500
110	276 000	5.6 / 5.81	397 200 / 640 000
100	352 000	5.71 / 5.92	513 500 / 827 500

Table.24. Multivariable regression prediction for 2mm thickness. Two variable equation under tensile mode.

Gurney / MPa	Gurney / Cycles	MVR / log N	MVR / N
180	102 000	4.84	69 700
140	184 000	5.12	132 700
110	276 000	5.39	246 400
100	352 000	5.5	314 500

Gurney found that decreasing stressed plate thickness lead to decrease in fatigue life in the case of longitudinal attachments for other geometry being constant. This could have been due more rapid crack propagation through the plate, possibly influenced by the double stress gradient present in longitudinal attachment. Swedish standard, BKS takes into account “thinness effect” for plates thinner than 25mm.

$$\frac{S}{S_{ref}} = \left(\frac{25}{t} \right)^{0.0763} \quad (56)$$

where $S = S_{ref}$ for $t \geq 25mm$. S_{ref} refers to fatigue strength of the joint and S is the fatigue strength after correction. For 6mm plate $S = 1.115 \cdot S_{ref}$ and for 2mm plate $S = 1.212 \cdot S_{ref}$, however, fatigue strength tends to decrease with decreasing plate thickness in longitudinal attachment. As a result, validity of Swedish standard may not apply to longitudinal attachment. Collected data contained symmetrical and unsymmetrical longitudinal attachments. Unsymmetrical attachments would exhibit higher fatigue strength than symmetrical attachments due secondary bending stress occurring in the weld toe region which would induce compressive stress component at the weld toe. As a result, stress peak would be lower than in symmetrical joint. Maddox’s unsymmetric longitudinal attachment was investigated with multivariable regression results. Refer to Table.25 for preliminary results.

Table.25. Multivariable prediction for 12.7mm thickness. Two variable equation is used.

Maddox / MPa	Maddox / Cycle	MVR / log N	MVR / N
150	266 350	5.51	323 000
100	787 880	5.96	914 000
50	8 014 700	6.73	5 404 000

Case study from UKOSRP project was 38mm stressed plate thickness subjected to four point bending. Application of multivariable prediction would not take into account thickness correction based on IIW or BS 7608 recommendations. This is because derived equations are based on regression analysis from collected data. Refer to Table.26 for bending results.

Table.26. Longitudinal attachment under four point bending from UKOSRP. Predicted fatigue life is based on three variable equation.

UKOSRP MPa	UKOSRP Cycles	MVR / log N	MVR / N
280	207 300	5.01	103 100
200	482 000	5.41	255 200
140	1426 400	5.82	666 600

Cruciform joints from UKOSRP project were subjected to four point bending. Two stressed plate thicknesses were considered, 25mm and 38mm.

$$\log N = -1.6337 \cdot \log s - 0.049517 \cdot \log t + 9.16535 \quad (57)$$

$$\log N = -1.41 \cdot \log s - 0.1 \cdot \log t + 0.165 \cdot \log r + 8.765 \quad (58)$$

Table.27. Cruciform joints under four point bending (UKOSRP), 38mm plate thickness with three variables.

UKOSRP, MPa	UKOSRP, Cycles	MVR / log N	MVR / N
200	171 520	5.68	477 000
120	833 000	5.99	980 000
90	2 326 000	5.17	1 470 600

Table.28. Cruciform joints under four point bending (UKOSRP), 25mm plate thickness with three variables.

UKOSRP MPa	UKOSRP Cycles	MVR / log N	MVR / N
230	127 300	5.57	375 600
160	712 400	5.80	626 600
100	2 915 400	6.08	1 215 600

Two variable equation and three variable equation were also applied to tensile mode. Equation is applied to load-carrying cruciform joint under tensile mode. Joint has full penetration welds. Failure location is at the weld toe. Weld leg length is 12 mm. Tests were conducted in air under varying mean stress. The effect of mean stress is not taken into account.

Table.29. Cruciform joints under tensile mode (UKOSRP), 25mm plate thickness with three variables.

UKOSRP MPa	UKOSRP Cycles	MVR / log N	MVR / N
280	98 100	5.72	523 000
160	393 000	6.06	1 151 600
100	2 349 600	6.35	2 234 200

Table.30. Cruciform joints under tensile mode (UKOSRP) 25mm plate thickness with two variables.

UKOSRP MPa	UKOSRP Cycles	MVR / log N	MVR / N
280	98 100	5.24	172 300
160	393 000	5.63	429 800
100	2 349 600	5.97	926 400

12 DISCUSSION

12.1 Multivariable regression

One obvious drawback of multivariable regression performed here is that linear relationship is assumed between different variables. This may not be the case as seen earlier. For example, relationship between fatigue strength and thickness in butt joints loaded in tension based on collected data may not be linear, rather exponential.

Derived equations that approximate fatigue behavior in certain details do not take into account, for example, welding process, amount of residual stress at the joint, joint environment, testing frequency and mean stress. One thing in common to all failures in tests is a weld toe failure. As multivariable regression was performed to all three details, following observations were made. In all tested cases, multivariable regression caused clockwise rotation of fatigue estimation curve as compared to data regression curve based on one thickness. Point of intersection of multivariable regression curve and data regression curve lies around $\log N = \sim 4.8$ to ~ 5.7 , 65 000 to 500 000 cycles, respectively. In general, this was the case in most tested joints and thicknesses. Therefore at these cycles multivariable regression line predicts higher fatigue life than regression line based on data and predicted fatigue strength at 2 000 000 cycles would be lower. Refer to Figure.43 for sample from longitudinal attachment database.

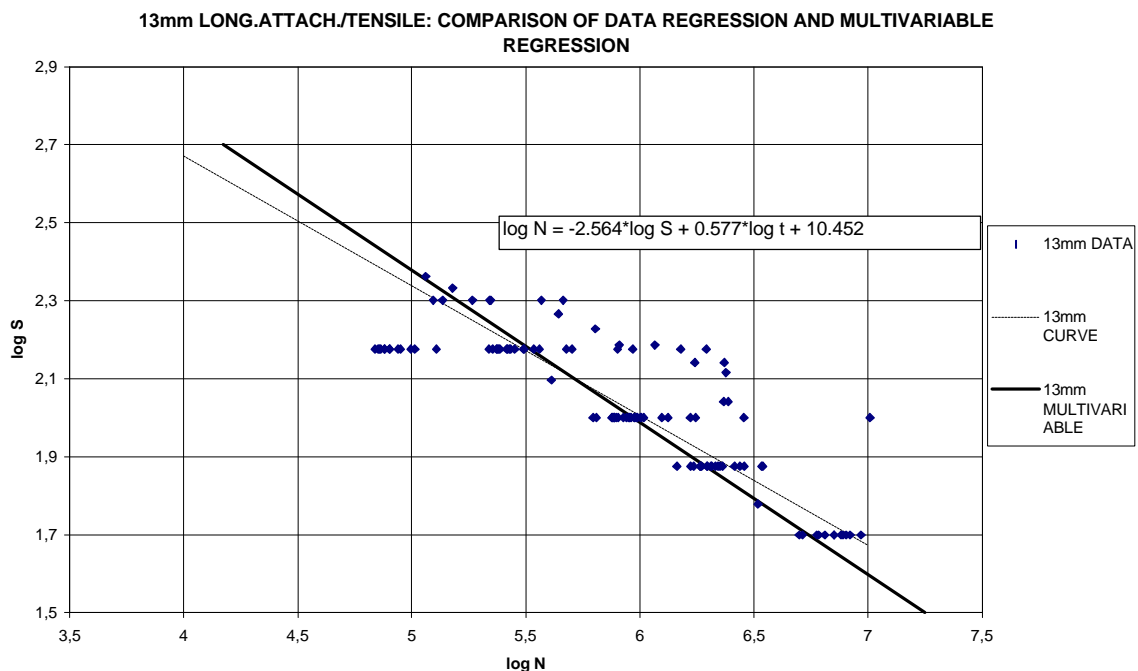


Figure.43. Comparison of multivariable regression to 13mm thickness regression in longitudinal attachment joint.

Based on derived equations in multivariable regression, it would seem logical to draw the following conclusion as far as fatigue life of joint is concerned. Of the variables considered, butt joints might be most sensitive to stress range then loading mode followed by thickness. Same relationships are observed in cruciform joints. However, longitudinal joints would appear to be most sensitive to stress range and main plate thickness followed by loading mode. Stress range used in multivariable regression equations is nominal stress. If hot-spot stress is calculated from FE-model, nominal value needs to be multiplied by a relevant stress concentration factor. Based on results, it is necessary to collect more data under bending mode in all three joint types. Collected data needs to be broken down more, for example, weld leg length in cruciform and longitudinal attachments could be chosen as a variable. Derived equations have been applied to some test results to see how well does equation describe the data or if at all.

All tensile results considering stress range and thickness fell almost on single line based on derived equation. This suggests that multivariable regression equation describes poorly thickness effect in butt joints under tensile loading. Earlier, relationship between fatigue strength and thickness had been established to follow exponential model. Another variable, bending mode, was added into the equation.

As an example from tensile case, 16mm thick butt joint tested at 220 MPa under tensile loading in tests gave fatigue life of 93 300 cycles. Now, applying equation multivariable equation gives estimated fatigue life of 324 000 cycles. Single result does not provide much information about overall fit, so coefficient of determination was calculated based on all 16mm tensile butt data.

As a result, r^2 was equal to 0.28. Relationship is poor.

As an example for bending loading, 10mm butt joint was considered and coefficient of determination was computed. The result r^2 was 0.11.

Similar procedure was done to cruciform joints. All tensile results fell close to single line with only slight variation. Bending curves were above tensile curves, however, bending curves seem converge to tensile curves at longer lives, over 2 000 000 cycles.

Scatter under tensile loading in longitudinal attachment was more than for butt joint or cruciform joint. Significant scatter was observed under bending mode. Under both, tension and bending, fatigue strength decreased as plate thickness decreased. Overall, correlation of multivariable curve in longitudinal attachment was better than in butt or cruciform joints. Main controlling geometrical parameters in butt joint are plate thickness, weld cap width, weld toe angle and amount of penetration. Few of the collected test data reported weld

cap width and weld toe angle. Amount of penetration was reported but at the moment it was ignored. Thus, only plate thickness was considered. Other non-geometrical parameters such as stress ratio, welding process and residual stress were ignored. In order to improve the fit in multivariable regression percent fit has to increase and residual standard deviation decrease. Residual standard deviation was calculated as the difference between predicted fatigue life based on linear model and test result. Residuals were graphed against stress range and thickness. If thickness has a strong relationship to fatigue strength in butt joint, then residual versus variable graph should show this correlation as better percent fit and decrease in residual standard deviation. Model based on linear regression was expressed as

$$\log N = -1.4807 \log s + 8.896 \quad (59)$$

and residual as

$$Residual = \log N_{test} - \log N_{predicted} \quad (60)$$

For the first case, residual was the difference in fatigue life based on one independent variable equation. In the second case, residual was based on two independent variable equation, stress range and thickness.

$$\log N = -1.4878 \log \Delta s - 0.03317 \log t + 8.929 \quad (61)$$

Figure.44 shows residuals as each variable is added in butt joint. [26]

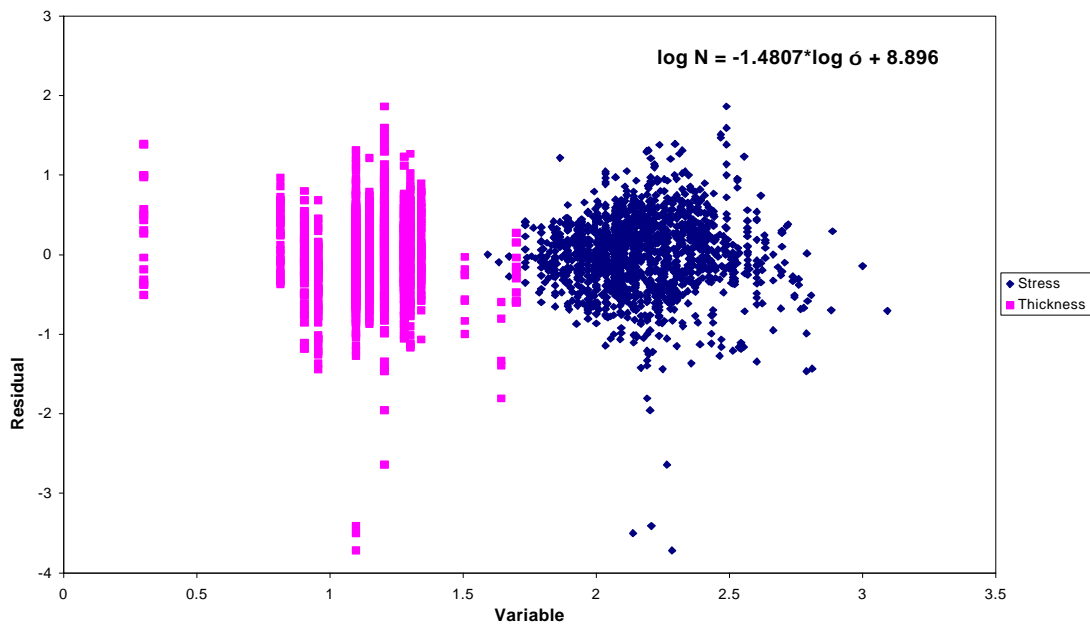


Figure.44. Residual correlation to each variable in butt joint.

Visual inspection of Figure.44 shows that residual standard deviation is increased as a result of adding a plate thickness into multivariable regression. Results are shown in Table.31.

Table.31. Percent fit and residual standard deviation for the butt joint.

EQUATIONS	Percent Fit	RSD	TEST VALUE
$\log N = -1.4807 \log \mathbf{s} + 8.896$	28.3 %	0.49	2.08
$\log N = -1.4878 \log \mathbf{s} - 0.03317 \log t + 8.929$	28.3 %	0.493	0.103
$\log N = -1.4809 \log \mathbf{s} - 0.0701 \log t + 0.331 \log r + 8.976$	28.4 %	0.492	0.147

In the case of longitudinal attachment percent fit increased as thickness of the stressed plate was entered into the equation, but residual standard deviation increased as well. In order to introduce better fit RSD needs to decrease. Refer to Figure.45 for residuals as each variable is added.

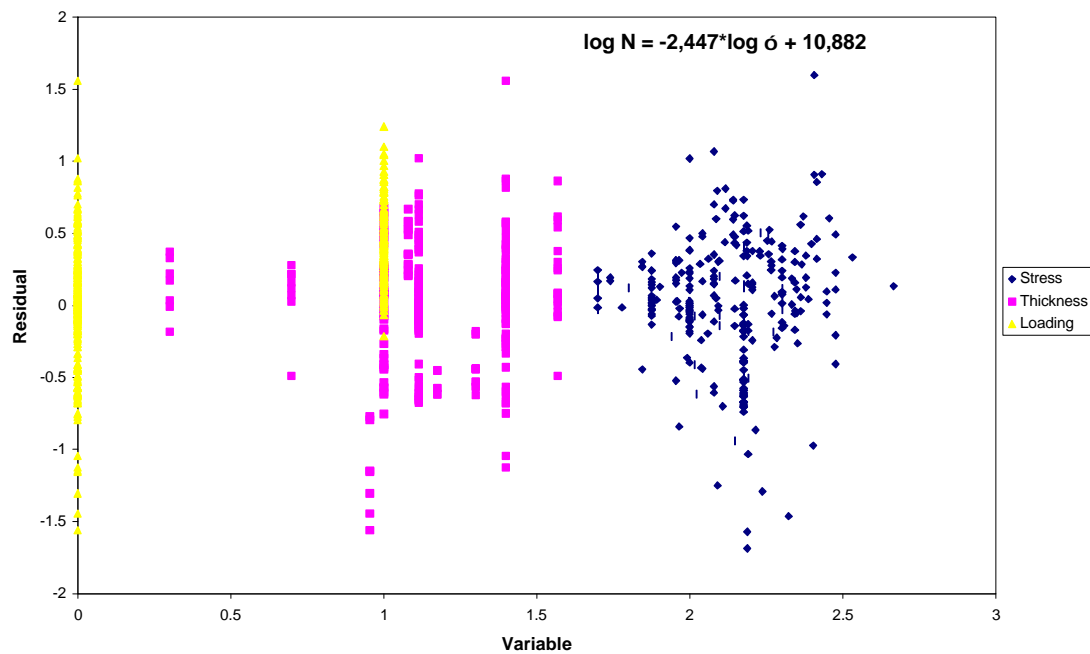


Figure.45. Longitudinal attachment residual correlation to each variable.

$$\log N = -2.447 \log \mathbf{s} + 10.882 \quad (62)$$

Table.32. Percent fit RSD for longitudinal attachment.

Equation	Percent Fit	RSD	TEST VALUE
$\log N = -2.447 \log \mathbf{s} + 10.882$	51 %	0.43	17.9
$\log N = -2.564 \log \mathbf{s} + 0.577 \log t + 10.452$	56 %	0.41	5.91
$\log N = -2.692 \log \mathbf{s} + 0.4939 \log t - 0.2073 \log r + 10.821$	50 %	0.54	-

So called t statistic was calculated for the set of data which was based on 95% confidence interval. This means that true value lies within ± 1.96 times the standard deviation away from the mean value. 5% significance level was calculated as 1.965, this shows that thickness is significant and should be included in the model. Decrease in percent fit was observed when loading mode was included. Therefore, no test value was computed. Linear model is valid between thickness and fatigue strength as well as loading mode and fatigue strength. Clear relationship was established earlier for the thickness based on two variable equation. Fatigue strength tends to decrease with decreasing plate thickness. This trend was seen as decrease in residual standard deviation and increase in percent fit. Residual standard deviation was calculated as follows

$$RSD = \sqrt{\frac{\sum_{i=1}^n (\log N_i - c - a_1 \log s_i - a_2 \log t_i \dots)^2}{n - (m + 1)}} \quad (63)$$

where $\log N_i$ is the test result and c, a_1, a_2 are the solved coefficients. Here n is the number of entries and m is the number of independent variables. Percent fit was calculated as follows

$$PercentFit = \frac{S_t - S_r}{S_t} \quad (64)$$

where S_t and S_r are defined earlier.

Most encouraging results from multivariable regression were for longitudinal attachment. Fatigue life prediction has discrepancy but general trend from derived equation follows along with test results. Derived model predicts decrease in fatigue life as stressed plate thickness is decreased. Gurney [6] made same observation from his tests. Severe approximation is caused by ignoring other local and global geometry of the joint. This issue is clear downfall for fatigue life estimates. Refer to Figure.46 for multivariable prediction. Lowest plate thickness shows lowest fatigue strength.

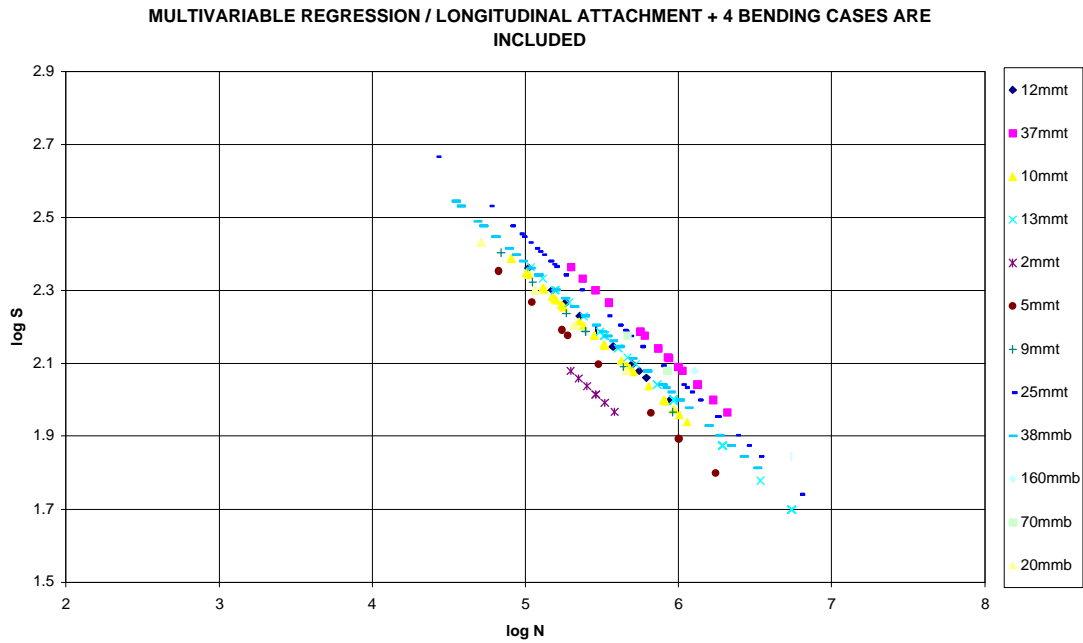


Figure.46. Multivariable regression for longitudinal attachment under tensile mode.

Thickness effect prediction using multivariable regression. Coefficient in thickness is about twice as in standards. Result should be treated with care.

$$\log N = -2.564 \log S + 0.577 \log t + 10.452 \quad (65)$$

Effect of loading mode was considered as follows. Same behavior was observed under bending. As plate thickness decreased fatigue strength tended to decrease.

$$\log N = -2.692 \log S + 0.4939 \log t - 0.2073 \log r + 10.821 \quad (66)$$

Coefficient in thickness is about same as in (65), however, difference is large enough to cause variation in fatigue life estimates. Cruciform joint has not been separated by load or non-load carrying joint. Refer to Table.33 for percent fit and residuals.

Table.33. Percent fit and RSD for cruciform joints.

Equation	Percent Fit	RSD	TEST VALUE
$\log N = -1.824 \log S + 9.673$	39.4 %	0.464	27.8
$\log N = -1.6337 \log S + 0.0495 \log t + 9.165$	39.5 %	0.463	0.99
$\log N = -1.41 \log S + 0.1 \log t - 0.165 \log r + 8.765$	41.4 %	0.457	6.2
$\log N = -1.6944 \log S + 0.16127 \log r + 9.231$	41.6 %	0.455	6.69

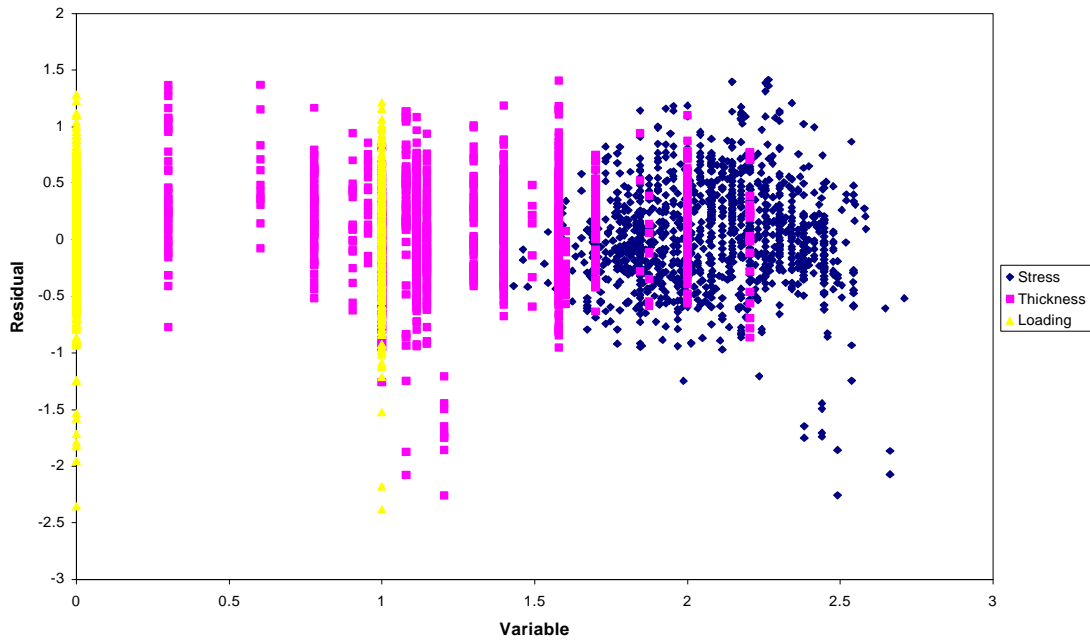


Figure.47. Residual correlation to each variable for cruciform joint.

Percent fit has increased as thickness and loading mode have been added. Residual standard deviation in turn has decreased. This means that parameters have significant effect and are favourable in the use multivariable regression. Changes in percent fit and RSD are not large, but trend is seen as positive.

Test value was computed as follows

$$TestValue = \sqrt{\frac{(Increase_ \% fit)(dof)}{100 - (new_ \% fit)}} \quad (67)$$

12.2 Case study I

Fatigue life predictions for thin longitudinal attachment were rather conservative. Stress concentration factors for 6mm and 2mm plates were all over two. Comment is based on the following element selection. Shell modeling was made with 8-node reduced integration elements. Modeling was also made with linear elements, however, 8-node element was chosen. Linear elements might give reasonable results as pure bending for symmetric attachment is modelled. On the other hand, mesh density would have to be greater. Solid modeling was made with 20-node reduced integration elements rather than 8-node linear elements for the same reasons. Even under tensile mode element selection has an effect on stress distribution in the vicinity of the attachment end. Refer to Figures.44 through 49 for principal stress distributions for different element types. Transverse principal stress distribution for

symmetrical longitudinal attachment under tensile and bending mode are shown in Figures.48 and 49. Solid elements are used for modeling.

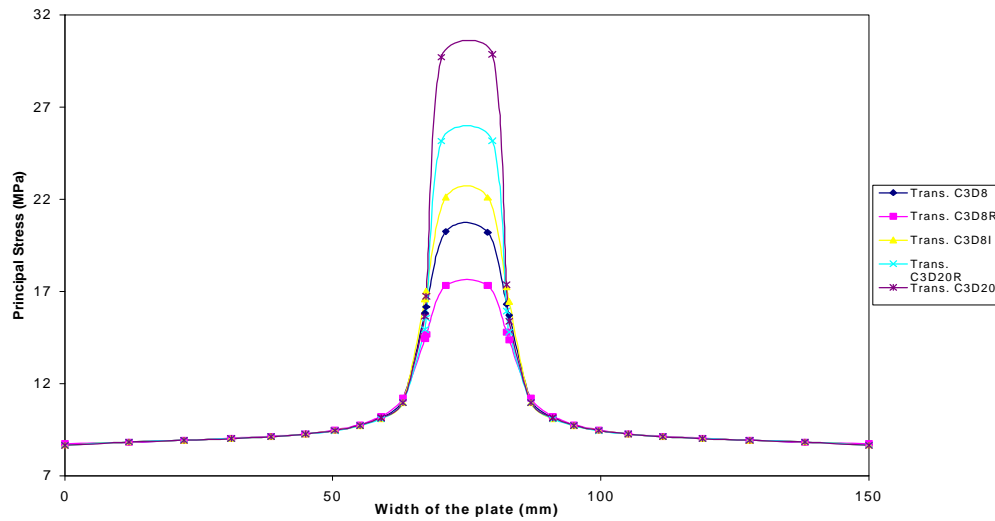


Figure.48. Solid symmetric 6mm longitudinal attachment under tensile mode.

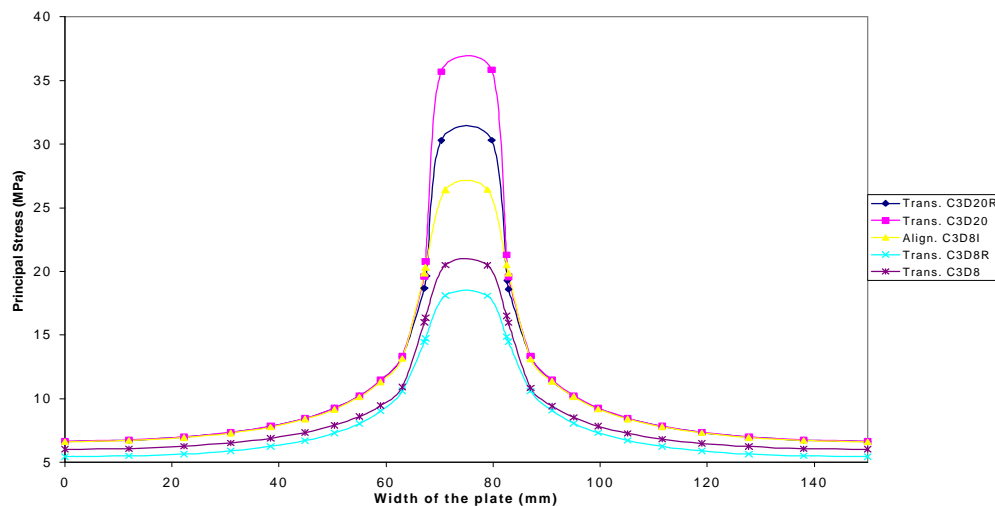


Figure.49. Solid symmetric 6mm longitudinal attachment under bending mode.

Tensile mode causes more abrupt stress peak at the attachment end than bending mode. Stress peak, however, is higher under bending mode than under tensile mode. In bending principal stress rises more gradually to the peak value. Incompatible linear mode elements CPE8I behave better than linear elements under bending mode. Because longitudinal attachment exhibits double stress gradient, effect of element selection to principal stress distribution approaching the weld toe was investigated. Refer to Figures.50 and 51 for the effect of element selection.

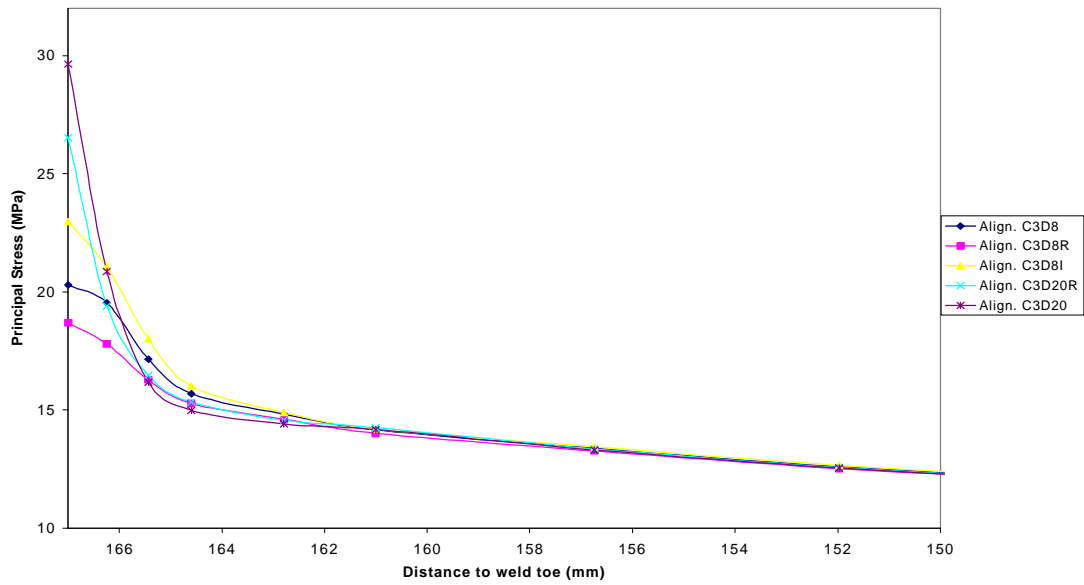


Figure.50. Solid symmetric 6mm longitudinal attachment under tensile mode. Principal stress distribution approaching weld toe.

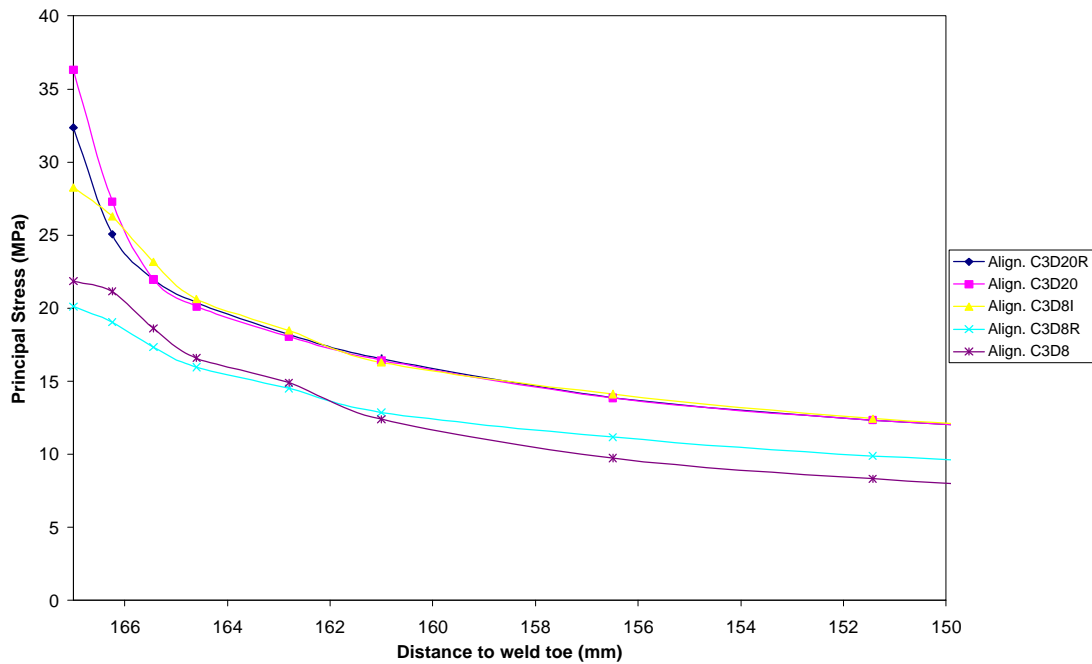


Figure.51. Solid symmetric 6mm longitudinal attachment under bending mode. Principal stress distribution approaching the weld toe.

As seen in Figures.50 and 51, principal stress distribution is more gradual and severe under bending mode than under tensile mode. Stress paths are taken on the surface from tensile side. Comparison is made with 20-node fully integrated solid elements. These elements should work fine under tensile and bending modes. One reason for higher

principal stress peak along the surface of the joint for bending case was lesser stiffness on the tensile side of the joint. Under pure bending both attachment end welds contribute to the stiffness of the joint. As joint is subjected to pure bending, mainly one attachment end weld is supporting the bending stress on the tensile side, as a result weld toe region on the tensile side is seeing more strain. No membrane stress is present as end is fixed on “frictionless” roller. These thoughts hold true for linear elastic material.

Principal stress distributions based on different elements were studied in 2mm symmetric longitudinal attachment. Figure.48 illustrates quite sudden stress rise from nominal value and the importance of boundary conditions. Small disturbances are seen in the vicinity of stress peaks. These are caused by wrong location of one of the boundary conditions.

Transverse rigid body mode was fixed at one corner of the joint rather in the center of the joint. Fixed corner caused unsymmetric loading to the joint which disturbed the peak principal stress. However, overall trend is still seen.

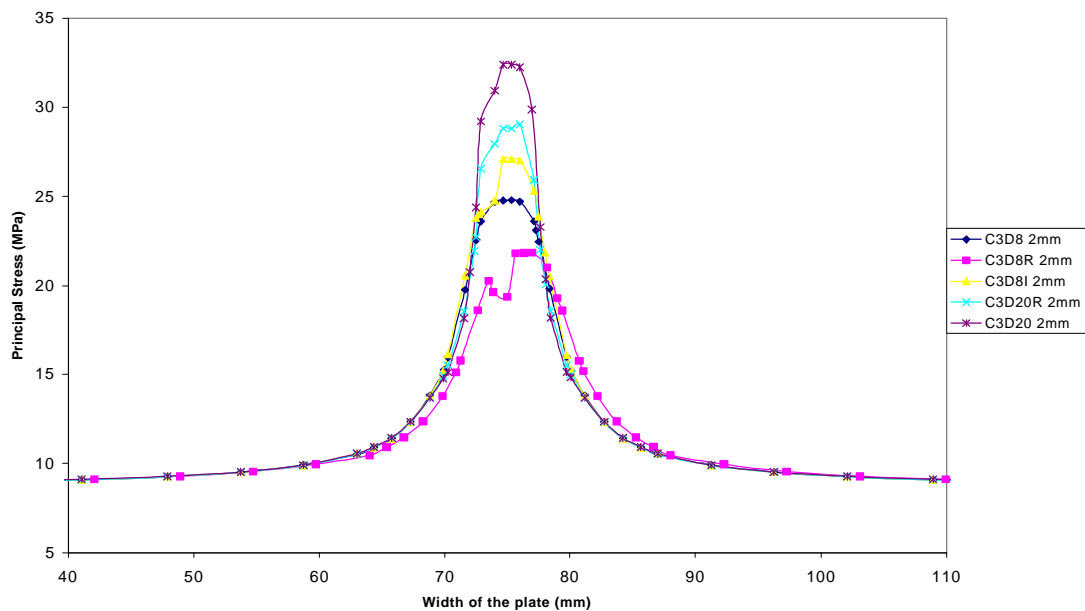


Figure.52. Symmetric 2mm longitudinal attachment under tensile mode. Transverse principal stress distribution to the weld toe.

Principal stress distribution for the 2mm plate shows same behaviour as for 6mm plate. Peak stress is higher in 2mm plate as compared to 6mm plate. Interestingly, despite of this Gurney concluded that 2mm showed higher fatigue strength than 6mm plates. Clearly, uncertainties exist and more data would have to analyzed. On the other hand, material model is linear elastic. Local plasticity is likely at the attachment end due to high stress

concentration factor and applied stress ranges. As a result, linear model over estimates stress results which causes conservative fatigue life estimation. Refer to Figure.53 for 2mm stress paths.

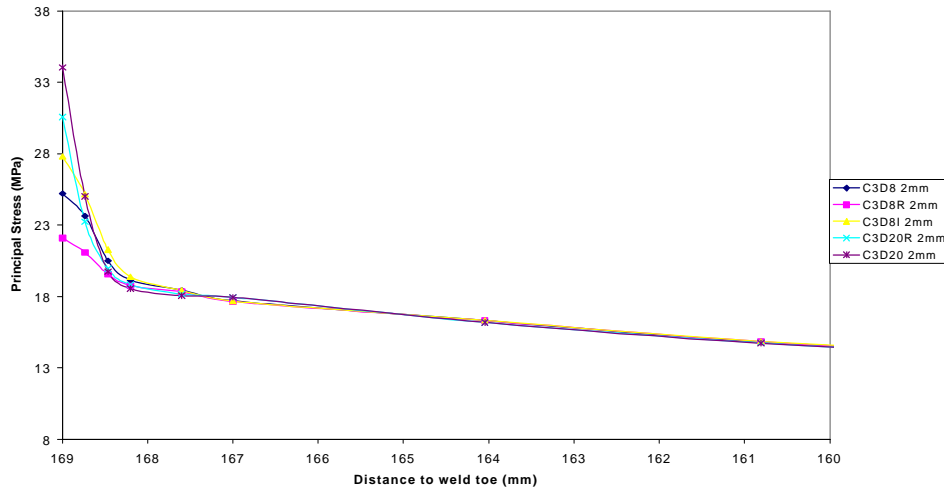


Figure.53. Symmetric 2mm longitudinal attachment under tensile mode. Principal stress distribution approaching the weld toe.

12.3 Case study II

Maddox’s unsymmetrical longitudinal attachment was studied. Principal stress distributions are plotted for both sides of the attachment. Principal stress distribution transverse to the weld toe for unsymmetrical longitudinal attachment are shown in Figure.54. Plot contains shell and solid element results.

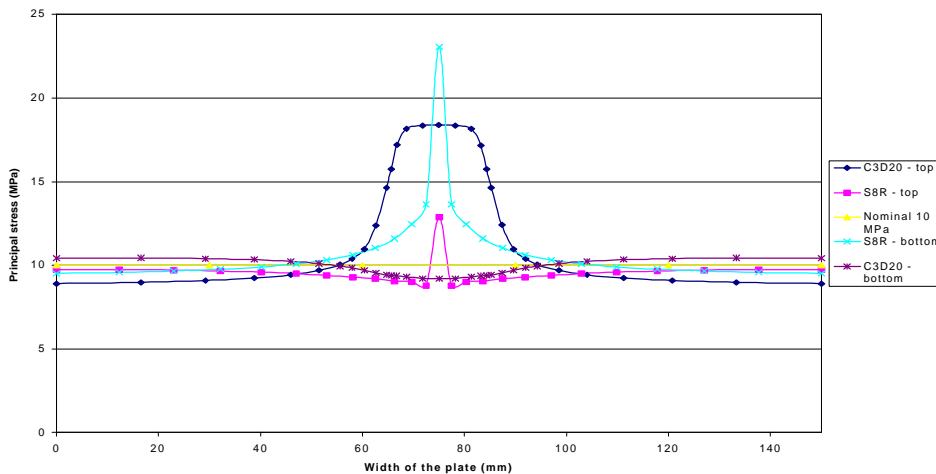


Figure.54. Principal stress distributions for shell and solid models transverse to the weld toe.

First, shell model has been modeled without inclined elements representing welds. On the attachment side shell element predicts lower peak stress at the weld toe than solid element. In addition, shell element predicts decrease of principal stress below its nominal value approaching the weld toe transverse to the loading direction. Lower peak stress in shell element is due to linear stress distribution in shell element. Thus, non-linear portion of the principal stress close to the weld toe cannot be represented by shell element. Dip below the nominal value close to the weld toe is due to the same reason. Shell element is unable to pick up the non-linear portion of the stress transverse from the weld toe.

On the bottom side, principal stress dips below its nominal value at the weld toe in solid model. In the shell model, high principal stress peak is observed rising directly from the nominal value. Dip at the weld toe in principal stress in solid model is due to secondary bending stress introduced by single sided attachment. Secondary bending stress introduces compressive stress on the attachment side at the weld toe region. Stiffness caused by single sided attachment does reach on the other side of the stressed plate, however, stress peak caused by the attachment end is not seen on the bottom side. Strain on the flat side of the stressed plate is reduced due to stiffening effect. This is seen as dip in nominal stress. This is partly due to linear elastic material as well, although stress values are below yield strength anyway.

High peak at the bottom side in shell model is due to linear stress distribution across shell element, bottom surface loaded in tension and reduced stiffness caused by the attachment. Attachment in shell model does not provide as much stiffness as in solid model, especially because welds are not modeled. This reduces the attachment stiffness, therefore adding onto stress peak in linear elastic material. These thoughts in mind, it would seem reasonable to see high peak in principal stress on the flat side of the attachment. Figure.55 illustrates the difference in principal stress distribution between shell model and solid model as approaching the weld toe.

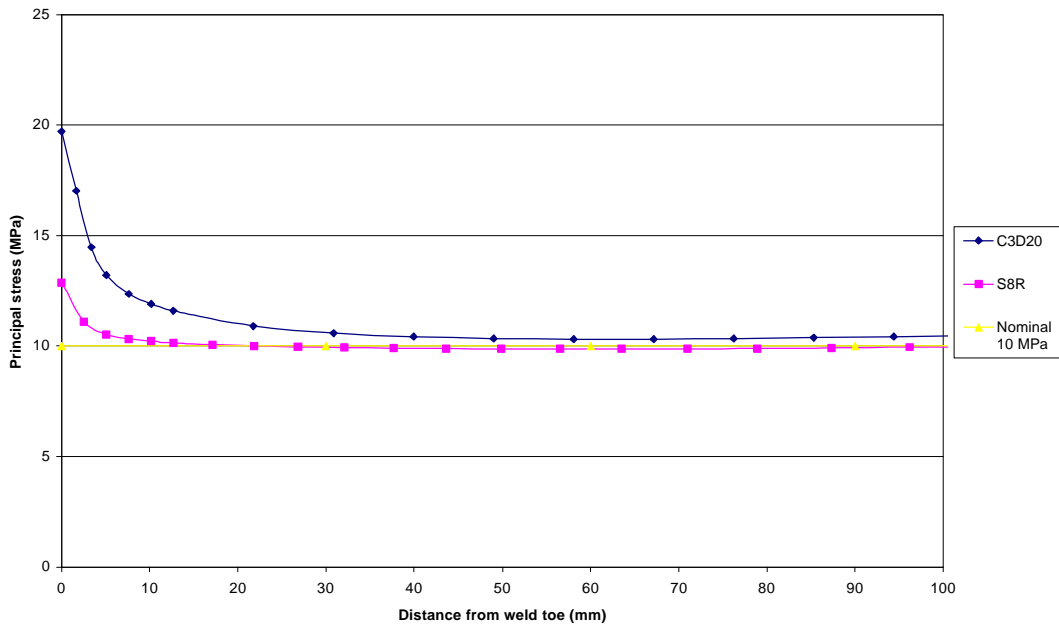


Figure.55. Solid and shell element comparison for principal stress distribution approaching the weld toe.

Principal stress distributions were studied for tested unsymmetrical longitudinal attachment by Maddox as well as symmetrical one. Main purpose was to see the effect of single sided attachment into stress distributions in the vicinity of the weld toe. Refer to Figures.56 through 58.

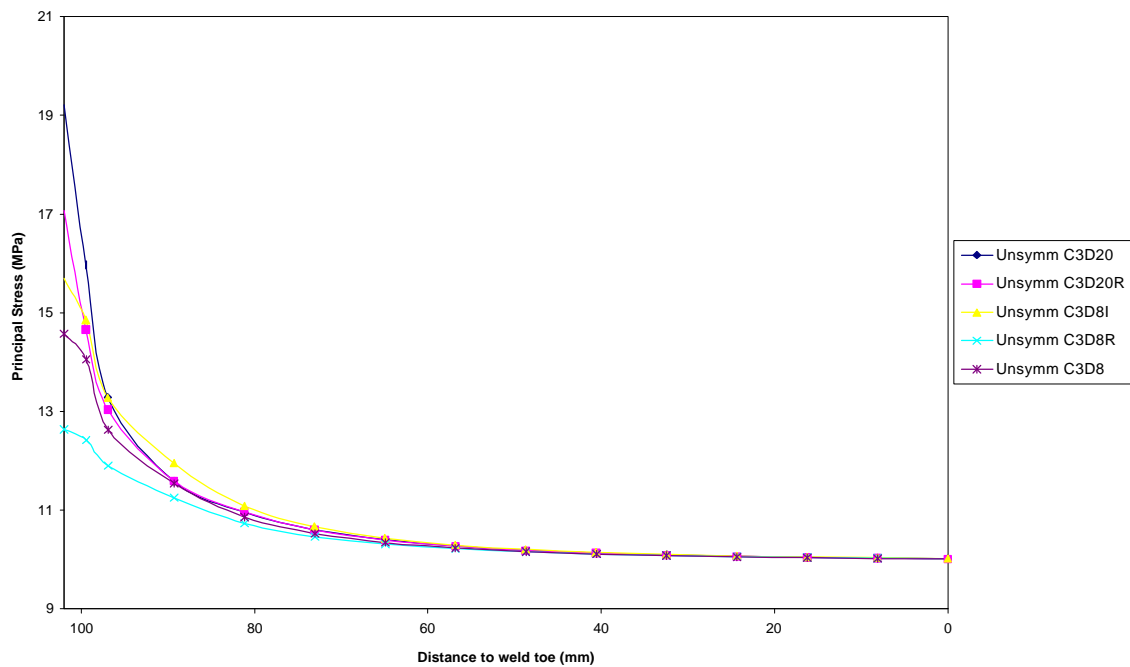


Figure.56. Axial stress distribution approaching the weld toe for unsymmetrical longitudinal attachment under tensile mode. Plate thickness is 12.7mm.

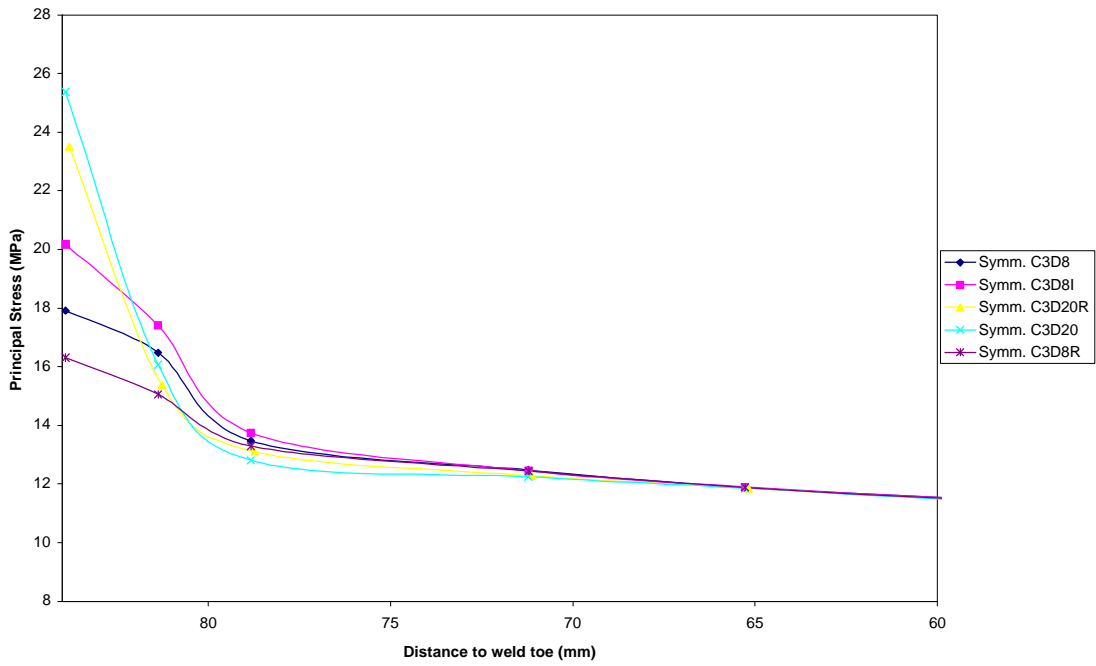


Figure.57. Axial stress distribution for symmetrical longitudinal attachment under tensile mode. Plate thickness is 12.7mm.

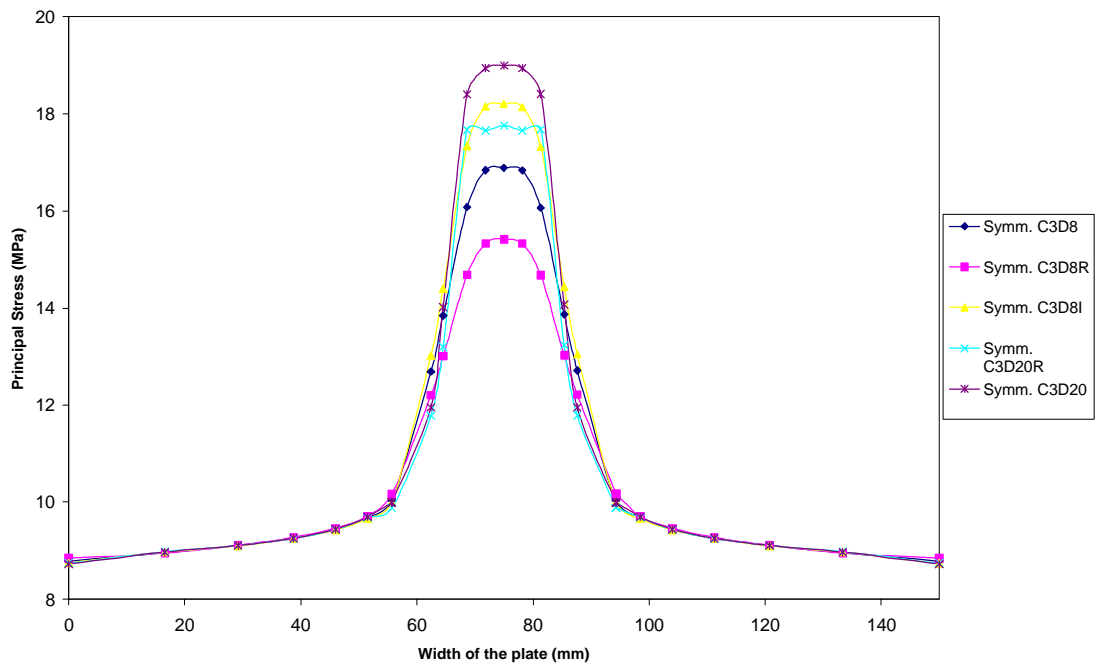


Figure.58. Transverse principal stress distribution for symmetric longitudinal attachment.

Symmetric attachment exhibits higher peak stress at the weld toe. This is due to secondary bending stress occurring in unsymmetrical attachment. Unsymmetrical attachment causes secondary bending moment at the weld toe which is compressive. As a result, lower stress peak would be expected.

12.4 Case study III

Contact model in this case study did not provide any different results than compared to simplified modelling. All predicted fatigue lives were conservative. Linear surface extrapolation provided best estimate to test result as compared to quadratic extrapolation method or through thickness integration. Only solid modelling was performed due to issue of double stress gradient which is present in longitudinal attachment.

12.5 Case study IV

Cruciform joint under consideration was subjected to pure bending. This results a constant bending stress in between the loading points. Under pure bending this bending stress dips below its nominal value (far away from weld toe) at about half plate thickness away from weld toe before rising from its nominal value due to discontinuity at the weld toe. This may be caused by the stiffening effect of welds and attachment plate in the middle of the joint, thus causing decrease in strain in front of the weld toe. As a result, all three surface extrapolation methods failed under 2D-modeling procedures under plane stress and plane strain conditions.

Difference between nominal stress and extrapolated hot spot stress was not large, nevertheless, stress concentration factor was below 1. Linear fully integrated plane stress elements overestimated stress. Plane stress assumption in 140mm wide specimen may not give valid results as out-of-plane normal stress component is present. Linear reduced integration elements gave lower principal stress as compared to quadratic elements. They are unable to curve under bending loading and due to one integration point have limited load carrying capacity. On the surface, stress at the node is a result from two integration points. This causes conservative fatigue life approximation.

Nominal stress approach gave non-conservative results. Issue with nominal approach here is that it does not account for stress raising effects caused by welds and attachment. Thus, non-conservative results could be expected.

Through thickness integration at the weld toe gave more encouraging results. As a comparison, full penetration welds were considered as well. In all cases fillet welds exhibited slightly larger structural stress at the weld toe than full penetration welds. Fatigue life prediction for fillet welded joints was higher at high stress ranges. This may be due to the m values obtained from UKOSRP testing program. Values were based on various testing conditions. Full penetration welds gave higher fatigue lives at lower stress

ranges. Decrease in plate thickness caused increase in fatigue life. Fatigue lives at lower stress ranges tended to be conservative. Therefore, slopes based on regression from tests describe data well at mid and high cycle range.

Fracture mechanics analysis gave comparable results, however, limited geometries were analyzed and one should treat the results accordingly. Numerical integration was based on best coefficient of determination of nine least-squares regression analyses. Exponential model provided best fit in all cases. By visual inspection it is clear that exponential fit describes data poorly, even though coefficient of determination is best. Exponential fit underestimates crack growth and crack length relationship at small crack lengths, however, more significant error results from $a = 0.5\text{mm}$ to $a = 7\text{mm}$. In this region exponential model overestimates the data. Logarithmic model dips on negative side at about $a = 11\text{mm}$. As a result integration can be performed up to this point only. Power model underestimates data in the region $a = 0.5\text{mm}$ to $a = 7\text{mm}$. Logarithmic model has same problem as exponential model. Table.31 lists fatigue lives predicted by four models and test result. Sectioned result is also shown

Table.34. Fatigue lives using four models comparison to UKOSRP.

UKOSRP	Power	Exponential	Logarithmic	Sectioned
833 000	480 000	1 117 400	1 266 700	266 000

By visual inspection it would seem reasonable that fracture mechanics solution is most accurate to actual test result. More accurate curve fitting technique is required. Data points could be broken down into sets of 2 or 3 along with curve fitting. Then, numerical integration could be performed by section basis for more accurate result. Same behavior was true for all three loading cases.

Failure criteria in test specimens was half thickness of plate, $\sim 20\text{mm}$. This causes approximation into the analysis. However, this is not significant as crack propagation rate increases as a function of crack length. Based on exponential model, for example, to grow a crack quarter way through the plate thickness consumes 80% of fatigue life. Along with results, one would not expect large difference in fatigue life when comparing fillet welds to full penetration welds under pure bending. Relatively little load is carried close to the neutral axis under pure bending. Thus, gap in fillet welded joint is fairly harmless in bending.[1]

Four point bending does not really cause pure Mode 1 except perhaps at early stages of crack growth. However, Mode 1 and Mode 2 are not additive to produce K_{total} . [14] Only Mode 1 was considered in this study. Refer to Figure.59 for curve fits.

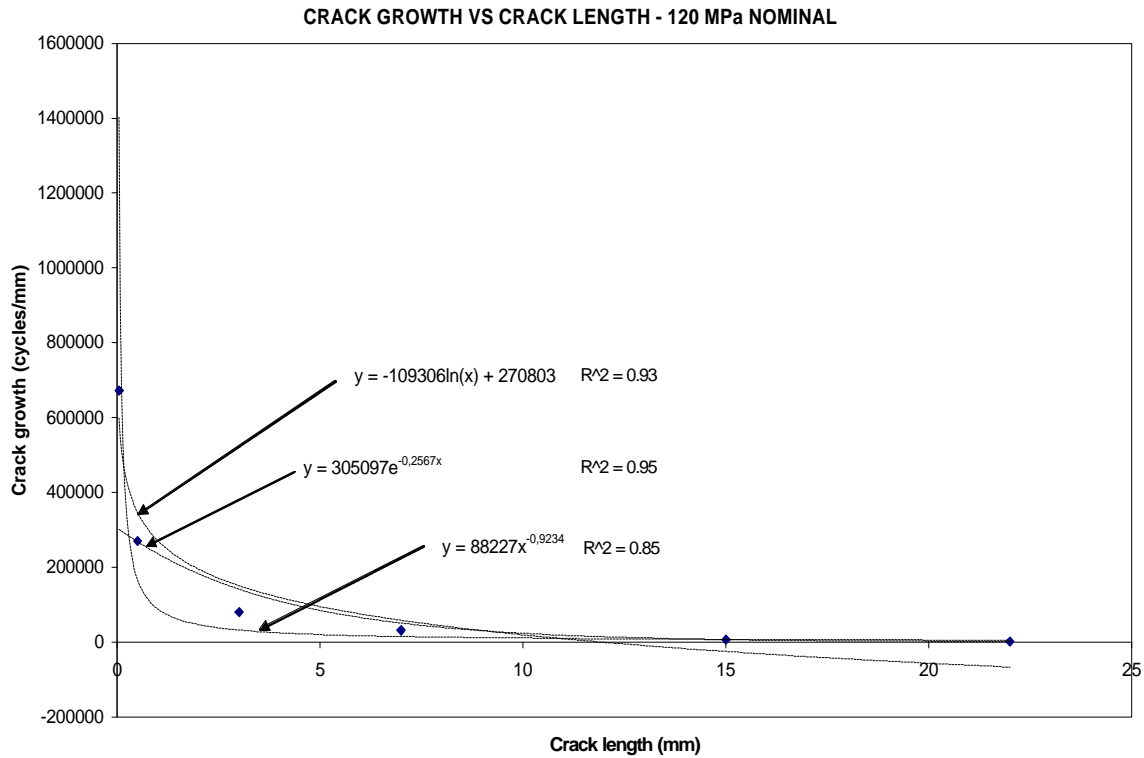


Figure.59. Basis for numerical integration for cruciform joint under four point bending.

13 CONCLUSIONS

Coefficients in multivariable regression are solved by setting up sum of the squares of the residuals, taking partial derivatives with respect to each variable and arranging resulting equations into matrix form. Coefficients are not predetermined but follow from solving the matrix. Some significant variables affecting fatigue life of a joint are stress range, plate thickness and loading mode. As comparing stress range and plate thickness, stress range may have much larger effect to fatigue life than plate thickness. Considering multivariable regression in three welded details and four case studies it would seem reasonable to draw the following conclusions:

- Multivariable regression does not presently work for butt joints which is based 1556 test results from 50 references. Model predicts difference of 300 000 cycles in fatigue life going from 2mm thick plate to 50mm thick plate.

- Multivariable regression predicts general behaviour in cruciform joints as far as fatigue strength is concerned. Model is built on 1189 test results from 29 references. Fatigue lives cannot be accurately determined, because other global and local geometry is omitted at this stage. Model predicts decrease in fatigue strength as stressed plate thickness is increased.
- Most encouraging results are seen in longitudinal attachment through multivariable regression. Model is built on quite limited amount data, 456 test results from 11 references. Opposite trend in thickness effect is as compared to butt joints or cruciform joints. Fatigue strength of longitudinal attachment tends to decrease as stressed plate thickness is decreased, given other geometry of the joint stays constant. Fatigue life estimates are rough as other important parameters are omitted in multivariable regression, such as plate width, attachment thickness and length.
- Hot-spot method does not appear to work for thin longitudinal attachments. Stress concentration factors are all over two, some close to three depending on the element. As a result, fatigue life estimates are quite conservative. Linear elastic material model most likely contributes over estimated stresses, at test stress ranges local plasticity at the attachment end is likely. This would results increase fatigue life estimation.
- Surface extrapolation methods failed in cruciform joint under four point bending. Predicted structural hot-spot stress was below nominal stress. Through thickness integration at the weld toe gave conservative fatigue life estimate. Both, effective notch method and fracture mechanics approach gave conservative results.
- Contact modelling with attempt to simulate relative sliding in four bending did not differ from simplified approach. Advantage would become significant if large strains would be present.
- Solid model in Maddox's experiment gave conservative fatigue life estimates as shell model gave non-conservative results. Shell model does not accurately take into account double stress gradient in longitudinal attachment. Welds are omitted which makes a severe approximation into the analysis.

In determining a fatigue life of a structure, it is advisable to use different methods for fatigue life estimates. As results are compared, designer can make educated approximations without losing important details, after all fatigue design is all about details. More important, thorough understanding of real world structures and how they deform under loads is essential. Moreover,

understanding how to apply boundary conditions correctly as close to real world as possible and ever going uncertainty of real loads that structure sees are areas of continuous work.

14 RECOMMENDATIONS

Based on exploratory work carried out to investigate the possibility of applying multivariable regression analysis into fatigue life estimations of welded joints, no recommendations should be done at this stage. Even though some encouraging results were obtained from longitudinal attachment, reference data is quite limited. As a result, derived equations should be treated with caution even though they predict general trend from test results. This is, fatigue strength of longitudinal attachment tends to decrease with decreasing stressed plate thickness. One of the major tests was by Gurney [6] with 6mm and 2mm stressed plate thicknesses.

It would seem reasonable, first to double check all collected data and plot individual test results to see whether odd test series are included. This comes from the fact that linear regression performed for butt joints gave $m = 1.5$ which seems too low. Altogether, over 1 500 test results were included in the analysis.

REFERENCES FOR THE PAPER

- [1] UKOSRP (United Kingdom Offshore Steels Research Project), Final Report to ECSC, No. 7210 KB/8/801, Volume 2, May 1971
- [2] Getting Started with ABAQUS, vs. 6.4, 2003.
- [3] Analysis User's Manual, Volume II: Analysis, Version 6.4, Fracture Mechanics section, 2003.
- [4] Hobbacher, A. , Fatigue Design of welded joints and components, International Institute of Welding, XIII-1539-96, 1996.
- [5] Marquis, G. and Niemi, E. , Introduction to the Structural Stress Approach to Fatigue Analysis of Plate Structures, Proceedings of The IIW Fatigue Seminar, Tokyo Institute of Technology, 2002.
- [6] Gurney, T.R. , The Fatigue Strength of Transverse Fillet Welded Joints – A study of the influence of joint geometry, Abington Publishing Special Report, 1991.
- [7] Bastid, Philip, *Development of Meshing Techniques for Cracks using ABAQUS CAE*, PowerPoint presentation, 09/03/04, Structural analyst at TWI Ltd. in FEA section
- [8] Fricke, W., Evaluation of Hot Spot Stresses in Complex Welded Structures, Proceedings of The IIW Fatigue Seminar, Tokyo Institute of Technology, 2002.
- [9] Dowling, N.E., Mechanical Behavior of Materials: Engineering Methods for Deformation, Fracture, and Fatigue, 2nd Edition, 1999.
- [10] Chapra, S.C. and Canale, R.P., Numerical Methods for Engineers: With Software and Programming Applications, 4th Edition, 2002.
- [11] Poutiainen, I., FEM – vasymiskestavyyden parantamisen apuvalineena, Lappeenranta University of Technology, PowerPoint presentation
- [12] Smith, Simon., Structural analyst at TWI – FEA section, discussions about CTOD and its relevance to SIF in LEFM
- [13] Anderson, T.L., Fracture Mechanics – Fundamentals and Applications, 2nd Edition, 1995.
- [14] Gurney, T.R, Fatigue of thin walled joints under complex loading, Abington Publishing Special Report, 1997
- [15] Castiglioni, C.A & Bremen, U, “Influence of some geometrical parameters on stress concentration in longitudinal attachments”, *Costruzioni Metalliche*, Vol.41, No.4, 1989.

- [16] Castiglioni, C.A & Gianola P, "Parametric analysis of weld toe stress concentration in longitudinal attachments", *Welding International*, Vol.6, No.4, 1992, pp.267-286.
- [17] Fricke W, "Evaluation of Hot-Spot Stresses in Complex Welded Structures", *Proceedings of The IIW Fatigue Seminar*, Tokyo Institute of Technology, 2nd April, 2002.
- [18] Maddox SJ, "Influence of tensile residual stresses on fatigue behavior of welded joints in steel", "Residual Stress Effects in Fatigue", ASTM STP 776, American Society for Testing and Materials, 1982, pp.63-96.
- [19] Konter A, "How to Undertake a Contact and Friction Analysis", NAFEMS The International Association for the Engineering Analysis Community, 2000.
- [20] ABAQUS 6.5 Analysis User's Manual, Volume V: Prescribed Conditions, Constraints & Interactions, 2004.
- [21] Harris WJ, "The significance of fatigue", *Engineering Design Guides*, Oxford University Press, 1976.
- [22] Maddox SJ, "Fatigue strength of welded structures", 2nd Edition, 1991.
- [23] Hobbacher AF, "Application of the Effective Notch Stress Method for Fatigue Assessment of Welded Joints", *Proceedings of the IIW Fatigue Seminar*, 2002.
- [24] Gustafsson M, "Thickness effect in fatigue of welded extra high strength steel joints", *Design and Analysis of Welded High Strength Steel Structures*, Eighth International Fatigue Congress FATIGUE 2002, 2002.
- [25] Niemi E, "Stress Determination for Fatigue Analysis of Welded Components", IIW – 1221 – 93, 1995.
- [26] *Statistics for Industry*, "Multivariate Statistics", 4 Victoria Avenue, Knaresborough, N. Yorks. HG5 9EU
- [27] Leggatt R, structural analyst at TWI, discussion about forcing the exponent in stress range term to 3, 20.05.2006, progress meeting and presentation on multivariable regression analysis.
- [28] Draper N. & Smith H., "Applied regression analysis", 2nd Edition, 1966.
- [29] Cooper B.E., "Statistics for experimentalists", 1st edition, 1969.
- [30] Dong P, "Master S-N curve method for fatigue evaluation of welded components", *WRC Bulletin 474 – August 2002*.
- [31] Wei L., FE analyst at TWI Ltd / Finite Element Analysis Section, discussion about loading mode parameter r, 2/2006

REFERENCES – LONGITUDINAL ATTACHMENT

- [1] Gurney TR, Effect of peening and grinding on the fatigue strength of fillet joints, *Welding Research International*, Vol 3, No 4, 1973 pp.53
- [2] Gurney TR, Further fatigue tests on mild steel specimens with artificially induced residual stresses, *British Welding Journal*, Vol 9, No 11, 1962 pp.612
- [3] Gurney TR & Smith IFC, Changes in the fatigue life of plates with attachments due to geometrical effects, *Welding Research Supplement*, Sept. 1986.
- [4] Iwata T & Matsuoka K, Fatigue strength of CP Grade 2 titanium fillet welded joint for ship structure, *Welding in the World*, Vol. 48, No. 7/8 2004 pp.40
- [5] Boulton CF & Harrison JD, Fatigue tests on welds in 18% nickel maraging steel, *Welding Research International*, Vol. 3, No. 3, 1973.
- [6] Knight JW, Some basic fatigue data for various types of fillet welded joints in structural steel, *Welding Research International*, Vol. 9, No. 3, 1979.
- [7] Koskimaki A & Niemi E, “Fatigue strength of welded joints in three types of stainless steel”, IIW Document XIII-1603-95
- [8] Maddox SJ, “Influence of tensile residual stresses on the fatigue behaviour of welded joints in steel”, ASTM STP 776, American Society for Testing and Materials, 1982.
- [9] Maddox SJ, UKOSRP, Phase I, 1975.
- [10] Noordhoek C & Verheul A, “The influence of plate thickness on the fatigue behaviour of welded plates up to 160mm with an attachment or butt weld”, *Steel in Marine Structures, Proceedings of the 3rd International ECSC Offshore Conference on Steel in Marine Structures*, 1987.
- [11] Huther I & Lieurade HP & Buisson R, “Fatigue strength of longitudinal non-load carrying welded joints”, *Welding in the World*, Vol.41, 1998.

REFERENCES – CRUCIFORM JOINTS

- [1] Maddox SJ, “The effect of plate thickness on the fatigue strength of fillet welded joints”, TWI Publication, 1987.
- [2] Ferreira JA & Branco CA, “Influence of the radius of curvature at the weld toe in the fatigue strength of fillet welded joints”, *International Journal of Fatigue*, Vol.11, No.1, 1998.
- [3] Nihei & Kamakura & Sasaki and Inagaki, “Effect of specimen size on fatigue properties of SM50B non-load carrying fillet welded joints”, *Transactions of National Research Institute of Metals*, Vol.24, No.2, 1985.

- [4] Maddox SJ, "Fatigue of welded joints loaded in bending by SJ Maddox", Transport and Road Research Laboratory, Department of the Environment
- [5] Dongpo W & Yufeng Z & Lixing H and Junmei C, "Application of the local approach to the fatigue assesment for welded joints", China Welding, Vol.12, No.2, 2003.
- [6] Iwata T & Matsuoka K, "Fatigue strength of CP grade 2 titanium fillet welded joint for ship structure", Welding in the World, Vol.48, No.7/8, 2004.
- [7] Gurney TR, "Influence of thickness on the fatigue strength of welded joints", BOSS 1979.
- [8] Kainuma S & Kim IT, "Fatigue strength evaluation of load-carrying cruciform fillet-welded joints made with mild steel plates for different thickness", International Journal of Fatigue, Vol.27 (2205).
- [9] Gurney TR, "Fatigue of thin walled joints under complex loading", An Abington Publishing Special Report, 1997.
- [10] Peckover RS & Fraser RAW, "UKOSRP – Phase 1", Offshore Technology Report – Department of Energy.
- [11] Berge S, "On the effect of plate thickness in fatigue of welds", Engineering Fracture Mechanics, Vol.21, No.2, 1985.
- [12] Knight JW, "Some basic fatigue data for various types of fillet welded joints in structural steel", Welding Research International, Vol.9, No.3, 1979.
- [13] Gurney TR, "The fatigue strength of transverse fillet welded joints – A study of the influence of joint geometry", An Abington Publishing – Special Report, 1975.
- [14] Manteghi S, "Methods of fatigue life improvement for welded joints in medium and high strength steels", TWI Special Report, 6/1998.
- [15] Booth GS, " The effect of thickness on the fatigue strength of plate welded joints", Steel in Marine Structures, Proceedings of the 3rd International ECSC Offshore Conference on Steel in Marine Structures, 1987.
- [16] Noordhoek C, Verheul A "The influence of plate thickness on the fatigue behaviour of welded plates up to 160mm with an attachment or butt weld", Steel in Marine Structures, Proceedings of the 3rd International ECSC Offshore Conference on Steel in Marine Structures, 1987.
- [17] Ravichandran G, "Prediction of fatigue life of partial penetration fillet welds under bending load", Welding Research International Journal, Vol.23, No.3, 1998.

- [18] Gregory EN, “The mechanical properties of welds in zinc coated steel”, Welding Journal, October 1971.
- [19] Shimada W & Hoshiouchi S and Hijikata A, “Improvement of fatigue strength in fillet welded joint by CO2 soft plasma arc overlaying on weld toe”, IIW – Document No. XIII – 830 – 77.
- [20] Wildschut H & de Back J and Dortland W, “Fatigue behavior of welded joints in air and sea water”, European Offshore Steels Research Seminar, TWI Abington, 1980.
- [21] Booth GS, “Constant amplitude fatigue tests on welded steel joints performed in sea water”, European Offshore Steels Research Seminar, TWI Abington, 1980.
- [22] N.N., UKOSRP – Final report to ECSC, Contract No. 7210, Vol.1 & 2, 1980.
- [23] Neumann A, “Probleme der Dauerfestigkeit von Schweissverbindungen”, VEB Verlag Technik, Berlin, 1966.
- [24] Nishioka A and Ouchida H, “A study of fatigue strength of fillet welded joints”, Hitachi Review, Hitachi Research Laboratory, Japan, 1964.
- [25] Macfarlane DS and Harrison JD, “Some fatigue tests of load-carrying transverse fillet welds”, British Welding Journal, Vol.12, 1965.
- [26] Webber D, “The comparison of the fatigue strength of welded joints in structural steel (MEXE), Materials Research Wing Report, No.34, Christchurch, 1966.
- [27] Baxter DE and Modlen GF, “Some factors affecting the fatigue strength of fillet welds”, British Welding Journal, Vol.13, No.4, 1966.
- [28] Kloeppe K and Seeger T, “Experimentelle und theoretische Untersuchungen zum Schädigungsverhalten”, Technischen Hochschule Darmstadt, Heft 5, 1969.
- [29] Friis LE & Sperle JO and Wallin LE, “Fatigue of welded structures”, Proceedings of the Conference, Vol.1, Session 1 & 2, TWI, 1971.
- [30] Frank KH, “The fatigue strength of fillet welded connections”, Ph.D Dissertation, Lehigh University, Bethlehem, 1972.

REFERENCES - BUTT JOINTS

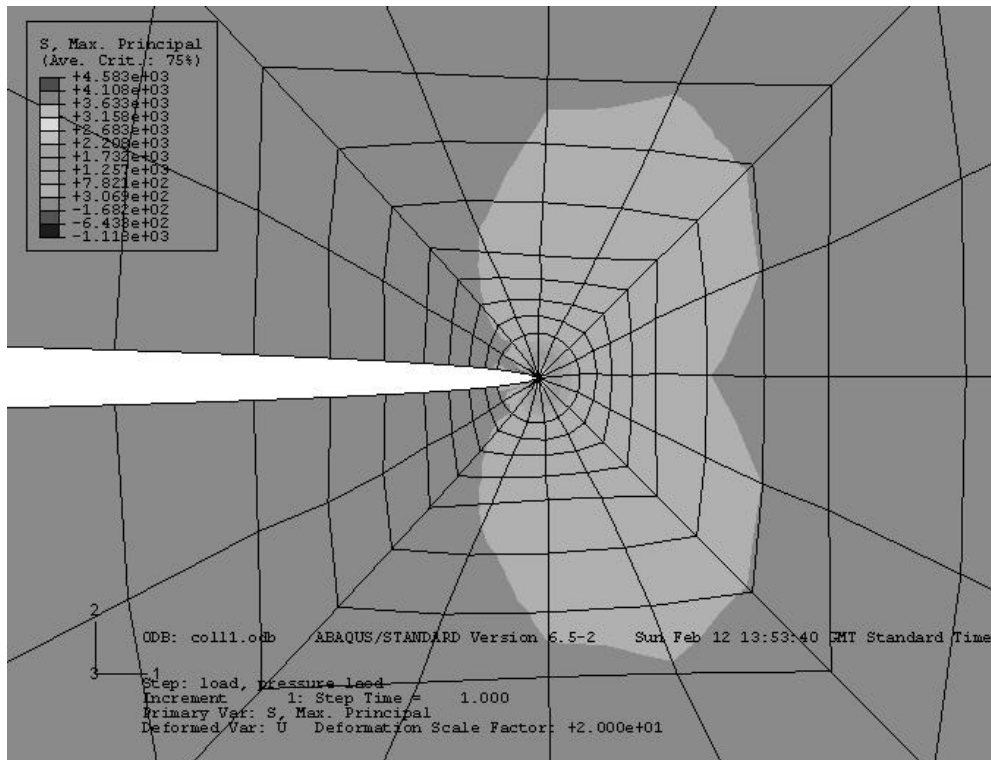
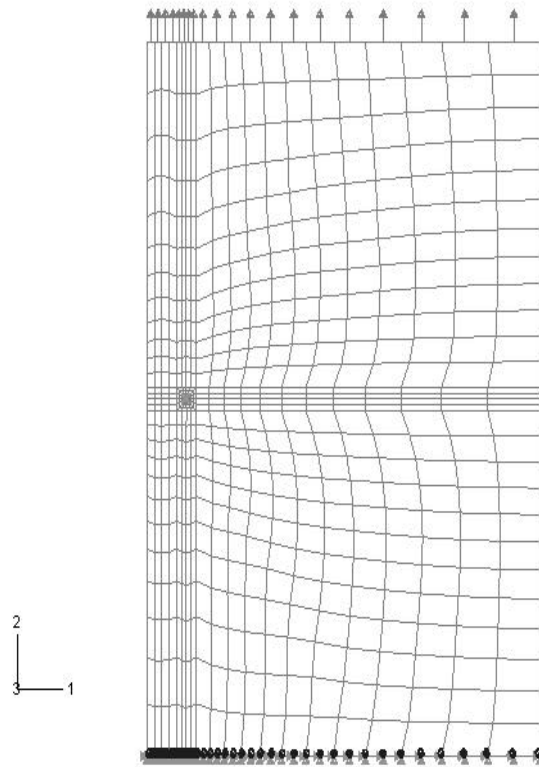
- [1] Dongpo W, Yufeng Z, Lixing H, “Application of the local approach to the fatigue assessment for welded joints”, China Welding, Vol.12, No.2, 2003.

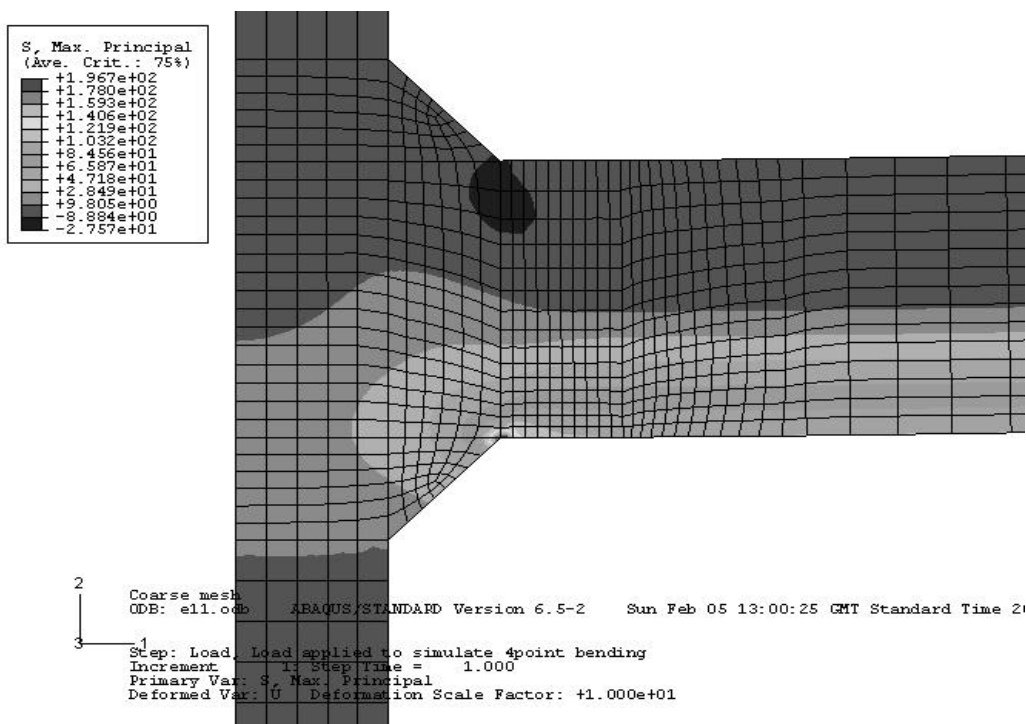
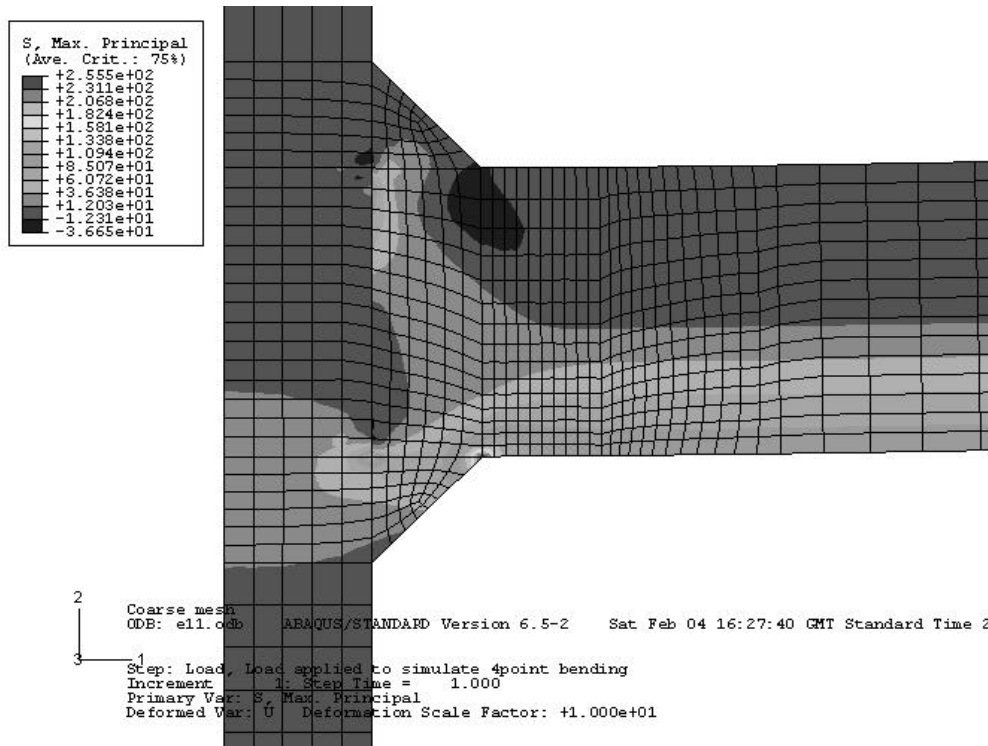
- [2] Iwata T & Matsuoka K, Fatigue strength of CP Grade 2 titanium fillet welded joint for ship structure, *Welding in the World*, Vol. 48, No. 7/8 2004 pp.40
- [3] Faulkner MG and Bellow DG, "Influence of testing frequency on the fatigue of butt welded steel joints", *Welding Research International*, Vol.9, No.3, 1979.
- [4] Burk JD and Lawrence FV, "Influence of bending stresses on fatigue crack propagation life in butt joint welds", *Welding Journal*, Feb. 1977.
- [5] Boulton CF and Harrison JD, "Fatigue tests on welds in 18% nickel maraging steel", *Welding Research International*, Vol.3, No.3, 1973.
- [6] Taylor D, "Some new methods for predicting fatigue in welded joints", *International Journal of Fatigue*, Vol.24, No.5, 2002.
- [7] Koskimaki A & Niemi E, "Fatigue strength of welded joints in three types of stainless steel", *IIW Document XIII-1603-95*
- [8] Scott GR & Stallmeyer JE and Munse WH, "Fatigue strength of transverse butt-welded joints in N-A-XTRA 100 steel", *Civil Engineering Studies / Structural Research Series No. 254*, 1979.
- [9] Frost NE and Denton K, "The fatigue strength of butt-welded joints in low-alloy structural steels", *British Welding Journal*, Vol.14, No.4, 1967.
- [10] Elliot S and Wylde JG, "The fatigue strength of electron beam transverse butt joints in C-Mn steels", *The Welding Institute Special Report No. 7752*, 1984.
- [11] Punshon CS and Wylde JG, "The fatigue strength of electron beam transverse butt welds in a low Ni-Cr-Mo alloy steel", *The Welding Institute Special Report No. 7752*, 1985.
- [12] Kuriyama Y & Saiga Y & Kamiyama T and Ohno T, "Low cycle fatigue strength of butt welded joints with angular distortion", *IIW Document XIII-621-71*, June 1971.
- [13] Petershagen H and Zwick W, "Fatigue strength of butt welds made by different welding process", *IIW Document XIII-1048-82*, 1982.
- [14] Solumsmoen OH, "Fatigue tests on specimens with holes, butt and fillet welds in mild steel and high tensile steels", *Met. Con.*, Vol.1, No.3, March 1969.
- [15] Gurney TR, "Fatigue tests on butt and fillet welded joints in mild and high tensile steels", *British Welding Journal*, Vol.9, No.11, 1962.
- [16] Friis LE and Steneroth ER, "Fatigue strength of welded joints in mild and high strength structural steel", *Jernkort. Ann.*, Vol.152, 1968.

- [17] Selby KA & Stallmeyer JE and Munse WH, "Influence of geometry on fatigue behavior of welded joints", University of Illinois Report No.297, 1965.
- [18] Yamaguchi I & Terada Y and Nitta A, "On the fatigue strength of steels for ship structures", IIW Document XIII-425-66, 1966.
- [19] Noordhoek C, Verheul A "The influence of plate thickness on the fatigue behaviour of welded plates up to 160mm with an attachment or butt weld", Steel in Marine Structures, Proceedings of the 3rd International ECSC Offshore Conference on Steel in Marine Structures, 1987.
- [20] Kloepfel K and Weihermuller H, "Neue Dauerfestigkeitsversuche mit Schweissverbindungen aus St 52", Der Stahlbau 26, Heft 6, 1957.
- [21] Garcia-Martin Z and Falco FC, "Estudio sobre la resistencia a la fatiga de uniones a tope soldadas automaticamente por FUSARC", Cien y Tecnica de la Soldadura, Vol.9, No.43, 1958.
- [22] Newman RP and Gurney TR, "Fatigue tests of plain plate specimens and transverse butt welds in mild steel", British Welding Journal, Vol.6, No.12, 1959.
- [23] Nacher A, "Influence of local heating and of surface peening of fatigue behavior of welded joints and details", British Welding Journal, Vol.7, No.8, 1960.
- [24] Newman RP and Gurney TR, "Fatigue tests on 1/2" thick transverse butt welds containing slag inclusions", British Welding Journal, Vol.11, No.7, 1964.
- [25] Muller G and Gregor V, "Ein Beitrag zum Problem der Dauerfestigkeit geschweisster Verbindungen aus Stahlen hoherer Festigkeit, ZIS – Mitteilungen 7, No.7, 1965.
- [26] Gurney TR and Smith GC, "Fatigue tests on 1.5" thick transverse butt welds containing slag inclusions", British Welding Journal, Vol.14, No.1, 1967.
- [27] Reemsnyder HS, "Some significant parameters in the fatigue properties of welded joints", Welding Research Supplement, Vol.34, No.5, 1969.
- [28] Harris FG & Douglas RB and Rowan RW, "Axial load and bending fatigue tests on welded normalized manganese – silicon steel", Department of Supply, Melbourne, 1969.
- [29] N.N., "Prufbericht uber Dauerfestigkeitversuche mit CO₂ – stumpf – geschweissten Prufstaben, Institut fur Statik und Stahlbau der TH Darmstadt Bericht vom 1969.
- [30] N.N., "N-A-XTRA-Schwingverhalten Huttenwerke Oberhausen AG", Stranski – Institut fur Metallurgie, Oberhausen, 1969.

- [31] Locati L & Bollani G and Massa A, "Metallographic influences on Fe 52 carbon steel fatigue strength", FIAT – Forschungsbericht, Turin, 1969.
- [32] Robakowski T, "L'influence de manque de penetration ala racine sur la resistance ala fatigue des joints", IIW Document No. XIII-582-70, 1970.
- [33] Odegard K and Hembre P, "Fatigue tests of ship building steel – Part 2: Tests with notched and welded test pieces of steel", IIW Document No. XIII-598-70, 1970.
- [34] Harrison JD, "Fatigue tests on large butt welds", CIRIA – Report 19, 1970.
- [35] N.N., "Untersuchung von MIG – CO₂ – stumpfgeschweissten Proben aus St 52 – 3", Institut fur Statik und Stahlbau der TH Darmstadt Bericht vom 1971.
- [36] Kunihiro T & Ando A & Nagai A & Ueda J and Oztaka T, "Low temperature fatigue behavior of 9% Ni steel weld joints", IIW Document No. XIII-649-72, 1972.
- [37] Donato L & Guerrera U & Sanpaolesi L and Bertero M, "Sugli acciai tipo T1 relativi giunti saldati", Centro studi costruzioni metalliche dell' Universita di Pisa, No.72, 1972.
- [38] Ekstrom DH and Munse WH, "The effect of internal weld defects on the fatigue behavior of welded connections", IIW Document No. XIII-678-73, 1973.
- [39] Disselmeyer H and Degenkolbe J, "Schwingverhalten eines hochfesten wasserverguteten legierten Feinkornbaustahles mit 70 kp/mm²", Schriftenreihe Schweißen und Schneiden, Bericht 2, 1973.
- [40] N.N., "Dauersschwingversuche an Quernahten in Sondergute mit Kreuzstrichraupen", Staatliches Materialprufungssamt fur Maschinenbau an der Tu Munchen, 1973.
- [41] Heckel K, "Die Dauerfestigkeit von Flachstahl aus St 37", Der Stahlbau 39, Heft 7, 1973.
- [42] Robakowski T, "Dauerfestigkeit und mechanische Eigenschaften UP-geschweisster Verbindungen des Stahles 14 HNMB Cu", ZIS – Mitteilungen 15, No.9, 1973.
- [43] Kado S & Ishiguro T and Ishii N, "Fatigue strength improvement of welded joints by plasma arc dressing", IIW Document No. XIII-774-75, 1975.
- [44] Gregory EN, "Galvanizing characteristics of steels and their weldments: Fatigue tests on butt welds", IIW Document No. XIII-796-76, 1976.

- [45] Iida K and Lino N, "Effect of angular distortion on fatigue strength of transverse butt-welds in high strength steels", Japan Welding Society, Vol.8, No.2, 1977.
- [46] Benoit D & Lieurade HP and Truchon M, "Comportement en fatigue a programme de differents types de joints soudes bout a bout en acier E 355", IIW Document No. XIII-886-78, 1978.
- [47] Nather F and Quel R, "MAG – geschweisste Stumpfnafte in dynamisch beanspruchten Bauteilen", DVS – Bericht Nr.50, Dusseldorf, 1978.
- [48] Minner HH and Seeger T, "Schwingfestigkeitsuntersuchungen an MAGM – geschweissten Stumpf – und Kehlnahtverbindungen aushochfesten", Oerlikon Schweissmitteilungen 36, No.83, 1978.





SURFACE EXTRAPOLATION METHODS - CRUCIFORM JOINT IN FOUR POINT BENDING										
FULL PENETRATION						FILLET WELDED				
t=38mm, leg=14mm						t =38mm, leg = 18mm				
LINEAR 1	0.4t (MPa)	t (MPa)	ELEMENT		Hot_Spot	LINEAR 1	0.4t (MPa)	t (MPa)	ELEMENT	Hot_Spot
CPE8R	103,88	103,88	15mm		103,88	CPE8R	103,75	103,86	1.5mm	103,68
	103,77	103,87	5mm		103,70	LINEAR 2	0.5t	1.5t		
	103,68	103,87	2.5mm		103,55	CPE8R	103,57	103,88	1.5mm	103,41
	103,65	103,87	1.5mm		103,50	QUADRATIC	0.4t	0.9t	1.4t	ELEMENT
LINEAR 2						CPE8R	103,82	103,83	103,88	1.5mm
CPE8R	0.5t	1.5t	ELEMENT							
	103,88	103,88	15mm		103,88	LINEAR 1	0.4t	t	ELEMENT	
	103,67	103,88	5mm		103,57	CPE8	103,66	103,86	1.5mm	103,53
	103,65	103,88	2.5mm		103,53	CPS8	103,62	103,86	1.5mm	103,46
	103,64	103,88	1.5mm		103,52	CPS8R	103,65	103,87	1.5mm	103,51
QUADRATIC						LINEAR 1				
CPE8R	0.4t	0.9t	1.4t	ELEMENT		CPE4R	96,04	95,80	96,20	1.5mm
	103,88	103,88	103,88	15mm	103,88	CPE4	98,67	97,74	99,29	1.5mm
	103,77	103,85	103,88	5mm	103,66	CPE4I	103,76	103,86	103,69	1.5mm
	103,68	103,85	103,88	2.5mm	103,43	LINEAR 1				
	103,69	103,85	103,88	1.5mm	103,46	CPS4R	96,07	95,80	96,25	1.5mm
LINEAR 1						CPS4	104,41	104,29	104,49	1.5mm
CPE4R	97,33	97,67	97,10	1.5mm						
CPE4	99,50	98,76	99,99	1.5mm						
CPE4I	103,71	103,87	103,60	1.5mm						
CPE8	103,63	103,87	103,46	1.5mm						
LINEAR 1										
CPS4R	97,33	97,66	97,10	1.5mm						
CPS4	104,27	104,33	104,23	1.5mm						
CPS8R	103,68	103,88	103,54	1.5mm						
CPS8	103,63	103,87	103,48	1.5mm						
QUADRATIC										
CPE8	103,72	103,85	103,88	1.5mm	103,54					
CPS8R	103,72	103,85	103,88	1.5mm	103,54					
CPS8	103,62	103,85	103,88	1.5mm	103,28					
t=25mm, leg=10mm										
LINEAR 1	0.4t	t	Hot-Spot							
CPE8R	103,65	103,87	103,50	1.5mm						
QUADRATIC	0.4t	0.9t	1.4t							
CPE8R	103,81	103,85	103,88	1.5mm	103,76					
CPE8	103,42	103,85	103,88	1.5mm	102,79					

